

*Supporting Information Part I for:*

## **Multi-Phosphine-Chelated Iron Carbide Clusters via Redox-Promoted Ligand Exchange on $[\text{Fe}_6(\mu_6\text{-C})(\mu_2\text{-CO})_4(\text{CO})_{12}]^{2-}$**

Caitlyn R. Cobb, Ren K. Ngo, Emily J. Dick, Vincent M. Lynch  
and Michael J. Rose\*

*Department of Chemistry, The University of Texas at Austin  
Austin, TX 78712 USA*

<b>Contents</b>	<b>Page</b>
<b>Synthetic and Experimental Procedures</b>	<b>S3-10</b>
<b>Figure S1.</b> FT-IR data for <b>1</b> .	<b>S11</b>
<b>Figures S2-S3.</b> FT-IR spectra of the synthesis of <b>2</b> in DCE and MeCN.	<b>S12-13</b>
<b>Figure S4.</b> FT-IR spectra for <b>1</b> , the formation of <b>2</b> in DCE, and the addition of PPhMe <sub>2</sub> in DCE.	<b>S14</b>
<b>Figures S5.</b> <sup>31</sup> P{ <sup>1</sup> H} NMR spectrum of the addition of PPhMe <sub>2</sub> in DCE to <b>2</b> .	<b>S15</b>
<b>Figures S6–7.</b> <sup>13</sup> C NMR and IR spectra for <b>3</b> .	<b>S16-17</b>
<b>Figures S8–11.</b> <sup>1</sup> H NMR, <sup>13</sup> C NMR, <sup>31</sup> P{ <sup>1</sup> H} NMR and IR spectra for <b>4</b> .	<b>S18-21</b>
<b>Figures S12–16.</b> <sup>1</sup> H NMR, <sup>13</sup> C NMR, <sup>31</sup> P{ <sup>1</sup> H} NMR, NOESY and IR spectra for <b>5</b> .	<b>S22-26</b>
<b>Figures S17-S20.</b> <sup>1</sup> H NMR, <sup>13</sup> C NMR, <sup>31</sup> P{ <sup>1</sup> H} NMR, and IR spectrum for <b>6</b> .	<b>S27-30</b>
<b>Figures S21–22.</b> <sup>31</sup> P{ <sup>1</sup> H} NMR and IR spectra for <b>7</b> .	<b>S31-32</b>
<b>Figures S23–26.</b> <sup>1</sup> H NMR, <sup>13</sup> C NMR, <sup>31</sup> P{ <sup>1</sup> H} NMR and IR spectra for <b>8</b> .	<b>S33-36</b>
<b>Figures S27–30.</b> <sup>1</sup> H NMR, <sup>13</sup> C NMR, <sup>31</sup> P{ <sup>1</sup> H} NMR and IR spectra for <b>9</b> .	<b>S37-40</b>
<b>Figures S31–34.</b> <sup>1</sup> H NMR, <sup>13</sup> C NMR, <sup>31</sup> P{ <sup>1</sup> H} NMR and IR spectra for <b>10</b> .	<b>S41-44</b>
<b>Figures S35.</b> IR spectrum for <b>11</b> .	<b>S45</b>
<b>Table S1.</b> IR spectral data for various carbidocarbonyl clusters.	<b>S46</b>
<b>Figures S36.</b> FT-IR spectra of the synthesis of <b>9</b> from <b>8</b> and MeCN.	<b>S47</b>

<b>Figures S37–45.</b> ORTEP diagrams of X-ray crystal structures for <b>3–11</b> . Experimental details for XRD and structure solution of <b>3–11</b> .	<b>S47-61</b>
<b>Table S2-S3.</b> Crystal data and refinement parameters for <b>3-11</b> .	<b>S62-64</b>
<b>Tables S4.</b> Selected bond distances for <b>3</b> .	<b>S65-66</b>
<b>Tables S5.</b> Selected bond angles for <b>3</b> .	<b>S66</b>
<b>Figure S46.</b> Fe <sub>5</sub> core framework and atom number visualization.	<b>S67</b>
<b>Tables S7.</b> Selected bond angles for <b>4, 5, and 8</b> .	<b>S67</b>
<b>Figure S47.</b> Visualization of Fe5 equatorial plane and C-plane distance.	<b>S67</b>
<b>Tables S8.</b> Selected bond distances for <b>4, 5, and 8</b> .	<b>S68</b>
<b>Table S9.</b> Selected bond distances for 3-iron cluster units in <b>6, 7, 10, and 11</b> .	<b>S69</b>
<b>Table S10.</b> Selected bond angles for 3-iron cluster units in <b>6 and 7</b> .	<b>S69</b>
<b>Table S11.</b> Selected bond angles for 3-iron cluster units in <b>10 and 11</b> .	<b>S70</b>
<b>Figure S48.</b> Visualization of simplified triphos and Fe <sub>4</sub> core of <b>9</b> .	<b>S70</b>
<b>Table S12.</b> Selected bond distances for <b>9</b> and literature values for other 4-Fe clusters.	<b>S70</b>
<b>Figure S49.</b> Visualization of Fe <sub>4</sub> butterfly dihedral angle and primary Fe-CFe angle.	<b>S71</b>
<b>Table S13.</b> Selected bond angle and torsion for <b>9</b> .	<b>S71</b>
Computational modeling of <b>2</b> : Design of approach and remarks on screening of functionals and basis sets using [Fe <sub>5</sub> (μ <sub>5</sub> -C)(CO) <sub>15</sub> ], <b>Tables S14-15</b>	<b>S72-73</b>
<b>Tables S16–S17.</b> Results of DFT functional screening for [Fe <sub>5</sub> (μ <sub>5</sub> -C)(CO) <sub>15</sub> ]: Selected bond distances, angles and RMSDs compared to experimental structure.	<b>S74-75</b>
<b>Tables S18–S21.</b> Results of DFT functional screening for [Fe <sub>5</sub> (μ <sub>5</sub> -C)(CO) <sub>15</sub> ]: Frequency simulations.	<b>S76-86</b>
<b>Figures S50-60.</b> Results of DFT functional screening for [Fe <sub>5</sub> (μ <sub>5</sub> -C)(CO) <sub>15</sub> ]: Frequency simulations.	<b>S86-97</b>
<b>Tables S22.</b> Results of DFT functional screening for [Fe <sub>5</sub> (μ <sub>5</sub> -C)(CO) <sub>15</sub> ]: RMSDs compared to experimental structure and HOMO-LUMO gaps.	<b>S98</b>
Remarks on computational method screening with [Fe <sub>5</sub> (μ <sub>5</sub> -C)(CO) <sub>15</sub> ].	<b>S98</b>
<b>Figure S61.</b> Visualization of optimized geometry [Fe <sub>5</sub> (μ <sub>5</sub> -C)(CO) <sub>15</sub> ] with C-PCM.	<b>S99</b>
<b>Table S23.</b> Vibrational analysis of [Fe <sub>5</sub> (μ <sub>5</sub> -C)(CO) <sub>15</sub> ] with C-PCM.	<b>S99-101</b>
<b>Remarks on model of 2 with and without C-PCM.</b>	<b>S101-102</b>
<b>Tables S24.</b> Comparisons of modeled geometries of <b>2</b> with C-PCM to gas-phase result.	<b>S102</b>
<b>Tables S25.</b> Comparisons of modeled vibrational spectra of <b>2</b> with C-PCM to gas-phase result.	<b>S102-104</b>
<b>Table S26.</b> Full coordinates of modeled gas-phase geometry for <b>2</b> .	<b>S105</b>

<b>Figure S62.</b> Calculated IR spectrum <b>2</b> .	<b>S106</b>
<b>Figure S63.</b> Calculated optimized gas phase geometry of <b>3</b> .	<b>S107</b>
<b>Table S27.</b> Full coordinates of modeled gas-phase geometry of <b>3</b> .	<b>S108-109</b>
<b>Figure S64.</b> Calculated IR spectrum <b>3</b> .	<b>S110</b>
<b>References</b>	<b>S111-113</b>

---

## Materials and Methods

### Solvents and Reagents

All non-deuterated solvents were dried through an alumina column system (Pure Process Technology). Fluorobenzene (FPh) (TCI America) was purchased as 99.0+% purity, and 1,2-dichloroethane (Fisher Chemical) was purchased as Certified ACS grade. All other solvents were purchased as HPLC grade from EMD, Fisher, Macron, TCI or J.T. Baker. Deuterated solvents ( $d_8$ -toluene and  $d_3$ -MeCN) were purchased from Acros Organics and used as received.  $C_6D_6$  was purchased from Cambridge Isotopes and underwent three freeze-pump-thaw cycles prior to use.

$(Et_4N)_2[Fe_6(\mu_6-C)(CO)_{16}]$  was prepared as described in our previous report.<sup>1</sup>  $Fe(CO)_5$  was purchased from Strem Chemicals and  $Na(s)$  was purchased from Fisher Chemical; both were used as received. Diethylene glycol was purchased from Acros Organics and used as received. Triphenylphosphine ( $PPh_3$ ), dimethylphenyl phosphine ( $PMe_2Ph$ ) and bis(2-diphenylphosphinoethyl)phenylphosphine (linear Triphos) were purchased from Acros Organics and used as received. Bis(diphenylphosphino)ethane (dppe) and (diphenylphosphino)propane (dppp) was purchased from TCI and used as received. The tripodal Triphos ligand 1,1,1-tris(diphenylphosphinomethyl)ethane and bis(diphenylphosphino)benzene (bdpb) were purchased from Alfa Aesar and used as received.

### Physical Measurements

The NMR spectra (except when otherwise indicated) were acquired at ambient temperature on a Varian VNMRs 600 MHz instrument equipped with a 5 mm AutoXDB PFG probe. The NOESY spectrum of **4** was obtained at ambient temperature.  $^{31}P$  NMR spectra were recorded at ambient temperature on a Varian 400 MHz NMR unless otherwise indicated. The probe was referenced to an external sample of 85%  $H_2PO_4$ . Solvent impurities were assigned according to Goldberg *et al.*<sup>2</sup> IR spectra were acquired using a Bruker Alpha spectrometer equipped with a diamond ATR crystal.

*Caution:* Metal carbonyls are extremely toxic. It is advised to handle these compounds in well-ventilated fume hoods under an inert gas atmosphere.

### Experimental Details

*Reaction of 2 with  $PPhMe_2$  and characterization of previously reported complex  $[Fe_5(\mu_5-C)(CO)_{12}(PMe_2Ph)_3]$*

In a glove box under N<sub>2</sub> atmosphere, a 20 mL screw-top vial was charged with a violet solution of (Et<sub>4</sub>N)<sub>2</sub>[Fe<sub>6</sub>(μ<sub>6</sub>-C)(CO)<sub>16</sub>] (300 mg, 0.284 mmol) in approximately 10 mL MeCN. Solid [Fc]PF<sub>6</sub> (198 mg, 0.597 mmol) was added, and the reaction mixture was stirred vigorously at room temperature for approximately 1 h, affording a red black solution (oxidation verified by FT-IR analysis). PMe<sub>2</sub>Ph (approximately 0.3 mL, 2.56 mmol) was added, and the reaction was stirred for 27h turning red brown.

Dropcast IR of reaction in **Figure S4**.

<sup>31</sup>P{<sup>1</sup>H}NMR (162 MHz, pentane, ppm) (**Figure S5**): δ 22.14 (s, 2P), 18.45 (s, 1P) ppm.

#### [Fe<sub>6</sub>(μ<sub>6</sub>-C)(μ<sub>2</sub>-CO)(CO)<sub>16</sub>] (**3**)

In a glovebox under N<sub>2</sub> atmosphere, a 20 mL screw-top vial was charged with a violet solution of (Et<sub>4</sub>N)<sub>2</sub>[Fe<sub>6</sub>(μ<sub>6</sub>-C)(CO)<sub>16</sub>] (132 mg, 0.125 mmol) in 10 mL of DCM. Solid [Fc]PF<sub>6</sub> (103 mg, 0.313 mmol) was added, and the reaction mixture was stirred vigorously at room temperature for 10 min, affording a black solution. Volatiles were removed *in vacuo*, affording a black solid. The solid was washed with pentane (2×10 mL), Et<sub>2</sub>O (2×10 mL), and toluene (5 mL) to remove ferrocene and Fe<sub>5</sub>(μ<sub>5</sub>-C)(CO)<sub>15</sub>. Extraction into FPh afforded a black solution from which black diffraction quality prisms of **3** were grown by slow evaporation at -20 °C. Yield: 42.3 mg, 0.0512 mmol (41.1%).

<sup>13</sup>C{<sup>1</sup>H} NMR (151 MHz, C<sub>6</sub>D<sub>6</sub>, ppm) (**Figure S6**): CO at δ 212.24, 212.11, 209.45 ppm

IR (solid state, in cm<sup>-1</sup>) (**Figure S7**): ν(CO) 2096 (w), 2023 (s), 1828 (m)

Anal. Calc.: C, 26.26; H 0.00; N 0.00

Anal. Exp.: C, 25.99; H, 0.26; N, 0.10

#### [Fe<sub>5</sub>(μ<sub>5</sub>-C)(CO)<sub>14</sub>PPh<sub>3</sub>] (**4**)

In a glovebox under N<sub>2</sub> atmosphere, a 20 mL screw-top vial was charged with a violet solution of (Et<sub>4</sub>N)<sub>2</sub>[Fe<sub>6</sub>(μ<sub>6</sub>-C)(CO)<sub>16</sub>] (300 mg, 0.284 mmol) in 10 mL of MeCN. Solid [Fc]PF<sub>6</sub> (200 mg, 0.604 mmol) was added, and the reaction mixture was stirred vigorously at room temperature for 1 h, affording a red-black solution (oxidation verified by FT-IR analysis). PPh<sub>3</sub> (684 mg, 2.559 mmol) was added, and the reaction was stirred for 24 h, turning red-brown. Volatiles were removed *in vacuo*, affording an oily black solid which were not dried to powders (drying completely prevents extraction of **4** into Et<sub>2</sub>O; this can be mitigated by adding a drop of MeCN after pentane extraction). The solid was washed with pentane (3×15 mL) to remove ferrocene and unreacted phosphine. Further extraction of the solid with Et<sub>2</sub>O gave a dark red solution from which black, block crystals of **3** were grown by slow evaporation at -20 °C. Yield: 34.6 mg, 0.0364 mmol (13%).

<sup>1</sup>H NMR (600 MHz, C<sub>6</sub>D<sub>6</sub>, ppm) (**Figure S8**): δ 7.93 (s 1H), 7.05 (t 2H), 6.93 (s 2H, overlapped free PPh<sub>3</sub> peak); free PPh<sub>3</sub>: 7.32, 6.98, possible overlap with solvent peak

<sup>31</sup>P{<sup>1</sup>H}NMR (162 MHz, Et<sub>2</sub>O, ppm) (**Figure S10**): δ 53.73, free PPh<sub>3</sub> -5.34

<sup>13</sup>C{<sup>1</sup>H} NMR (151 MHz, C<sub>6</sub>D<sub>6</sub>, ppm) (**Figure S9**): δ 490.11 (μ<sub>5</sub>-C), 214.04 (CO), 212.93 (CO), δ 133.54, 133.47 (d, J = 42 Hz); 131.27, 131.25 (d, J = 12 Hz); 130.13 (s); 128.89, 128.83 (d, J = 36 Hz)

IR (solid state, in  $\text{cm}^{-1}$ ) (**Figure S11**):  $\nu(\text{CO})$  2079 (m), 2005 (s), 1987 (s), 1959 (s)

Anal. Calc.: C, 41.91; H, 1.60; N 0.00

Anal. Exp.: C 42.42; H, 1.91; N, 0.14

### **$\text{NEt}_4[\text{Fe}_5(\mu_5\text{-C})(\mu_2\text{-H})(\text{CO})_{13}\text{PPh}_3]$ (**5**)**

During the workup described in the synthesis of **4**, the FPh extraction was collected and was passed through a silica gel column (2.5 cm  $\times$  8 cm), eluting a dark pink solution with FPh before yielding a reddish-black elution of **5** was collected from the silica in DCE. This solution was passed through a Celite filter, and vapor diffusion of  $\text{Et}_2\text{O}$  into FPh over several days at room temperature afforded dark-red plate crystals suitable for X-ray diffraction.

Yield: 34.3 mg, 0.0325 mmol (11%)

$^1\text{H}$  NMR (600 MHz,  $\text{CD}_3\text{CN}$ , ppm) (**Figure S12**): 7.42, 7.37 (aryl CH, 15H) 3.16, 3.15 ( $\text{Et}_4\text{N}$   $\text{CH}_2$ , 8H), 1.21 ( $\text{Et}_4\text{N}$   $\text{CH}_3$ , 12H),  $-11.71, -11.75$  (hydride,  $^2J_{\text{HP}} = 24$  Hz)

$^{13}\text{C}\{^1\text{H}\}$  NMR (151 MHz,  $\text{CD}_3\text{CN}$ , ppm) (**Figure S13**): interstitial carbide peak at  $\delta$  488.63 ppm, one singlet CO resonance at  $\delta$  -219.31 ppm,  $\text{PPh}_3$  aryl-C (doublets) at  $\delta$  136.14, 134.54, 131.17, 129.00;  $\text{NEt}_4$  at  $\delta$  53.00, 7.60

$^{31}\text{P}\{^1\text{H}\}$  NMR (162 MHz, FPh, ppm) (**Figure S14**):  $\delta$  62.17

NOESY (150.8 MHz,  $\text{CD}_3\text{CN}$ ) (**Figure S15**): coupling between peaks at 7.39 and  $-11.72$  ppm

Selected IR peaks in  $\text{cm}^{-1}$ , solid,  $\nu(\text{CO})$  (**Figure S16**): 2041 (m), 1988 (s), 1963 (s), 1947 (s), 1927 (s), 1898 (s), 1850 (s), 1817 (s), 1797 (s).

### *Reaction of 2 with bisphosphines dppe and dppp*

Reaction of **2** with dppe:

In a glovebox under  $\text{N}_2$  atmosphere, a 20 mL screw-top vial was charged with a violet solution of  $(\text{Et}_4\text{N})_2[\text{Fe}_6(\mu_6\text{-C})(\text{CO})_{16}]$  (302 mg, 0.286 mmol) in 15 mL of DCE. Solid  $[\text{Fc}]\text{PF}_6$  (209 mg, 0.631 mmol) was added, and the reaction mixture was stirred vigorously at room temperature for 1 h, affording a black solution (oxidation verified by FT-IR analysis). Dppe (229 mg, 0.575 mmol) was added, and the reaction was stirred for 24 h, turning dark brown. Volatiles were removed *in vacuo*, affording an oily black solid. During the course of the reaction workup for the dppe substitution reaction, 19 distinct fractions were collected by first extracting with solvents moving from non-polar to polar (namely pentane, toluene,  $\text{Et}_2\text{O}$ , FPh, DCE and MeCN) followed by performing silica gel columns on the extractions. This afforded three pentane column fractions, three toluene fractions, three  $\text{Et}_2\text{O}$  fractions, five FPh fractions, three DCE fractions and one MeCN fraction. Dropcast FT-IR spectra revealed that all exhibited features corresponding to carbonyls, and as such crystallizations were attempted. However, due to the multitude of fractions each crystallization was on a small scale and ultimately unsuccessful.

Reaction of **2** with dppp:

In a glovebox under N<sub>2</sub> atmosphere, a 20 mL screw-top vial was charged with a violet solution of (Et<sub>4</sub>N)<sub>2</sub>[Fe<sub>6</sub>(μ<sub>6</sub>-C)(CO)<sub>16</sub>] (300 mg, 0.284 mmol) in 15 mL of DCE. Solid [Fc]PF<sub>6</sub> (204 mg, 0.616 mmol) was added, and the reaction mixture was stirred vigorously at room temperature for 1 h, affording a black solution (oxidation verified by FT-IR analysis). Dppp (235 mg, 0.570 mmol) was added, and the reaction was stirred for 24 h, turning dark brown. Volatiles were removed *in vacuo*, affording an oily black-brown solid.

For the dppp substitution reaction 18 distinct fractions were collected after silica gel chromatography, all demonstrating carbonyl stretches in the FT-IR spectra, yet these also eluded structural characterization. As such, we hypothesize that since there was no major product fraction, rather an apparent abundance of carbonyl-containing products, cluster fragmentation occurred transforming the iron-carbonyl carbide cluster into smaller, iron-carbonyl-phosphine complexes.

### [Fe<sub>3</sub>(μ<sub>3</sub>-CH)(μ<sub>3</sub>-CO)(CO)<sub>9</sub>][(bdpb)<sub>2</sub>Fe(MeCN)<sub>2</sub>] (**6**)

In a glovebox under N<sub>2</sub> atmosphere, a 20 mL screw-top vial was charged with a violet solution of (Et<sub>4</sub>N)<sub>2</sub>[Fe<sub>6</sub>(μ<sub>6</sub>-C)(CO)<sub>16</sub>] (**1**: 261 mg, 0.247 mmol) in 10 mL of MeCN. Then, two equiv of solid [Fc]PF<sub>6</sub> (186 mg, 0.562 mmol) were added, and the reaction mixture was stirred vigorously at room temperature for ~10 min, affording a red-black solution (oxidation verified by FT-IR analysis). Next, two equiv of bdpb (225 mg, 0.504 mmol) were added, and the reaction was stirred overnight, turning reddish-brown. Volatiles were removed *in vacuo*, affording oily black solids. The solid was washed with pentane until colorless (8×10 mL) to remove ferrocene and unreacted phosphine; no ν(CO) features were present in IR analysis of the pentane extraction. Extraction of the remaining dark residue with Et<sub>2</sub>O afforded a pale reddish-pink solution, which upon slow evaporation provided red crystalline shards of **6** (first crop). Further extraction of the remaining crude solid with FPh affords a more concentrated, deep red solution of **6**. Filtration through Celite followed by vapor diffusion of pentane into Et<sub>2</sub>O over 24 h provided dark, red plate crystals of **6**.

Yield: 17.4 mg (4.81%).

<sup>1</sup>H NMR (600 MHz, CD<sub>3</sub>CN, ppm) (**Figure S18**): δ 12.36 (Fe<sub>3</sub>-CH, s), 7.67 (m), 7.54 (m), 7.47 (m), 7.42 (m), 7.32 (m), 7.16 (m), 7.10 (t), 6.69 (d), 6.38 (d), 1.96, (MeCN)

<sup>13</sup>C {<sup>1</sup>H} NMR (151 MHz, CD<sub>3</sub>CN, ppm) (**Figure S19**): δ 223.24, 221.25 (CO), δ 145.58, 137.40, 135.85, 134.65, 133.06, 131.08, 129.38, 129.13 (aryl-C)

<sup>31</sup>P{<sup>1</sup>H}NMR (243 MHz, CD<sub>3</sub>CN, ppm) (**Figure S17**): δ 98.35; contamination from some other minor decay products at 69.93, 66.09, 65.56. Possible free ligand at δ -7.91.

Selected IR peaks, solid, in cm<sup>-1</sup>, ν(CO) (**Figure S20**): 2051 (w), 1977 (s), 1949 (s), 1901 (s), 1725 (m).

Anal. Calc.: C, 60.40; H, 3.72; N 1.88

Anal. Exp.: C, 65.60; H, 4.55; N, 0.64

### [Fe<sub>3</sub>{μ<sub>3</sub>-C-P(Ph)<sub>2</sub>C<sub>2</sub>H<sub>4</sub>(PhP)C<sub>2</sub>H<sub>4</sub>(PPh<sub>2</sub>)}(CO)<sub>8</sub>] (**7**)

In a glovebox under N<sub>2</sub> atmosphere, a 20 mL screw-top vial was charged with a violet solution of (Et<sub>4</sub>N)<sub>2</sub>[Fe<sub>6</sub>(μ<sub>6</sub>-C)(CO)<sub>16</sub>] (257 mg, 0.243 mmol) in approximately 20 mL of MeCN. Solid [Fc]PF<sub>6</sub> (175 mg, 0.529 mmol) was added, and the reaction mixture was stirred vigorously at room temperature for approximately 10 minutes, and oxidation was verified by dropcast FT-IR of the reaction mixture. The linear Triphos ligand (150 mg, 0.281 mmol) was added, and the reaction was stirred for 2.5 h, turning reddish-brown. Solvent was removed *in vacuo*, with MeCN thoroughly removed by repeatedly triturating the semi-dried reaction mixture in Et<sub>2</sub>O and then removing solvent until black powder remained. The solid was washed with pentane (2×15 mL) to remove ferrocene and unreacted phosphine. No ν(CO) features were found by IR analysis of the pentane extraction. The crude solids were then washed Et<sub>2</sub>O, affording a pale brown solution. Extraction with toluene afforded a deep coffee-brown solution, which was filtered over Celite. Vapor diffusion of pentane into the toluene extraction at –20 °C over multiple weeks afforded brown needle crystals of **7** in brown oils, which provided atom connectivity via X-ray diffraction. Separation of the oils from the crystals proved intractable and product purification was not feasible.

<sup>31</sup>P{<sup>1</sup>H} NMR (243 MHz, *d*<sup>6</sup>-benzene, ppm) (**Figure S21**): δ 123.57 (s, 1P), 90.78 (s, 2P)

Selected IR peaks, solid, ν(CO) in cm<sup>-1</sup>(**Figure S22**): 2061 (w), 1963 (s), 1881 (s).

#### [Fe<sub>5</sub>(μ<sub>5</sub>-C)(κ<sub>1</sub>-Triphos)(CO)<sub>14</sub>] (**8**)

In a glovebox under N<sub>2</sub> atmosphere, a 20 mL screw-cap vial was charged with a violet- solution of (Et<sub>4</sub>N)<sub>2</sub>[Fe<sub>6</sub>(μ<sub>6</sub>-C)(CO)<sub>16</sub>] (258 mg, 0.244 mmol) in approximately 10 mL of DCE. Solid [Fc]PF<sub>6</sub> (183 mg, 0.553 mmol) was added, and the reaction mixture was stirred vigorously at room temperature for fifteen minutes, affording a dark brown solution. The tripodal Triphos ligand (300 mg, 0.480 mmol) was added, and the reaction was stirred for 0.5 h, now dark brown. Volatiles were removed *in vacuo* to afford a black powder. The solid was washed with pentane (3×10 mL), and the orange-tinged black pentane extraction was collected. The pentane extraction was passed through a silica gel column (2.5 cm × 8 cm) and flushed with pentane to remove ferrocene (bright yellow) and unreacted phosphine; then a greenish-black elution of **8** was collected from the silica in Et<sub>2</sub>O. After filtration through Celite, the Et<sub>2</sub>O solution of **8** was concentrated and set at –20 °C overnight, affording grey-green, diffraction quality needles of **8**.

Yield: a range from 3 to 7 %

<sup>1</sup>H NMR (600 MHz, C<sub>6</sub>D<sub>6</sub> in ppm) (**Figure S23**): 7.49 (s), 7.04 (s), 7.02, 7.01 (d), 2.71 (s, CH<sub>2</sub>), 1.16 (s, CH<sub>3</sub>)

<sup>13</sup>C{<sup>1</sup>H} NMR (151 MHz, *d*<sup>6</sup>-benzene, ppm) (**Figure S24**): interstitial carbide peak at δ 489.33, CO resonances at δ 214.33, 213.20, δ 140.81, 140.73, 133.79, 133.66, 128.89, 128.72 (aryl-C), δ 43.88 (CH<sub>2</sub>), 39.63 (CH<sub>3</sub>)

<sup>31</sup>P{<sup>1</sup>H} NMR (243 MHz, *d*<sup>6</sup>-benzene, ppm) (**Figure S25**): Bound Fe–P region: 48.50, 44.87, 41.57, 25.12; Free PR<sub>3</sub> region: –24.71, –25.64 (max peak, reported shift for free Triphos: –26 ppm), –25.98, –27.11 δ

Selected IR peaks, solid, ν(CO) in cm<sup>-1</sup>(**Figure S26**): 2078 (m), 2011 (s), 1995 (s), 1966 (s), 1949 (s), 1932 (s).

### [Fe<sub>4</sub>(μ<sub>4</sub>-C)(κ<sub>3</sub>-Triphos)(CO)<sub>10</sub>] (**9**) from MeCN reaction of **2** with Triphos

In a glovebox under N<sub>2</sub> atmosphere, a 50 mL flask was charged with a violet solution of (Et<sub>4</sub>N)<sub>2</sub>[Fe<sub>6</sub>(μ<sub>6</sub>-C)(CO)<sub>16</sub>] (**1**: 270 mg, 0.256 mmol) in approximately 20 mL of MeCN. Next, two equiv of solid [Fc]PF<sub>6</sub> (186 mg, 0.563 mmol) were added, and the reaction mixture was stirred vigorously at room temperature for ~10 min, affording a reddish-black solution. Two equiv of Triphos (335 mg, 0.536 mmol) were then added, and the reaction was stirred for 30 min, turning reddish-brown. The solvent was removed *in vacuo*, and the residual MeCN was thoroughly removed by triturating the residue with Et<sub>2</sub>O until a dry, black powder remained. The solid was extracted with pentane (4×20 mL) to afford a dark yellow solution containing ferrocene, unreacted Triphos and trace amounts of the desired product. The remaining black powder was extracted with Et<sub>2</sub>O (5×10 mL), generating a reddish-black solution that was concentrated to ~5 mL and loaded onto a silica gel column (2.5 cm × 8 cm). Further elution with Et<sub>2</sub>O provided a greenish-black fractions (a bright red material remained on the column). To guarantee reliable crystallization, the green-black fractions were re-concentrated to ~5 mL and re-purified over silica (more red impurities, including **10**, remained on the column). The final Et<sub>2</sub>O fractions were combined and filtered through Celite. Slow evaporation for 12 h at room temperature provided diffraction quality black prisms of **9**.

Yield: range 5 to 15%

<sup>1</sup>H NMR (600 MHz, C<sub>6</sub>D<sub>6</sub> in ppm) (**Figure S27**): 7.48 (s), 7.16 (s), 7.05 (s), 2.70 (s, CH<sub>2</sub>), 1.15 (s, CH<sub>3</sub>)

<sup>13</sup>C{<sup>1</sup>H} NMR (151 MHz, *d*<sup>6</sup>-benzene, ppm) (**Figure S28**): interstitial carbide peak at δ 485.34 ppm, CO resonances at δ 220.45, 216.23 (broad), 215.16; δ 140.81, 139.37, 133.79, 130.92, 128.38 (aryl-C), δ 43.82 (CH<sub>2</sub>), 39.53 (CH<sub>3</sub>)

<sup>31</sup>P{<sup>1</sup>H} NMR (243 MHz, *d*<sup>6</sup>-benzene, ppm) (**Figure S29**): Bound Fe-P region: δ 41.58 (broad, weak 1P); Free PR<sub>3</sub> region: -25.67 (2P, Reported shift for free Triphos: -26 ppm)

Selected IR peaks, solid, ν(CO) in cm<sup>-1</sup>(**Figure S30**): 2059 (m), 2045 (m), 2002 (s), 1971 (s), 1944 (s), 1918 (s), 1884 (s), 1799 (m).

Anal. Calc.: C, 54.78; H, 3.45; N, 0.00

Anal. Exp.: C, 56.38; H, 4.12; N, 0.34

### **9** from DCE reaction of Triphos with **2**

In a glovebox under N<sub>2</sub> atmosphere, a 20 mL screw-cap vial was charged with a violet solution of (Et<sub>4</sub>N)<sub>2</sub>[Fe<sub>6</sub>(μ<sub>6</sub>-C)(CO)<sub>16</sub>] (258 mg, 0.244 mmol) in 10 mL of DCE. Solid [Fc]PF<sub>6</sub> (183 mg, 0.553 mmol) was added, and the reaction mixture was stirred vigorously at room temperature for 15 min, affording a dark brown solution. Triphos (300 mg, 0.480 mmol) was added, and the reaction was stirred for 0.5 h, now dark brown. Volatiles were removed *in vacuo* to black powders. The solid was washed with pentane (3×10 mL), and the orange-tinged black pentane extraction was collected. Unexpectedly, no detectable compound **9** was found in the pentane extraction, unlike the MeCN reaction (*vide supra*). The crude reaction solid was then extracted with Et<sub>2</sub>O (5×10 mL), affording a reddish-brown black extraction that was passed through a silica gel column (2.5 cm × 8 cm) to collect more

of **9** as a greenish black elution, and leaving bright red color on the column. The Et<sub>2</sub>O solution of **9** was then filtered through Celite, and characterized by FT-IR.

#### *Formation of 9 from reaction of MeCN with crystals of 8*

In an N<sub>2</sub>-atmosphere glovebox, dried crystalline solid of **8** (~5-7 mg) was dissolved in ~2.5 mL of Et<sub>2</sub>O in a 20 mL vial, affording a pale greenish-beige solution. A dropcast FT-IR spectrum of this solution was acquired. Next, ~1 mL of MeCN was added to the reaction mixture while stirring vigorously at room temperature, immediately turning the solution a pale red. After ~3 min, the reaction mixture was distinctly red-brown, at which point another dropcast FT-IR spectrum was acquired, indicating complete disappearance of the characteristic ~2075 cm<sup>-1</sup> ν(CO) feature of **8** and an overall red-shift of all ν(CO) features (**Figure S28**). Volatiles were removed *in vacuo* and the crude solids were purified by pentane washes (removing trace **8** and free Triphos, evidenced by FT-IR) and then extraction into Et<sub>2</sub>O (**9**, **10** and other red impurities). The pale greenish brown Et<sub>2</sub>O extraction was purified over silica, and the greenish (first) fraction was filtered through Celite. Slow evaporation of Et<sub>2</sub>O afforded small black prisms of **9** suitable to establish the connectivity by X-ray diffraction.

#### **[(CO)<sub>9</sub>Fe<sub>3</sub>(μ<sub>3</sub>-CCO<sub>2</sub>-κ<sub>2</sub>)Fe(CO)(κ<sub>3</sub>-Triphos)] (10)**

During the workup described in the synthesis of **8** and **7**, cluster **10** is the second band encountered during silica chromatography of the Et<sub>2</sub>O extraction after removal of **9**. A bright red band is eluted from the column with THF, affording a ruby red solution. Volatiles were removed *in vacuo* and the red solid was extracted into toluene and filtered over Celite. The toluene solution was layered with pentane by vapor diffusion at room temperature, affording large red prisms of **10** suitable for X-ray diffraction.

<sup>1</sup>H NMR (500 MHz, CDCl<sub>3</sub>, ppm) (**Figure S31**): δ 7.67 (s), 7.45 (s), 7.34 (s), 7.18, 7.13 (d), 7.05, 6.98 (d), 6.78 (s), (aryl-C from free and bound triphos) 3.78 (s, CH<sub>2</sub>), 1.87 (s, CH<sub>3</sub>)

<sup>13</sup>C{<sup>1</sup>H} NMR (151 MHz, CDCl<sub>3</sub>, ppm) (**Figure S32**): δ 221.53, 219.89, 216.30, 212.13, (CO); 163.76, 162.13 (μ<sub>3</sub>-CCO<sub>2</sub>; μ<sub>3</sub>-CO); 133.14, 132.36, 131.68, 131.54, 130.65, 130.28, 129.84, 129.79, 129.64, 129.54, 128.96, 128.83, 128.51, (aryl-C); 39.84 (CH<sub>2</sub>), 38.92 (CH<sub>3</sub>)

<sup>31</sup>P{<sup>1</sup>H} NMR (162 MHz, CDCl<sub>3</sub>, ppm) (**Figure S33**): δ 46.47, 46.23 (d), 35.26, 35.02, 34.78 (t)

Selected IR peaks, dropcast solid from THF solution, ν(CO) in cm<sup>-1</sup> (**Figure S34**): 2059 (w), 2000 (s), 1973 (s).

Anal. Calc. without MeCN: C, 53.51; H, 3.24; N, 0.00

% occupancy MeCN from XRD: 42.2

Anal. Exp.: C, 54.29; H, 4.46; N, 0.26

#### **[Fe<sub>3</sub>(μ<sub>3</sub>-CPh){Triphos(PPh)<sub>2</sub>(PPh)}(μ<sub>2</sub>-CO)<sub>2</sub>(CO)<sub>5</sub>] (11)**

In an N<sub>2</sub>-atmosphere glovebox, silica-purified **9** was dissolved in toluene affording a dark brown solution. Attempts to crystallize **9** at -20 °C over several months by slow evaporation instead afforded dichromic

(yellow/brown), diffraction quality prisms of **11** in a brown supernatant, as well as some white solids — likely Triphos and FeTriphos(CO)<sub>2</sub>.

Selected IR peaks, solid,  $\nu(\text{CO})$  in  $\text{cm}^{-1}$  (**Figure S35**): 2048 (s), 2000 (s), 1963 (s), 1936 (m), 1918 (s), 1854 (s).

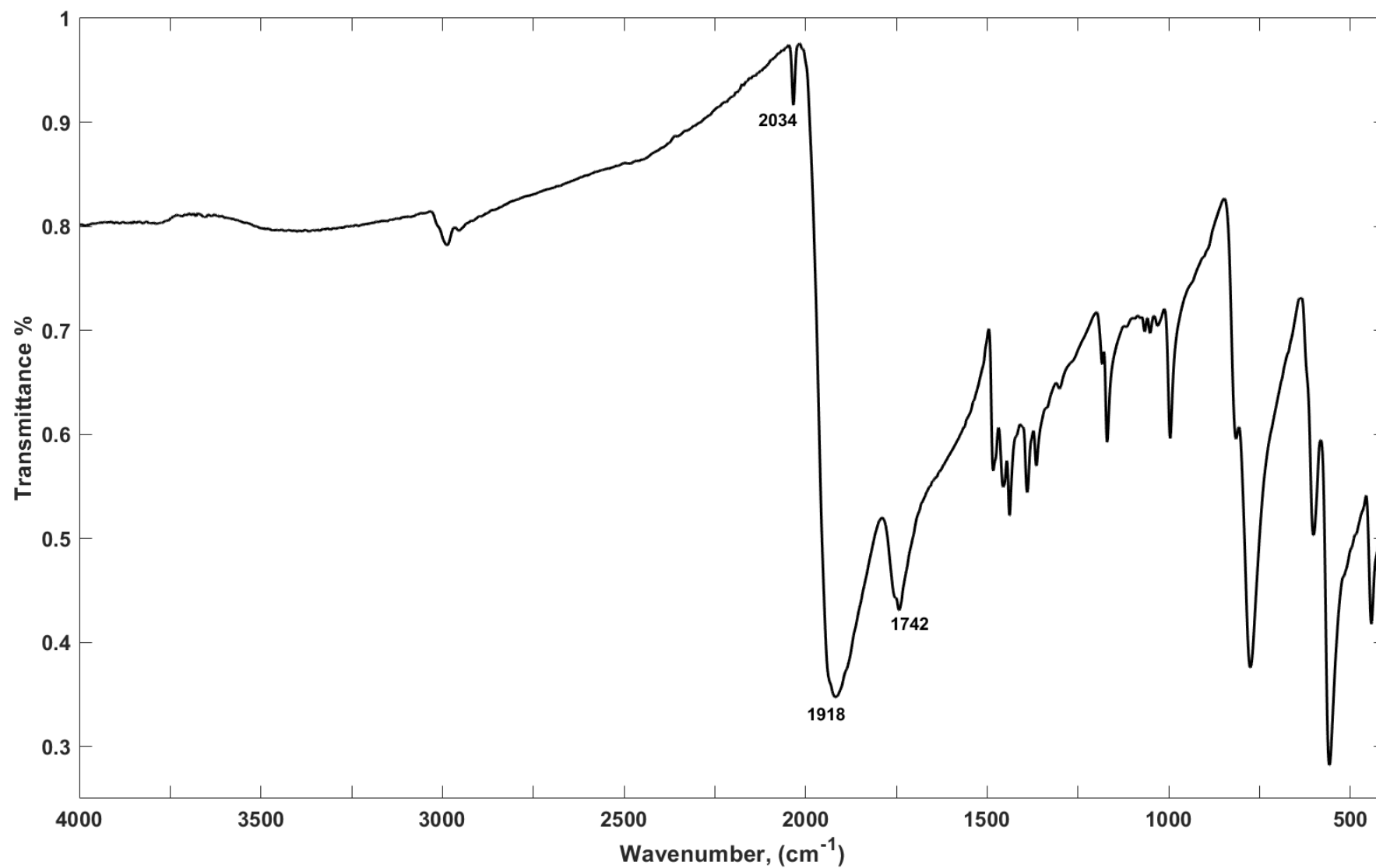


**Figure S1.** IR spectrum of [NEt<sub>4</sub>]<sub>2</sub>[Fe<sub>6</sub>(μ<sub>6</sub>-C)(CO)<sub>16</sub>] (**1**) in the solid state.

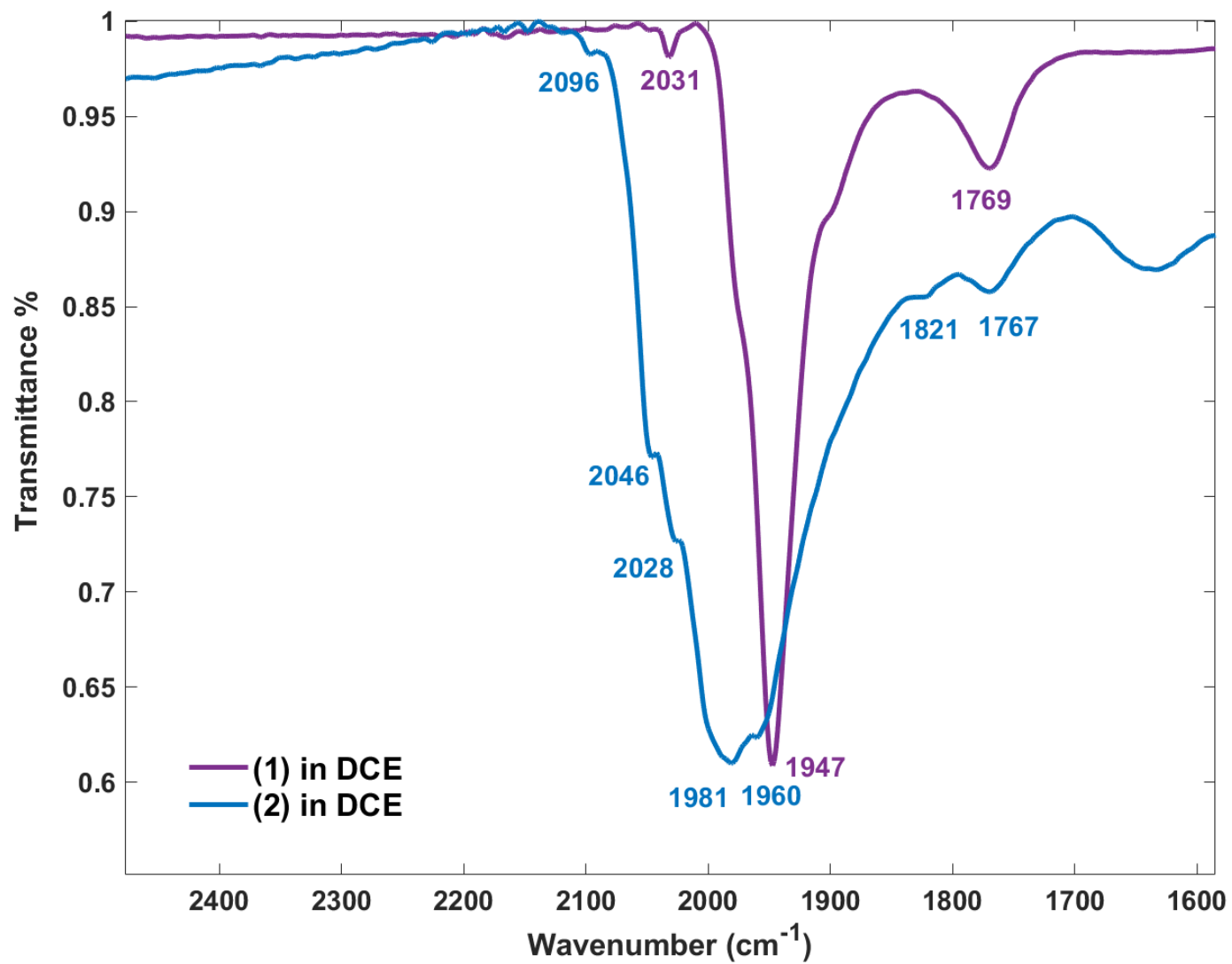


**Figure S2.** IR spectrum showing the  $\nu(\text{CO})$  region for **1** (purple trace) and the *in situ* oxidized compound  $[\text{Fe}_6(\mu_6\text{-C})(\text{CO})_{16}]$  (**2**) formed by the reaction of **1** and 2 equiv  $[\text{Fc}]\text{PF}_6$  (blue trace); all as dropcast samples from DCE.

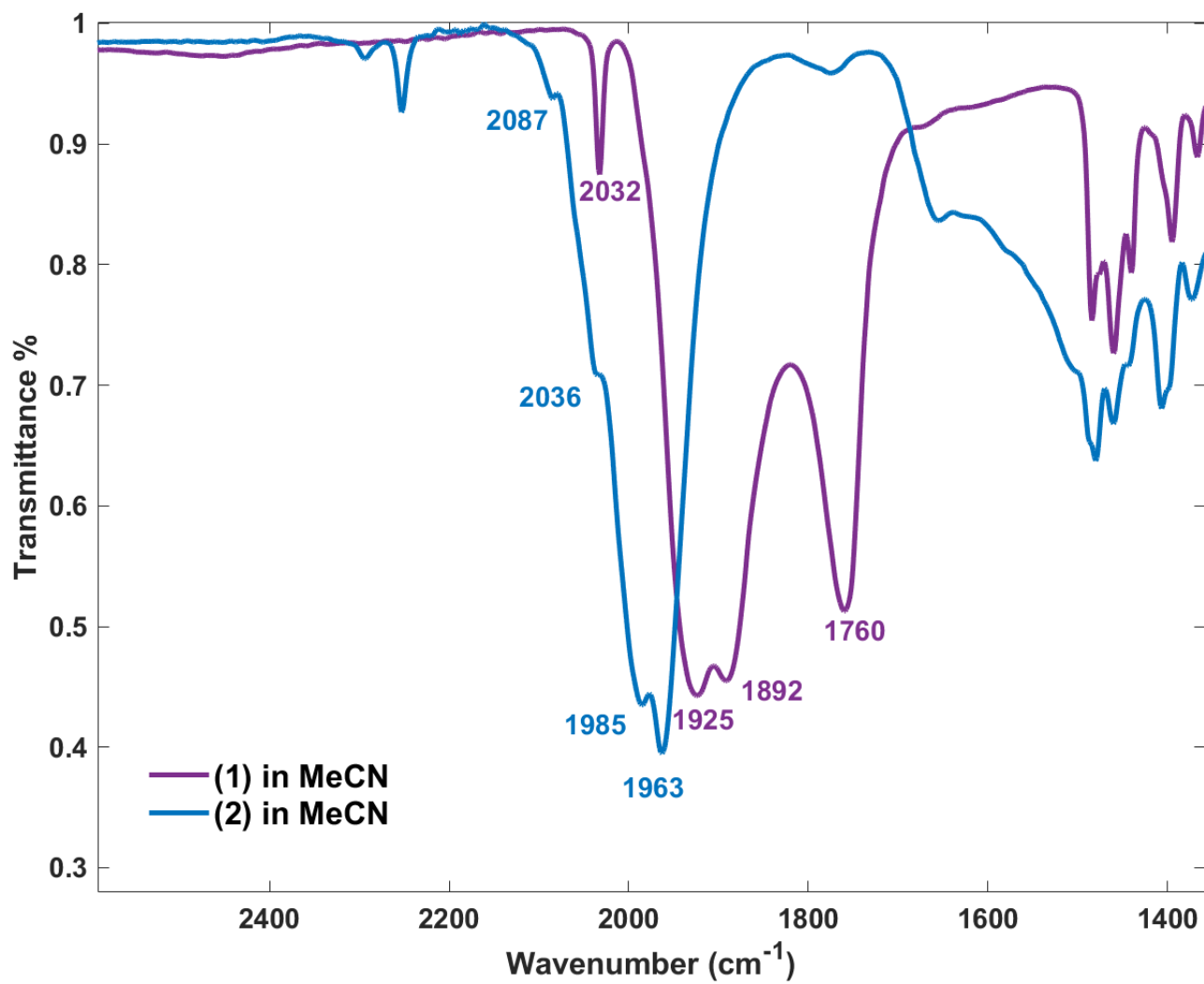


**Figure S3.** IR spectrum showing the  $\nu(\text{CO})$  region for **1** (purple trace) and **2** formed by the reaction of **1** and 2 equiv of  $[\text{Fc}]\text{PF}_6$  (blue trace); all as dropcast samples from MeCN.

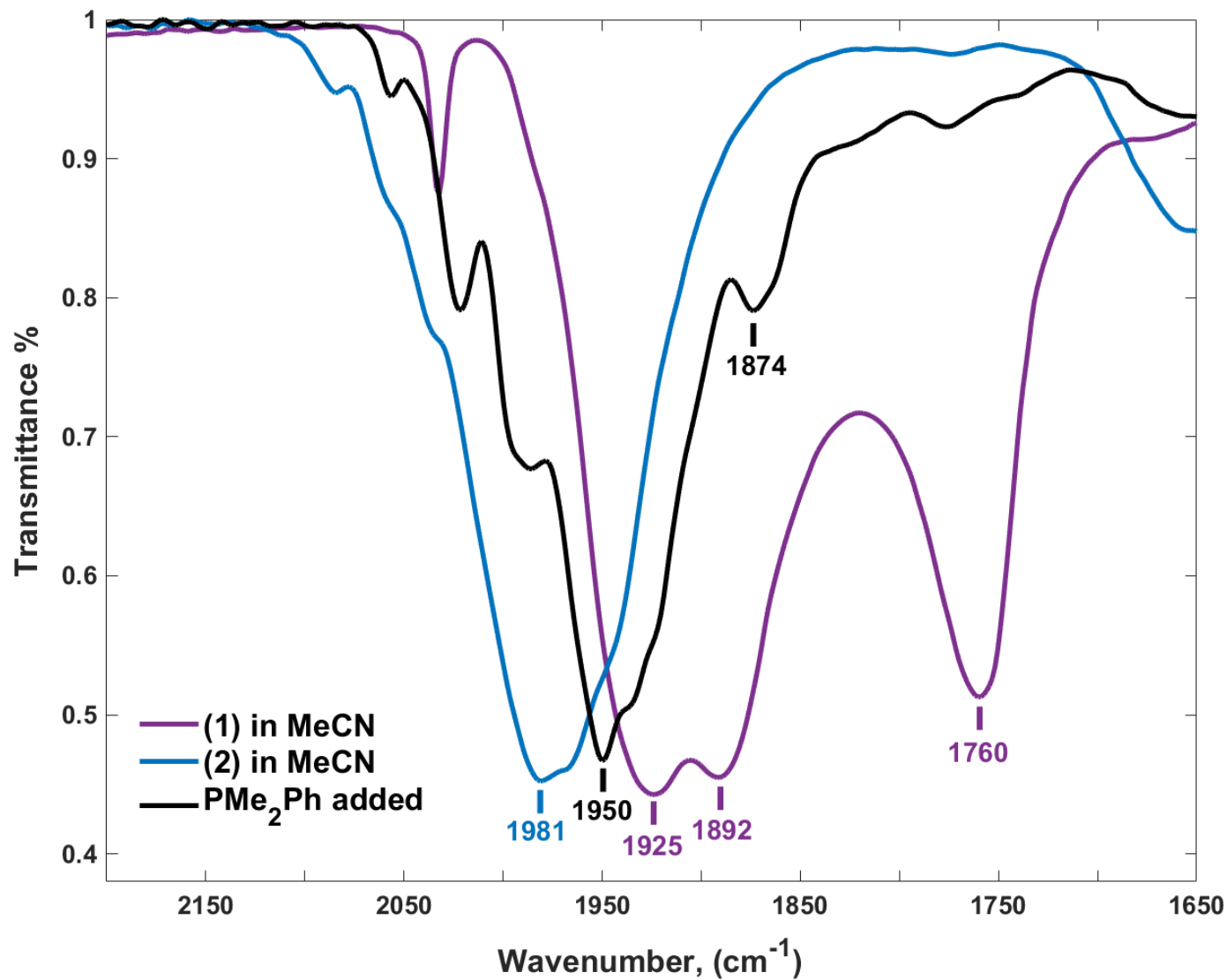


**Figure S4.** IR spectrum of **1** dropcast from MeCN (*purple trace*),  $\nu(\text{CO})$  features: 2032(w), 1925(s), 1892(s), 1760(s)  $\text{cm}^{-1}$ ; the reaction mixture of the oxidation of **1** with 2 equiv of  $[\text{Fc}]\text{PF}_6$  to form **2** in MeCN (*blue trace*),  $\nu(\text{CO})$  features: 2086(w), 2056(w sh), 2035(w sh), 1981(s)  $\text{cm}^{-1}$ ; and the reaction of **2** with  $\text{PMe}_2\text{Ph}$  in MeCN (*black trace*),  $\nu(\text{CO})$  features: 2055(w), 2022(m), 1988(m), 1950(s), 1874(m)  $\text{cm}^{-1}$ .

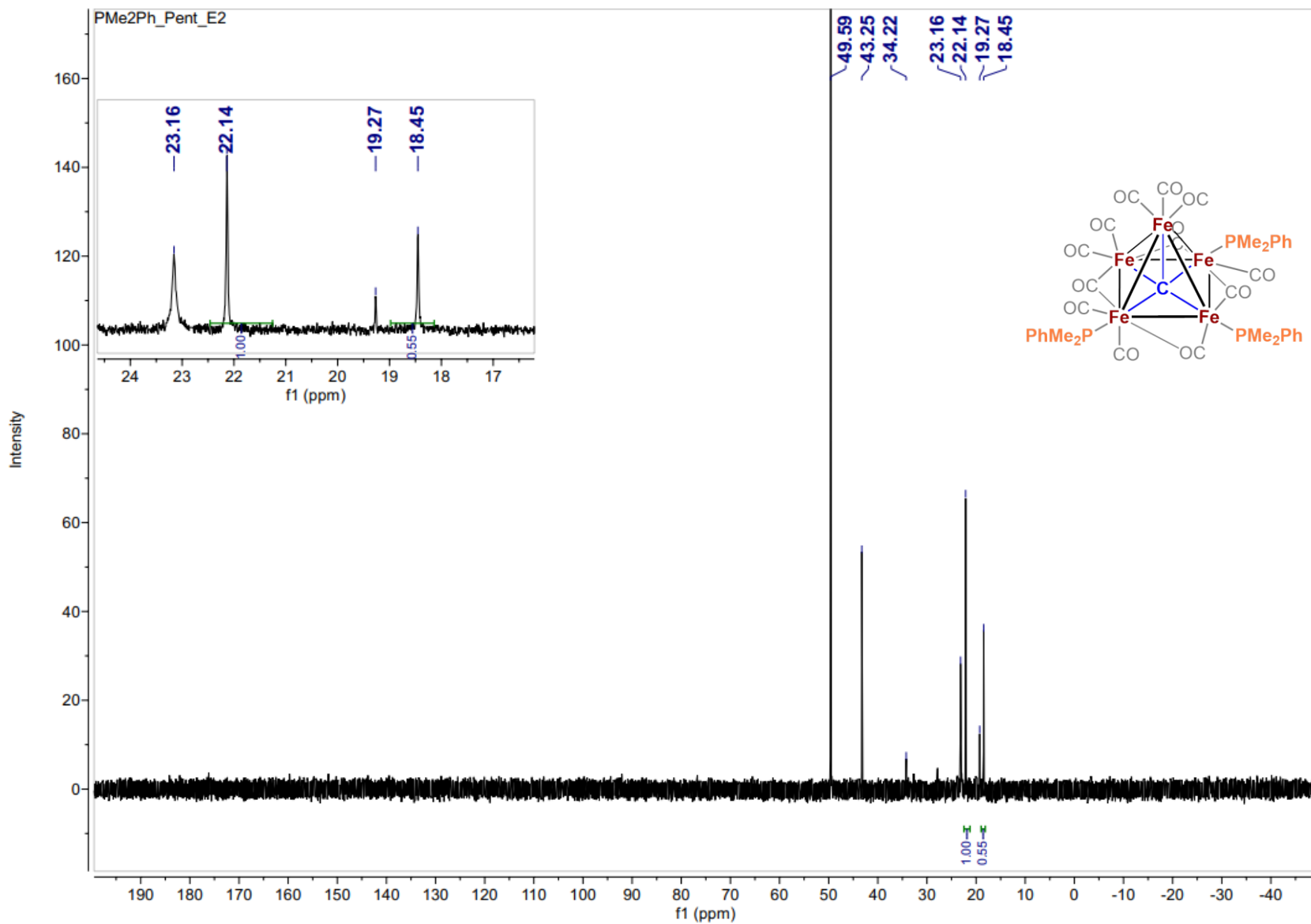


**Figure S5.**  $^{31}\text{P}$  NMR spectrum of the pentane extraction of the reaction of **2** with dmpp (acquired in pentane) with resonances for the bound phosphines in  $[\text{Fe}_5(\mu_5\text{-C})(\text{CO})_{12}(\text{PMe}_2\text{Ph})_3]$  at 22.14 and 18.45 ppm in relative intensities 2:1, for the 'down' and 'up' phosphine orientations.<sup>3</sup>

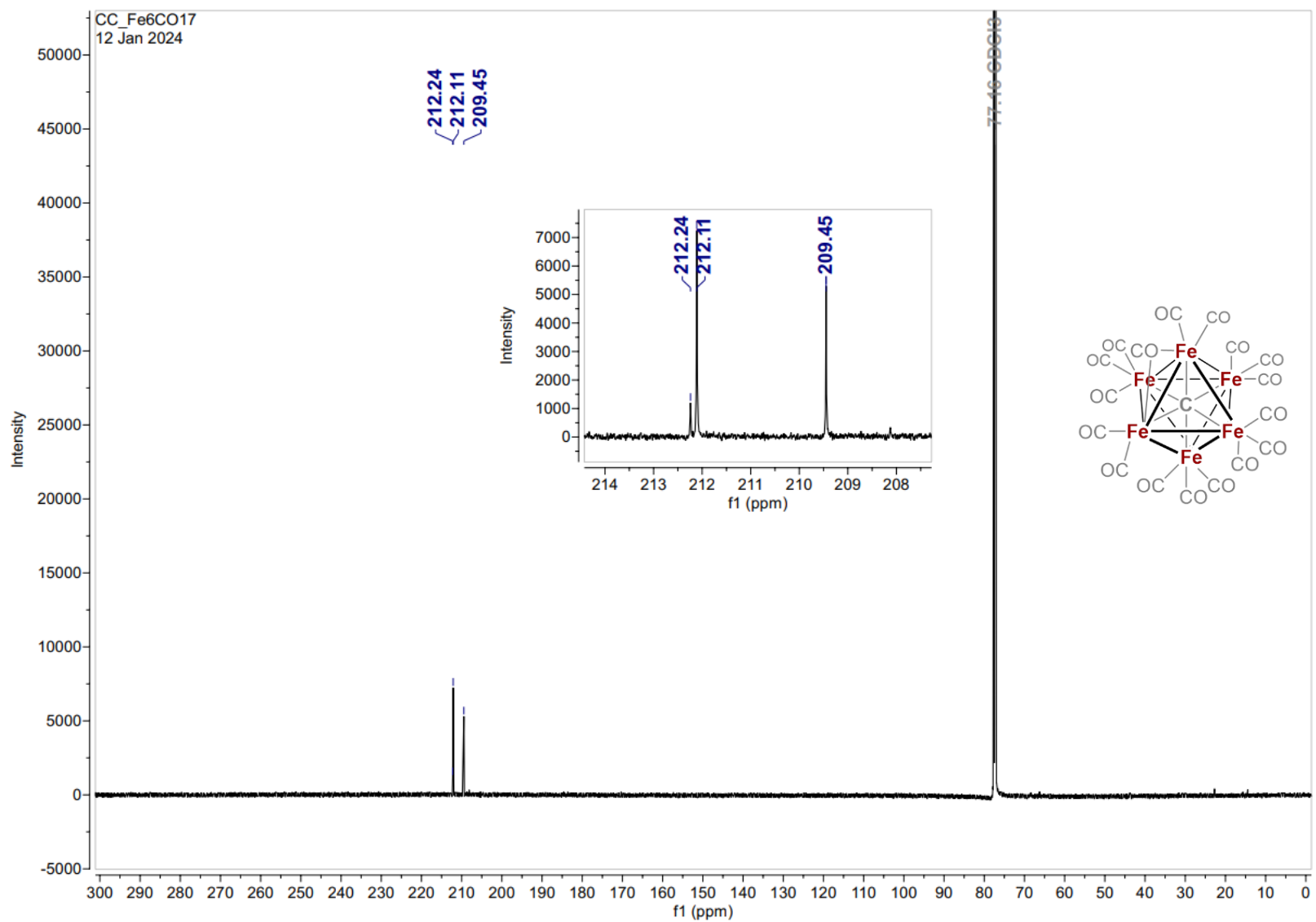


**Figure S6.**  $^{13}\text{C}$  NMR spectrum of  $[\text{Fe}_6(\mu_6\text{-C})(\mu_2\text{-CO})(\text{CO})_{16}]$  (3) in  $\text{CDCl}_3$  at  $25^\circ\text{C}$ .

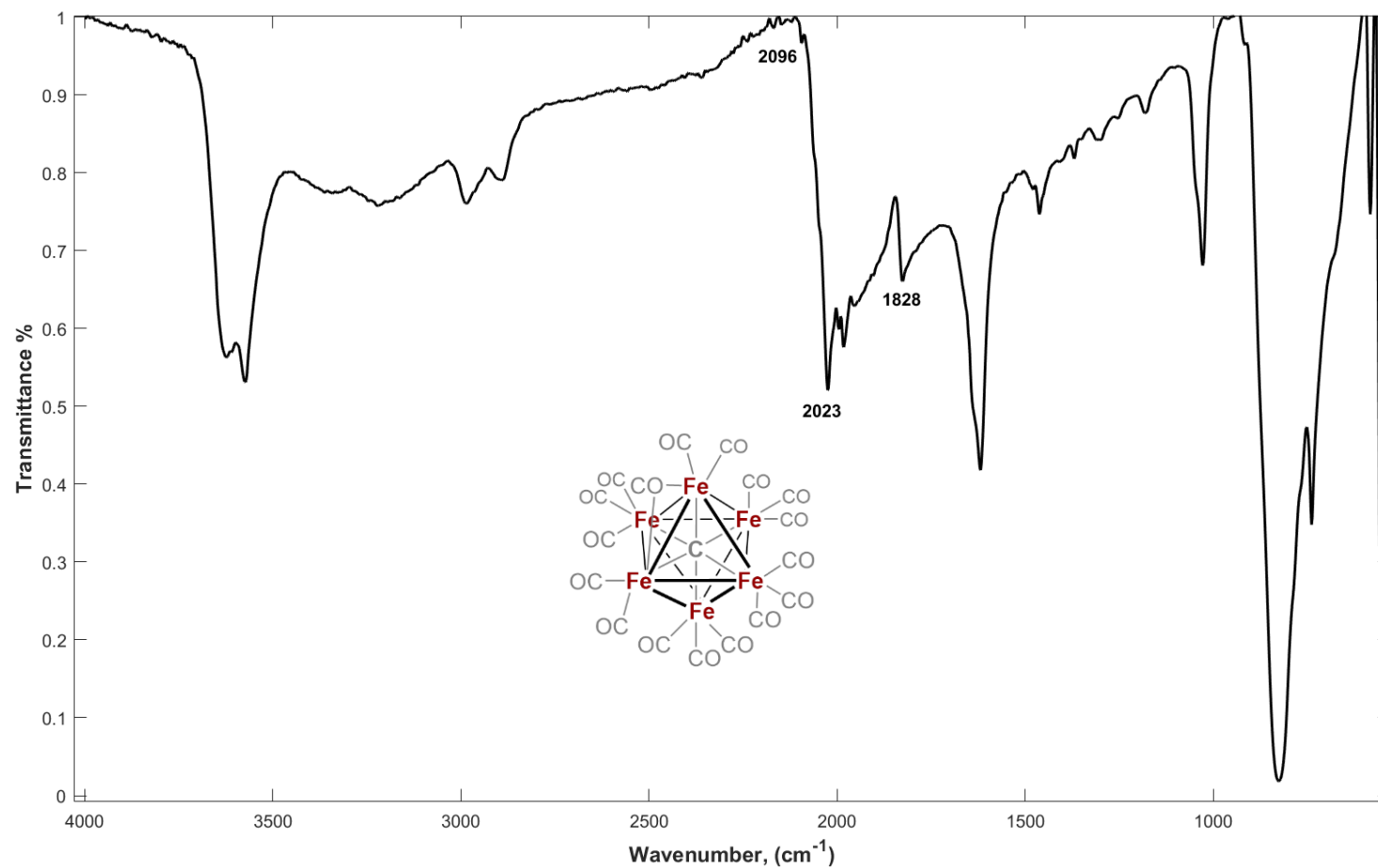


**Figure S7.** IR spectrum of  $[\text{Fe}_6(\mu_6\text{-C})(\mu_2\text{-CO})(\text{CO})_{16}]$  (**3**) in the solid state. Some contamination from paraffin oil (from crystal handling) is present but does not obscure the  $\nu(\text{CO})$  region.

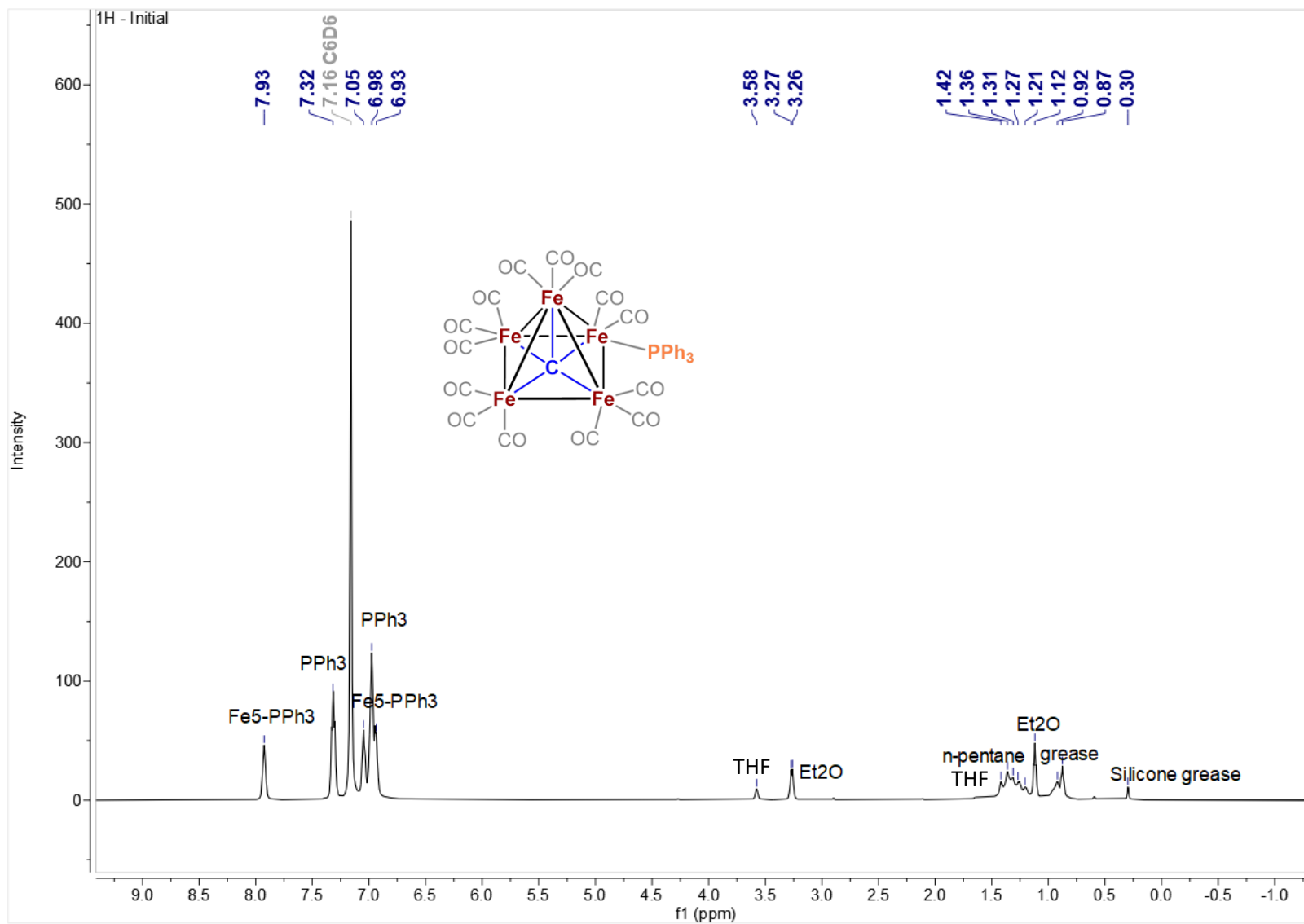


**Figure S8.**  $^1\text{H}$  NMR spectrum of  $[\text{Fe}_5(\mu_5\text{-C})(\text{CO})_{14}\text{PPh}_3]$  (**4**) in  $\text{C}_6\text{D}_6$  at  $25^\circ\text{C}$ .

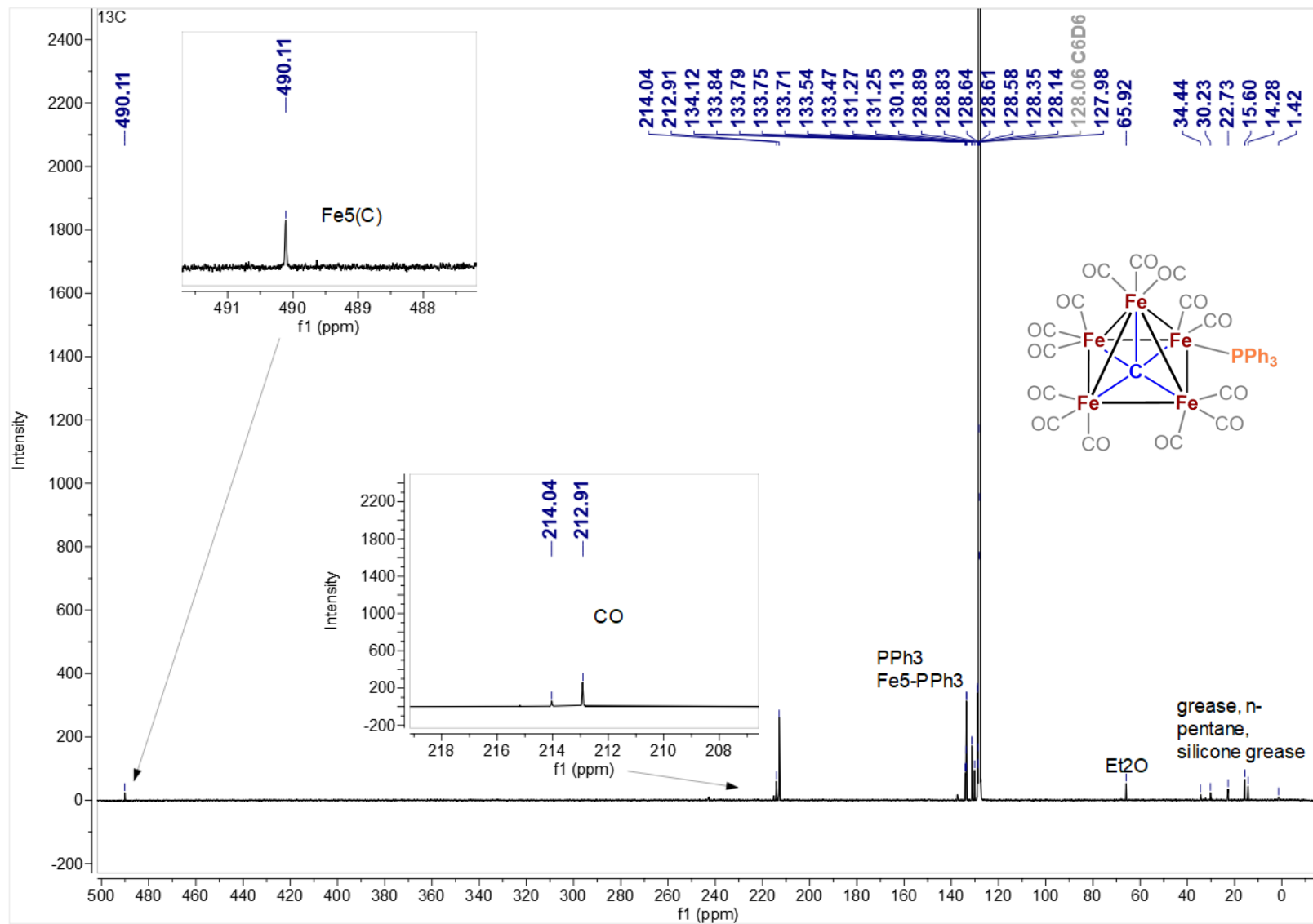


**Figure S9.**  $^{13}\text{C}$  NMR spectrum of  $[\text{Fe}_5(\mu_5\text{-C})(\text{CO})_{14}\text{PPh}_3]$  (**4**) in  $\text{C}_6\text{D}_6$  at  $25^\circ\text{C}$ , with carbide region and CO regions highlighted.

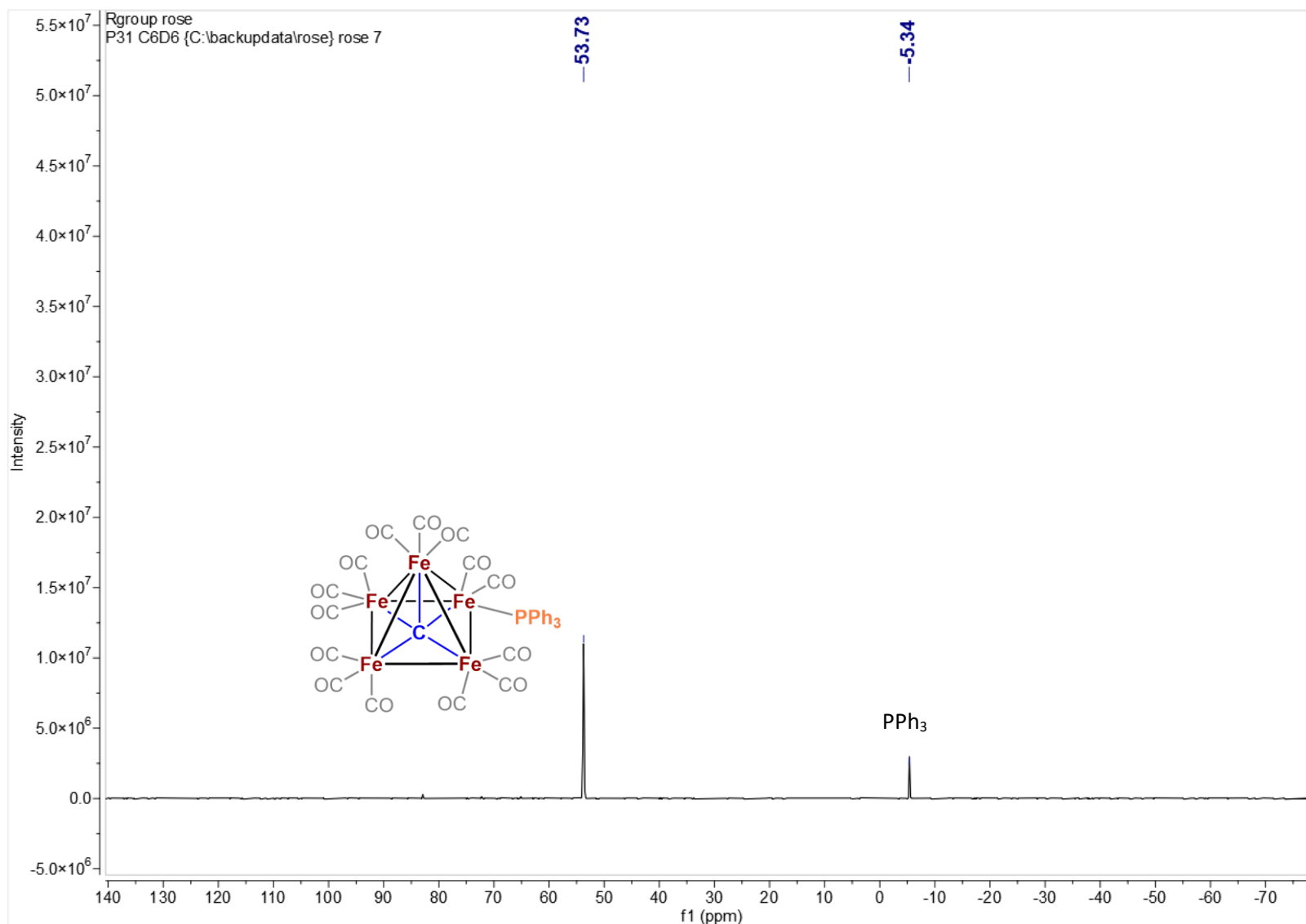


**Figure S10.** <sup>31</sup>P NMR spectrum of [Fe<sub>5</sub>(μ<sub>5</sub>-C)(CO)<sub>14</sub>PPh<sub>3</sub>] (**4**) in C<sub>6</sub>D<sub>6</sub> at 25 °C.

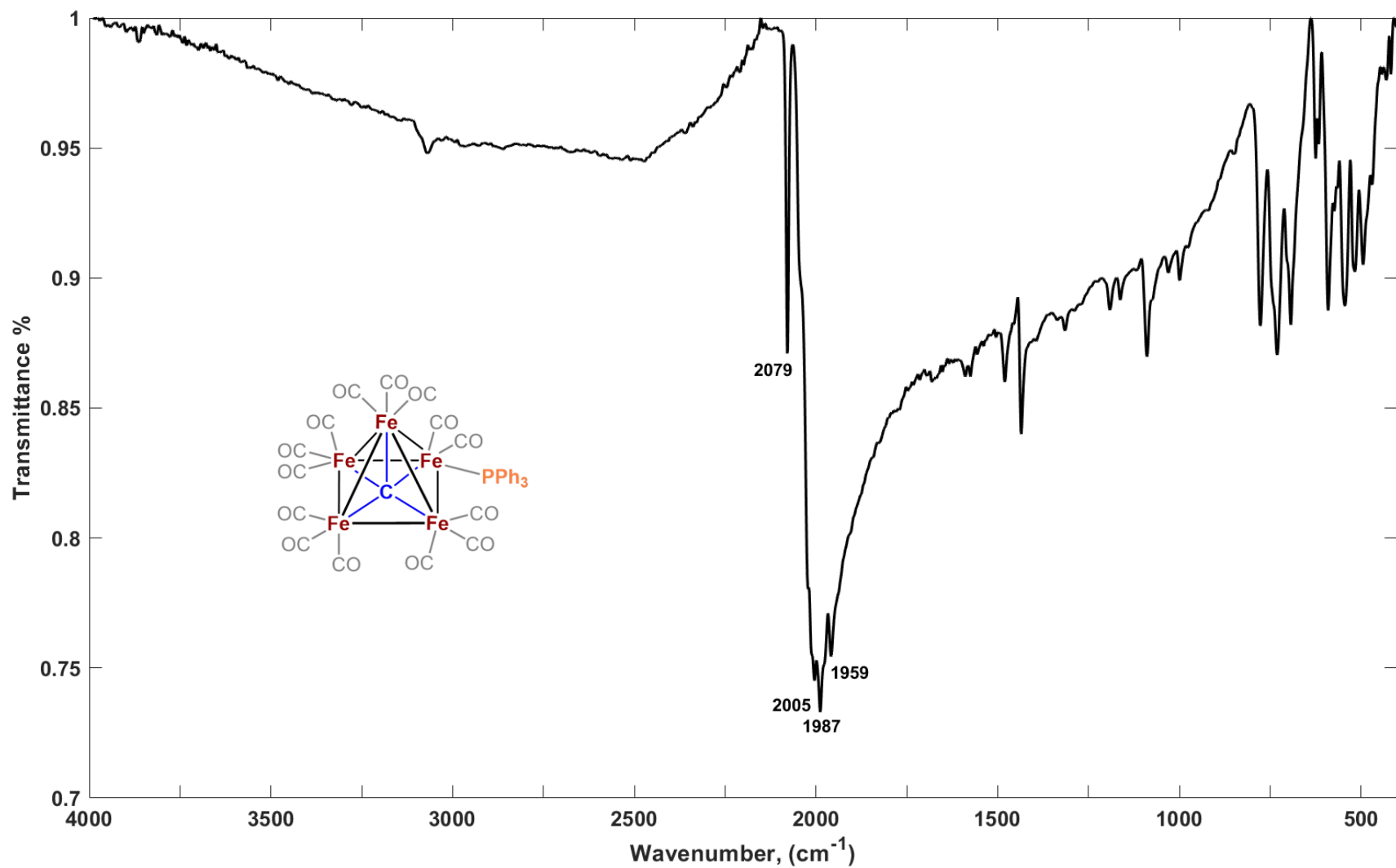


**Figure S11.** IR spectrum of  $[\text{Fe}_5(\mu_5\text{-C})(\text{CO})_{14}\text{PPh}_3]$  (**4**) in the solid state.

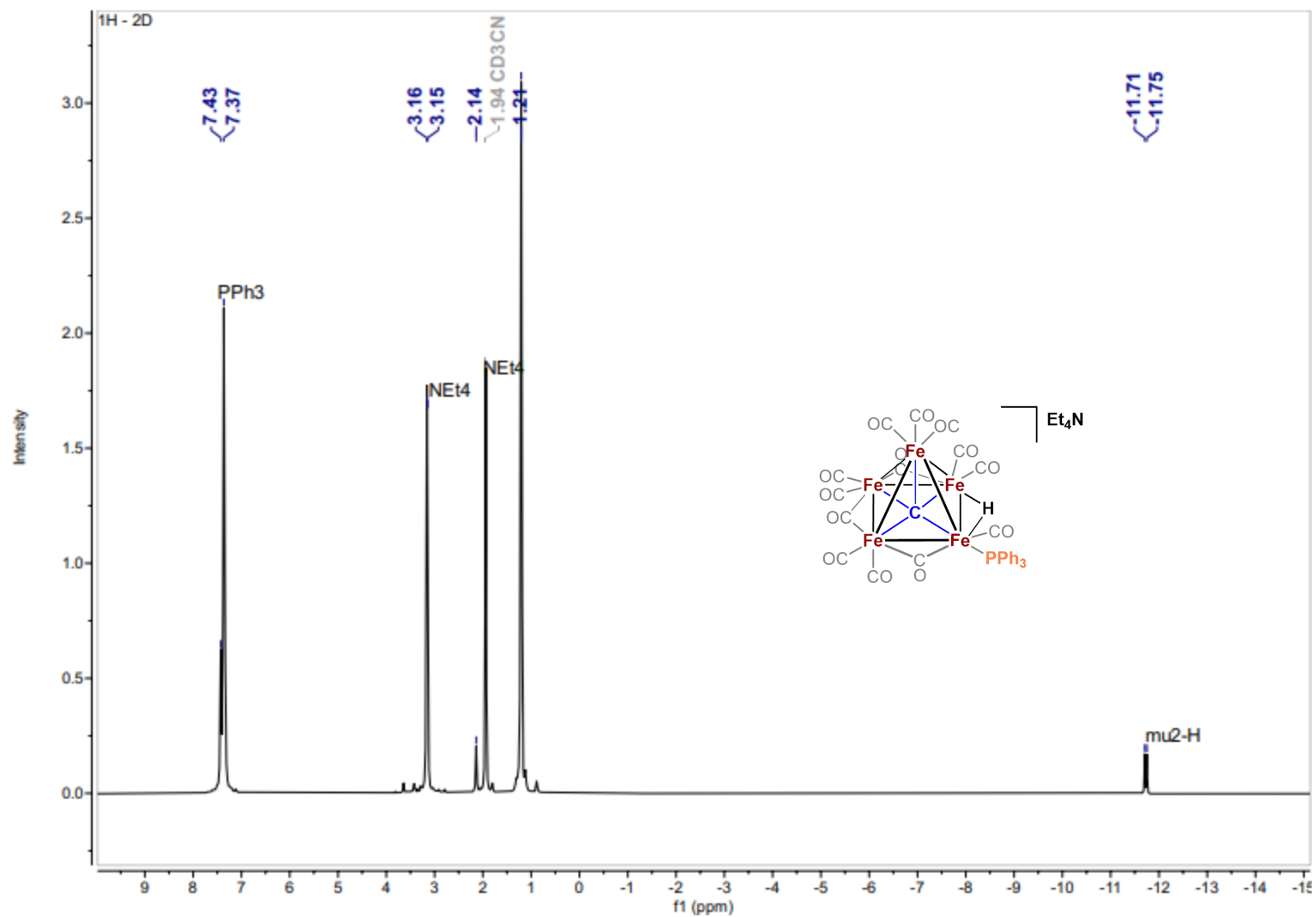


**Figure S12.**  $^1\text{H}$  NMR spectrum of  $\text{NEt}_4[\text{Fe}_5(\mu_5\text{-C})(\mu_2\text{-H})(\text{CO})_{13}\text{PPh}_3]$  (**5**) in  $d_3\text{-MeCN}$  at  $25^\circ\text{C}$ , with hydride region inset indicating doublet hydride peaks (due to coupling to  $^{31}\text{P}$  in  $\text{PPh}_3$ ,  $J = 24$  Hz).

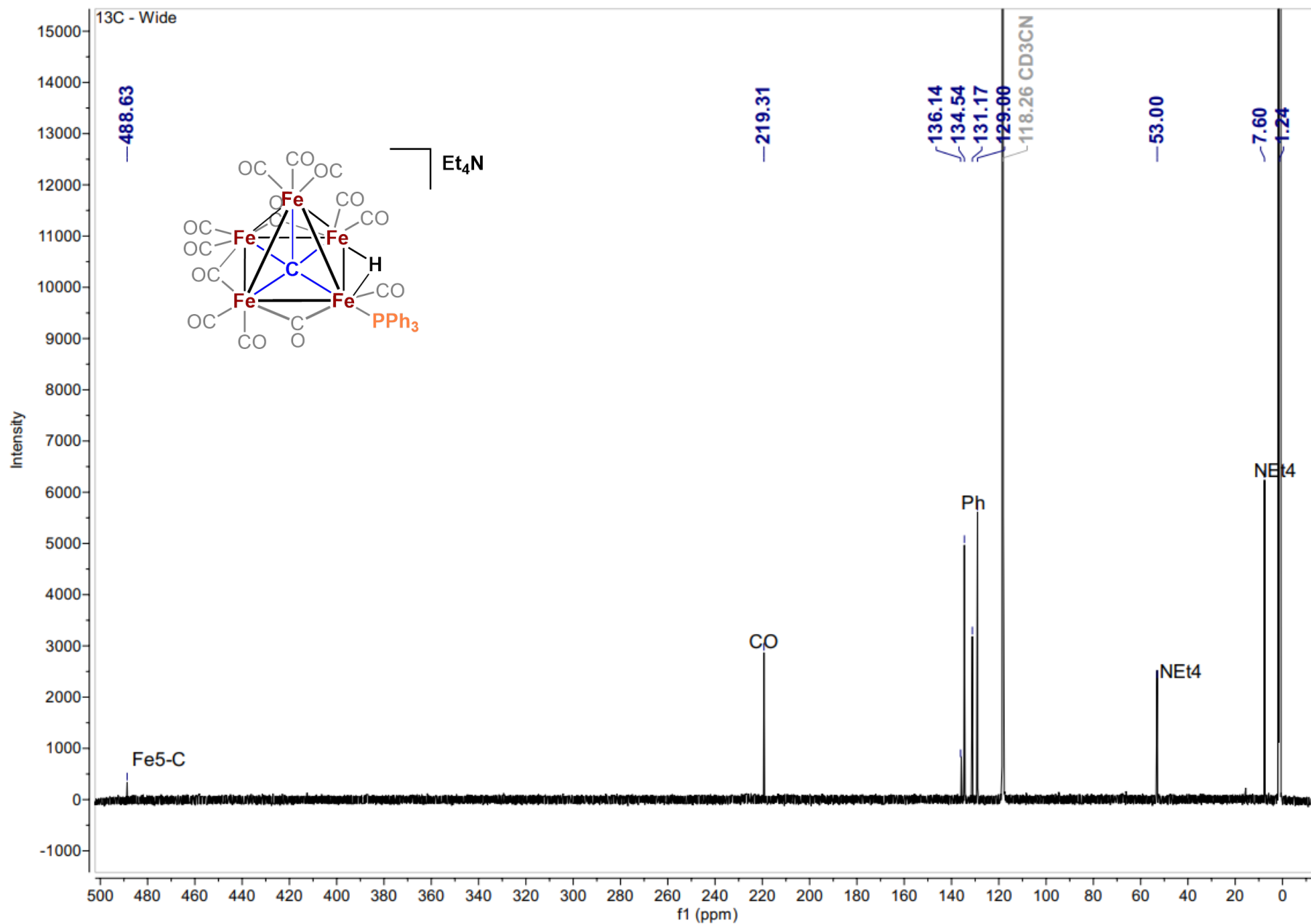


**Figure S13.** <sup>13</sup>C NMR spectrum of NEt<sub>4</sub>[Fe<sub>5</sub>(μ<sub>5</sub>-C)(μ<sub>2</sub>-H)(CO)<sub>13</sub>PPh<sub>3</sub>] (**5**) in *d*<sub>3</sub>-MeCN at 25 °C.

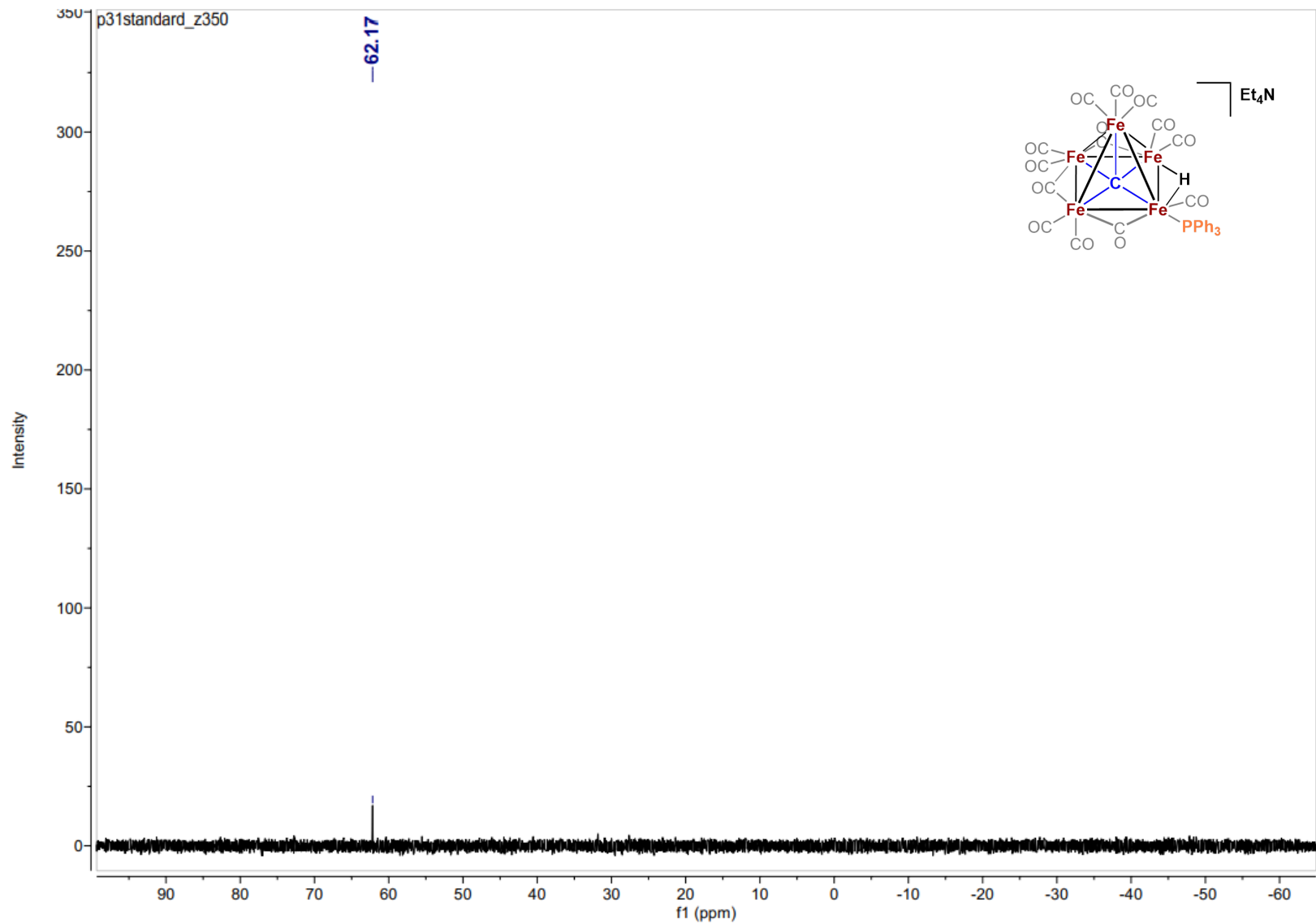


**Figure S14.**  $^{31}\text{P}\{^1\text{H}\}$  NMR spectrum of  $\text{NEt}_4[\text{Fe}_5(\mu_5\text{-C})(\mu_2\text{-H})(\text{CO})_{13}\text{PPh}_3]$  (**5**) in FPh at 25 °C.



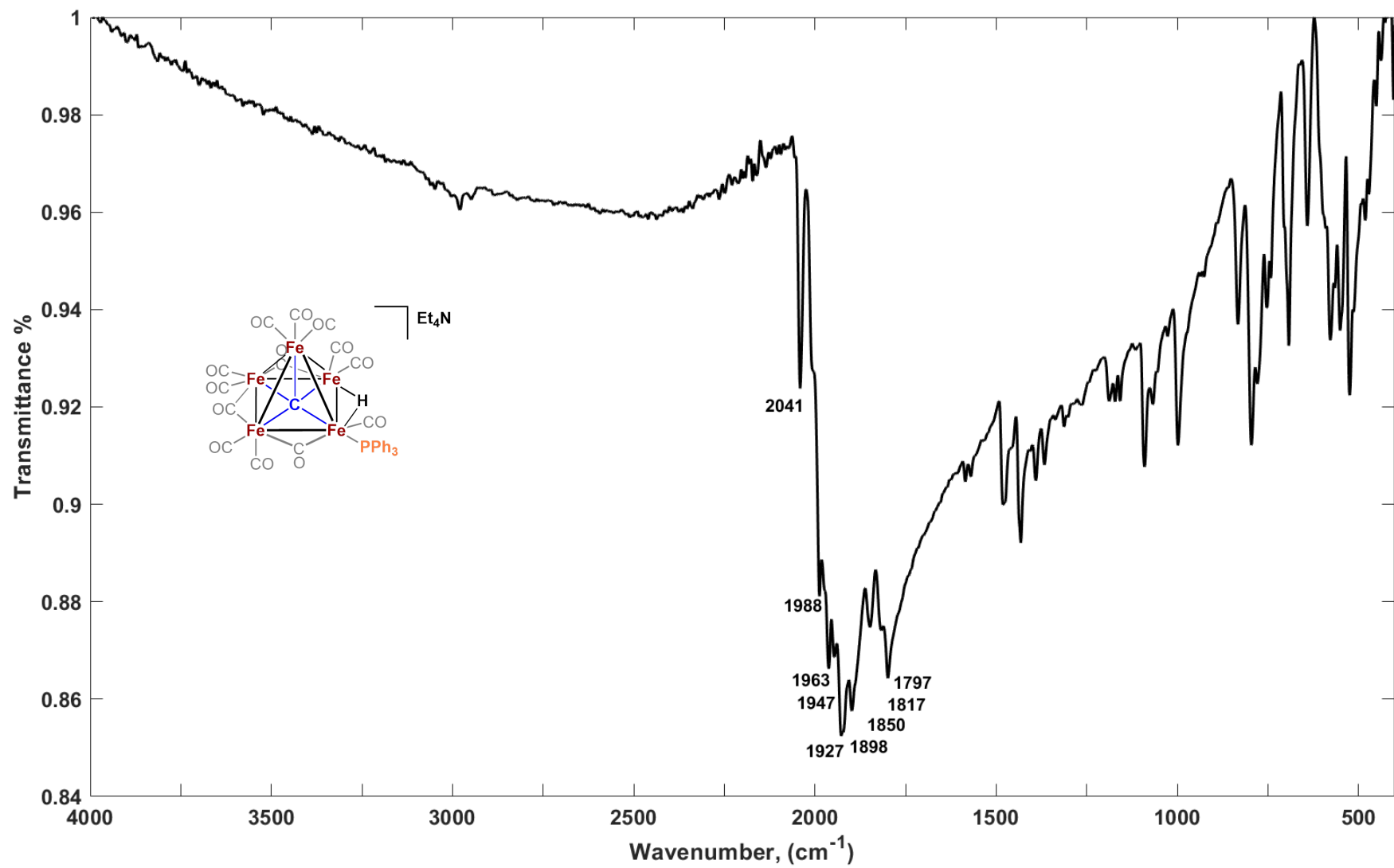


**Figure S16.** IR spectrum of  $\text{NEt}_4[\text{Fe}_5(\mu_5\text{-C})(\mu_2\text{-H})(\text{CO})_{13}\text{PPh}_3]$  (**5**) in the solid state.

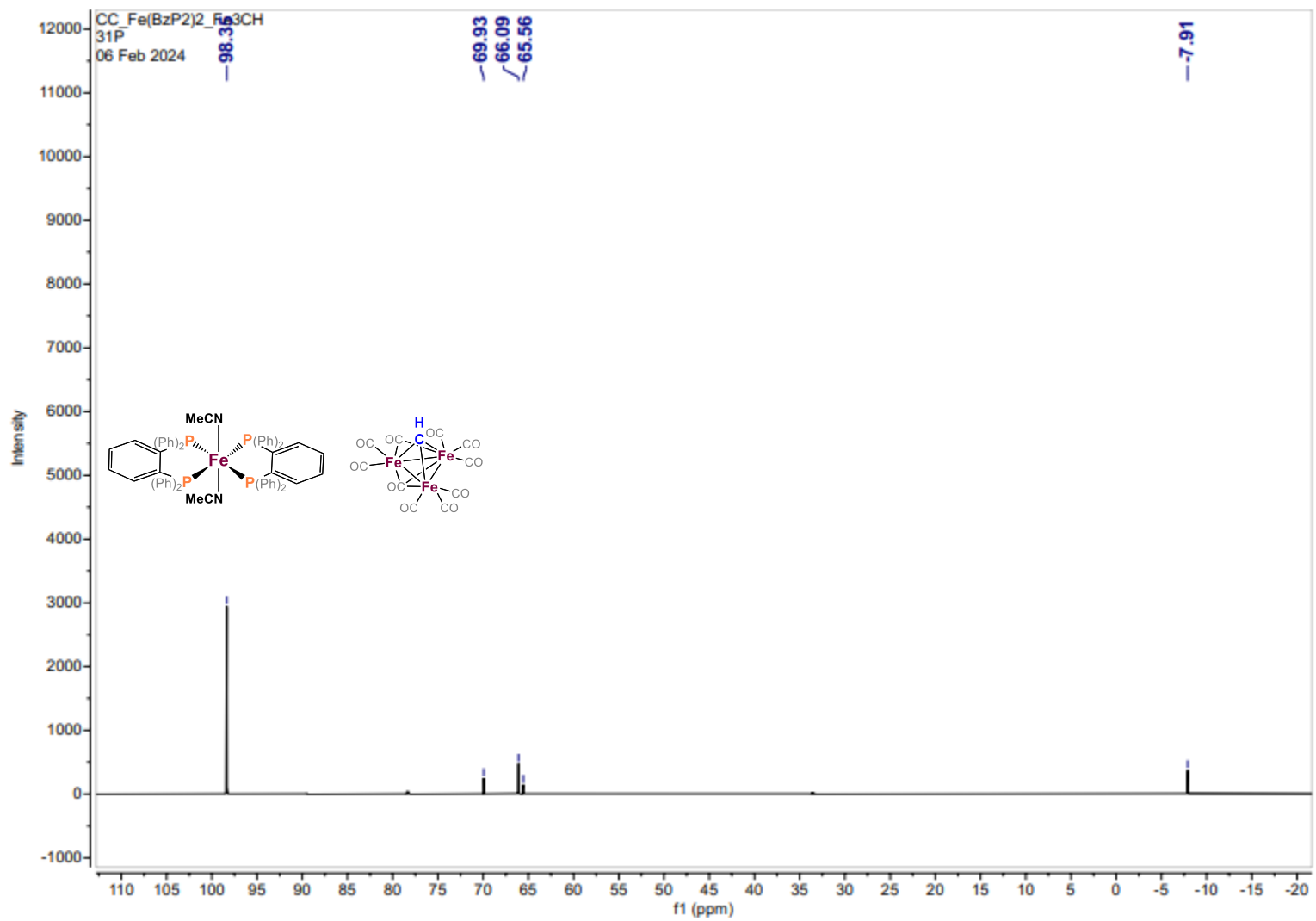


**Figure S17.**  $^{31}\text{P}$  NMR spectrum of  $[\text{Fe}_3(\mu_3\text{-CH})(\mu_3\text{-CO})(\text{CO})_9][(\text{bdpb})_2\text{Fe}(\text{MeCN})_2]$  (**6**) in  $d_3\text{-MeCN}$  at  $25\text{ }^\circ\text{C}$ .

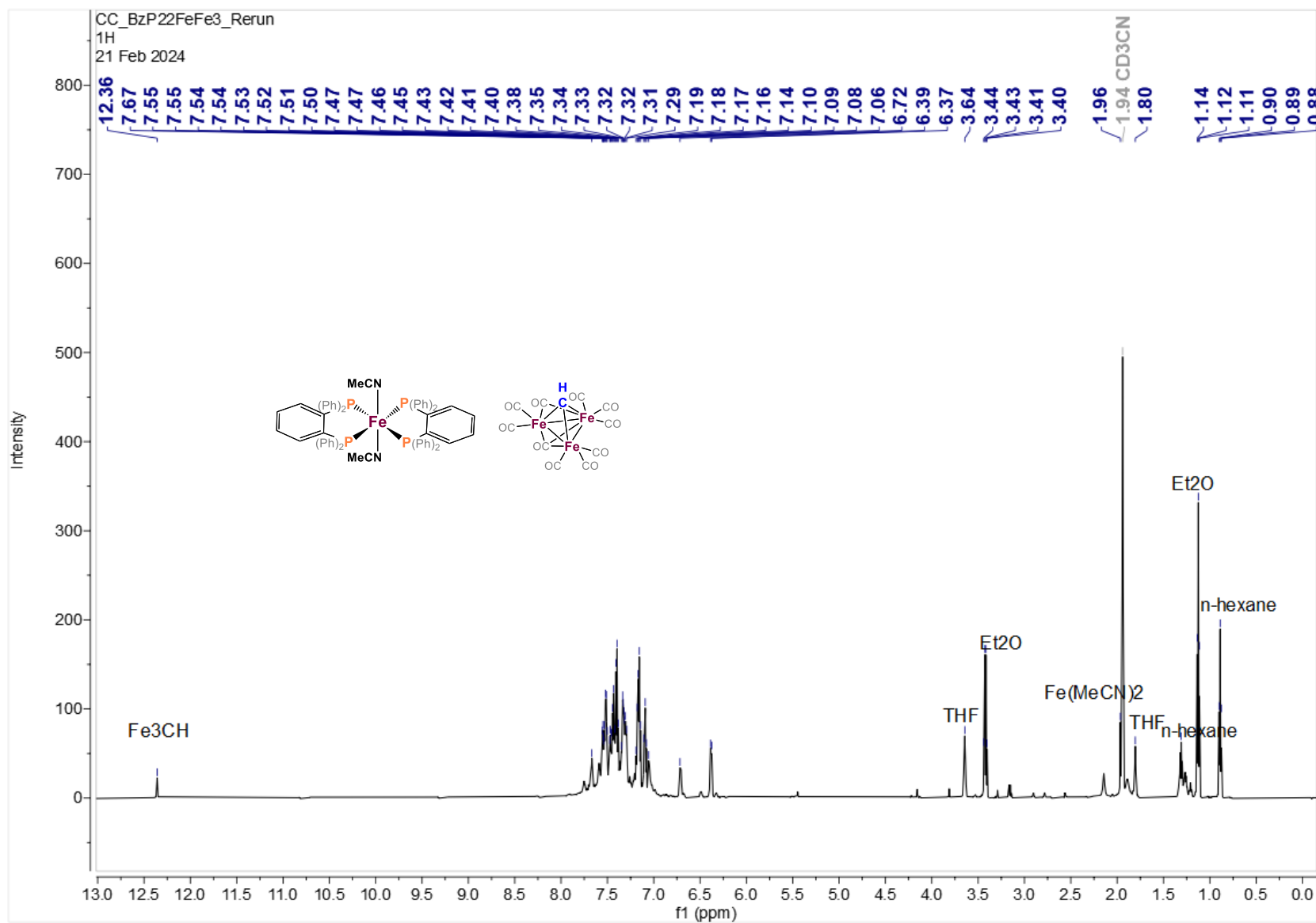


**Figure S18.**  $^1\text{H}$  NMR spectrum of  $[\text{Fe}_3(\mu_3\text{-CH})(\mu_3\text{-CO})(\text{CO})_9][(\text{bdpb})_2\text{Fe}(\text{MeCN})_2]$  (**6**) in  $d_3\text{-MeCN}$  at  $25\text{ }^\circ\text{C}$ .



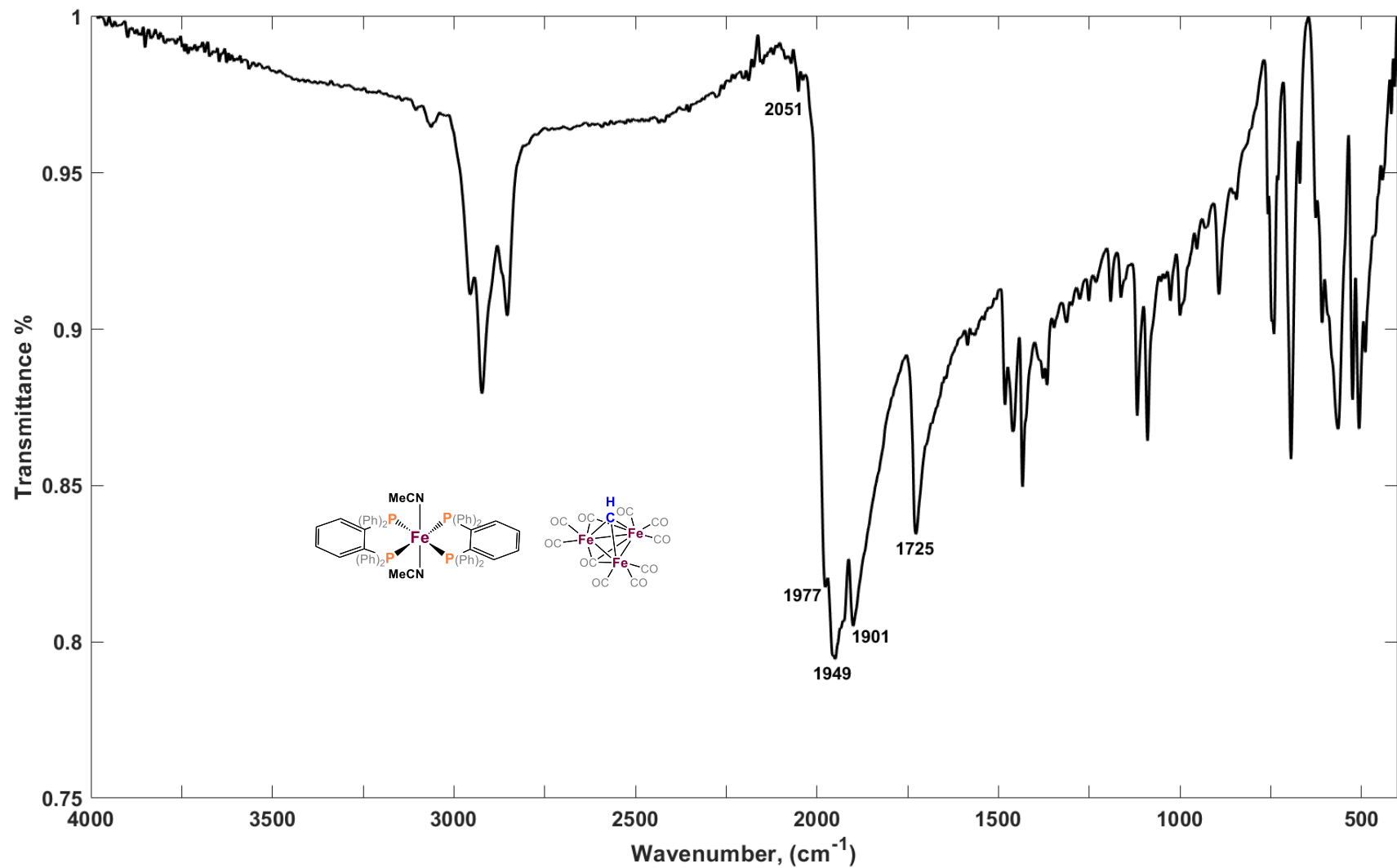


**Figure S20.** IR spectrum of  $[\text{Fe}_3(\mu_3\text{-CH})(\mu_3\text{-CO})(\text{CO})_9][(\text{bdpb})_2\text{Fe}(\text{MeCN})_2]$  (**6**) in the solid state.

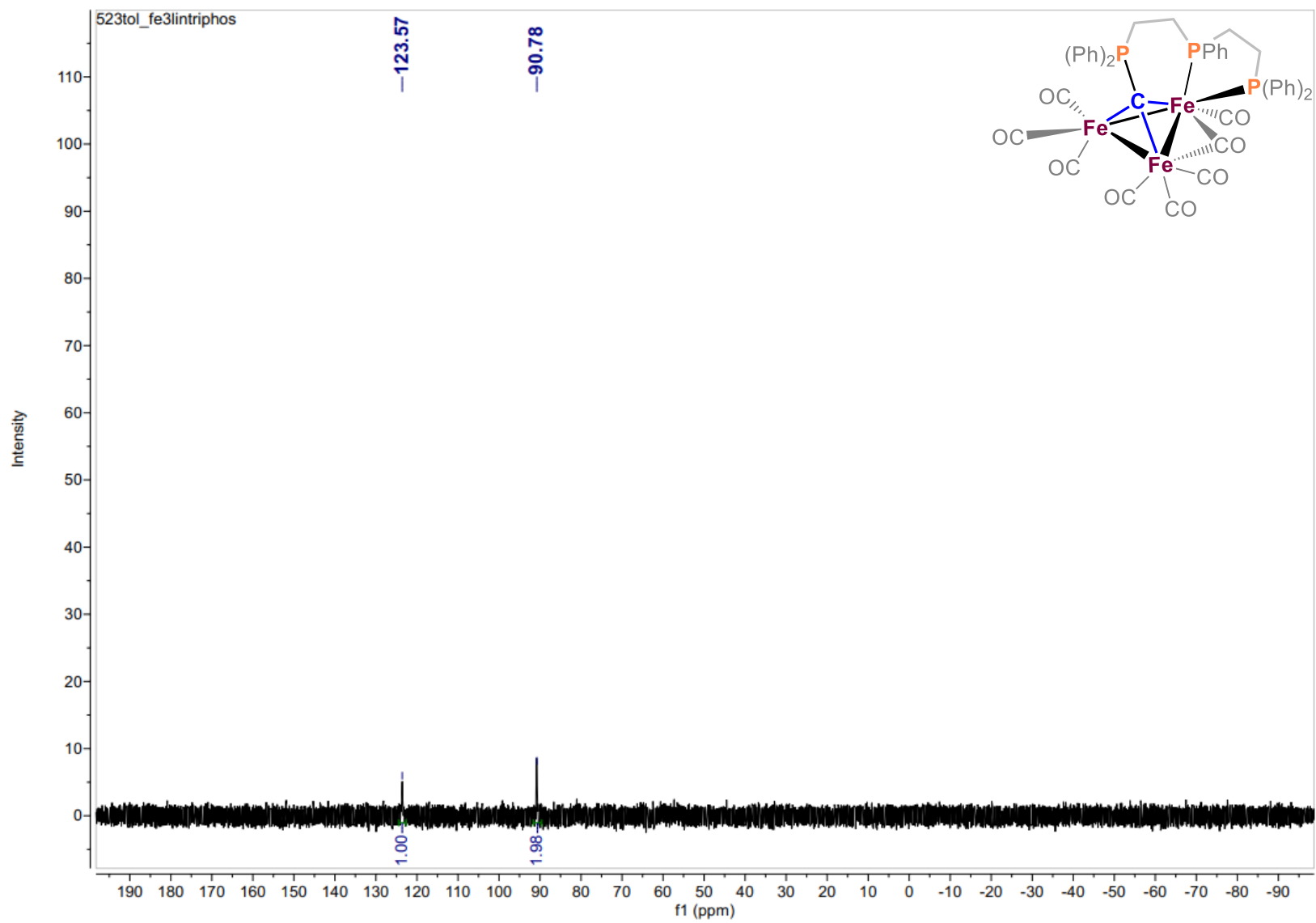


**Figure S21.**  $^{31}\text{P}\{^1\text{H}\}$  NMR spectrum of  $[\text{Fe}_3\{\mu_3\text{-C-P}(\text{Ph})_2\text{C}_2\text{H}_4(\text{PhP})\text{C}_2\text{H}_4(\text{PPh}_2)\}]$  (**7**) in  $d_8$ -toluene at 25 °C.

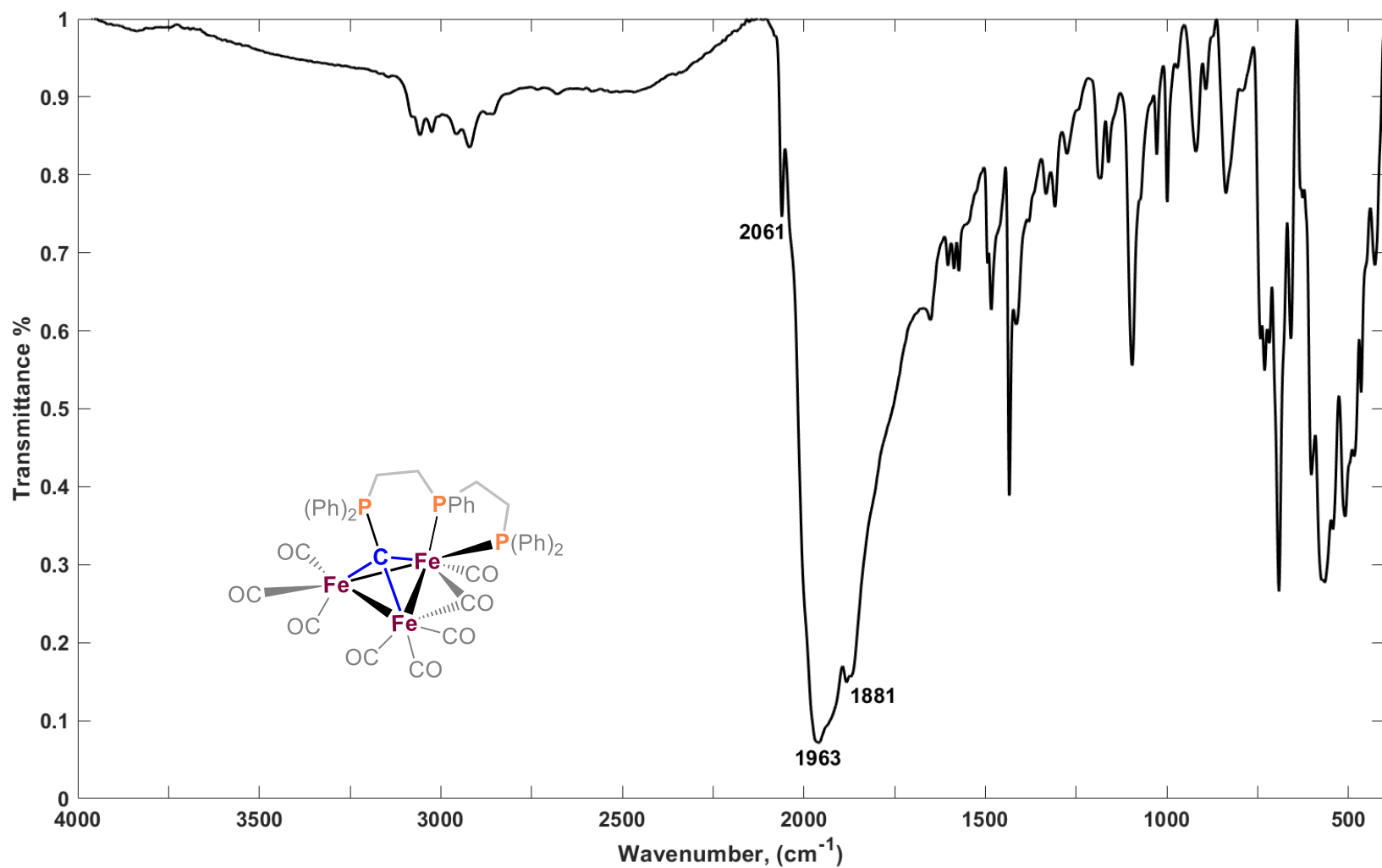


**Figure S22.** IR spectrum of  $[\text{Fe}_3\{\mu_3\text{-C-P}(\text{Ph}_2)\text{C}_2\text{H}_4(\text{PhP})\text{C}_2\text{H}_4(\text{PPh}_2)\}]$  (7) in the solid state.



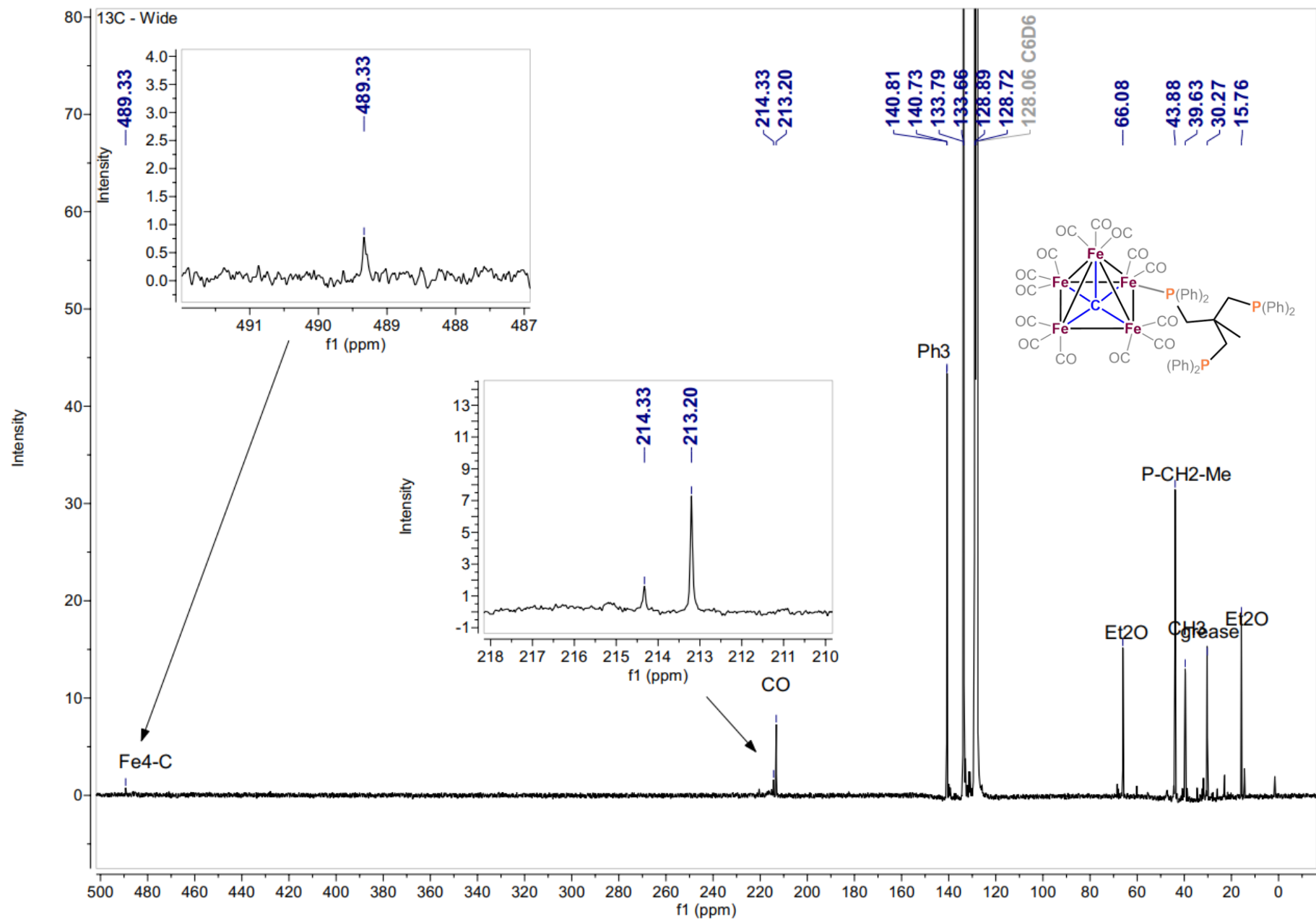


**Figure S24.**  $^{13}\text{C}$  NMR spectrum of  $[\text{Fe}_5(\mu_5\text{-C})(\kappa_1\text{-Triphos})(\text{CO})_{14}]$  (**8**) in  $\text{C}_6\text{D}_6$  at  $25^\circ\text{C}$ .

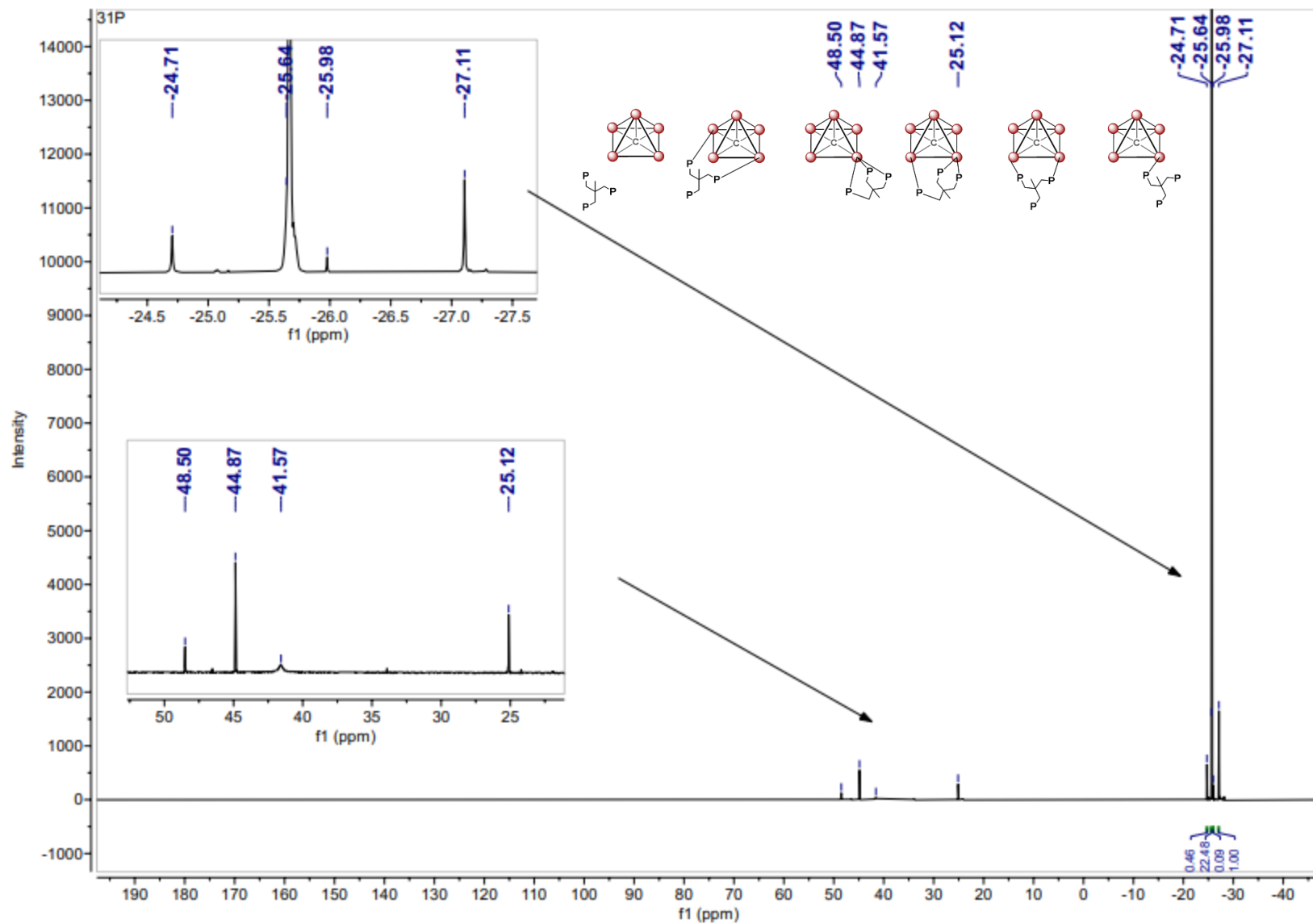


**Figure S25.** <sup>31</sup>P NMR spectrum of  $[\text{Fe}_5(\mu_5\text{-C})(\kappa_1\text{-Triphos})(\text{CO})_{14}]$  (**8**) in  $\text{C}_6\text{D}_6$  at 25 °C. Possible binding modes of the Triphos ligand in dynamic equilibrium shown as an overlaid scheme.

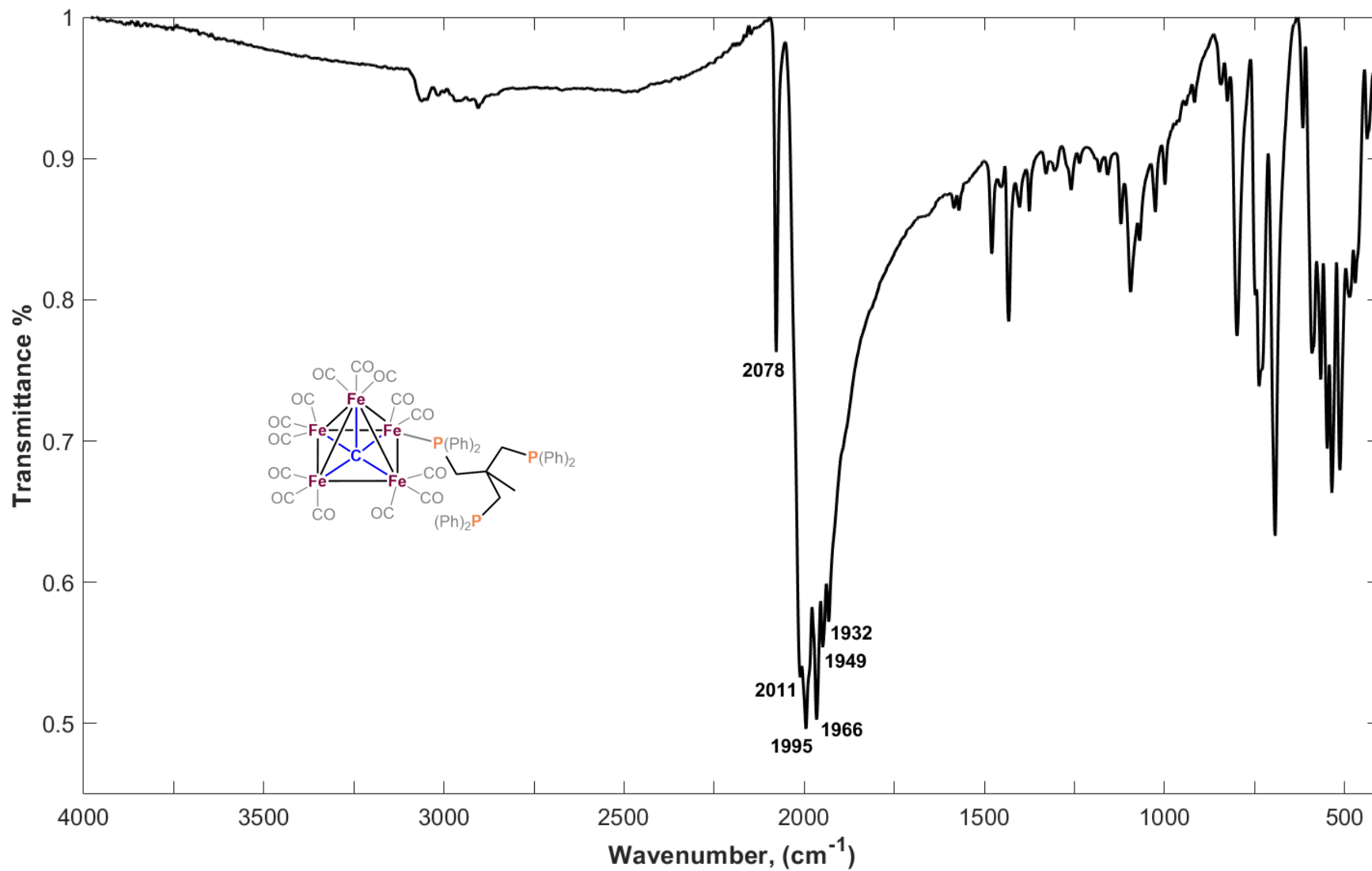


**Figure S26.** IR spectrum of  $[\text{Fe}_5(\mu_5\text{-C})(\kappa_1\text{-Tripfos})(\text{CO})_{14}]$  (**8**) in the solid state.

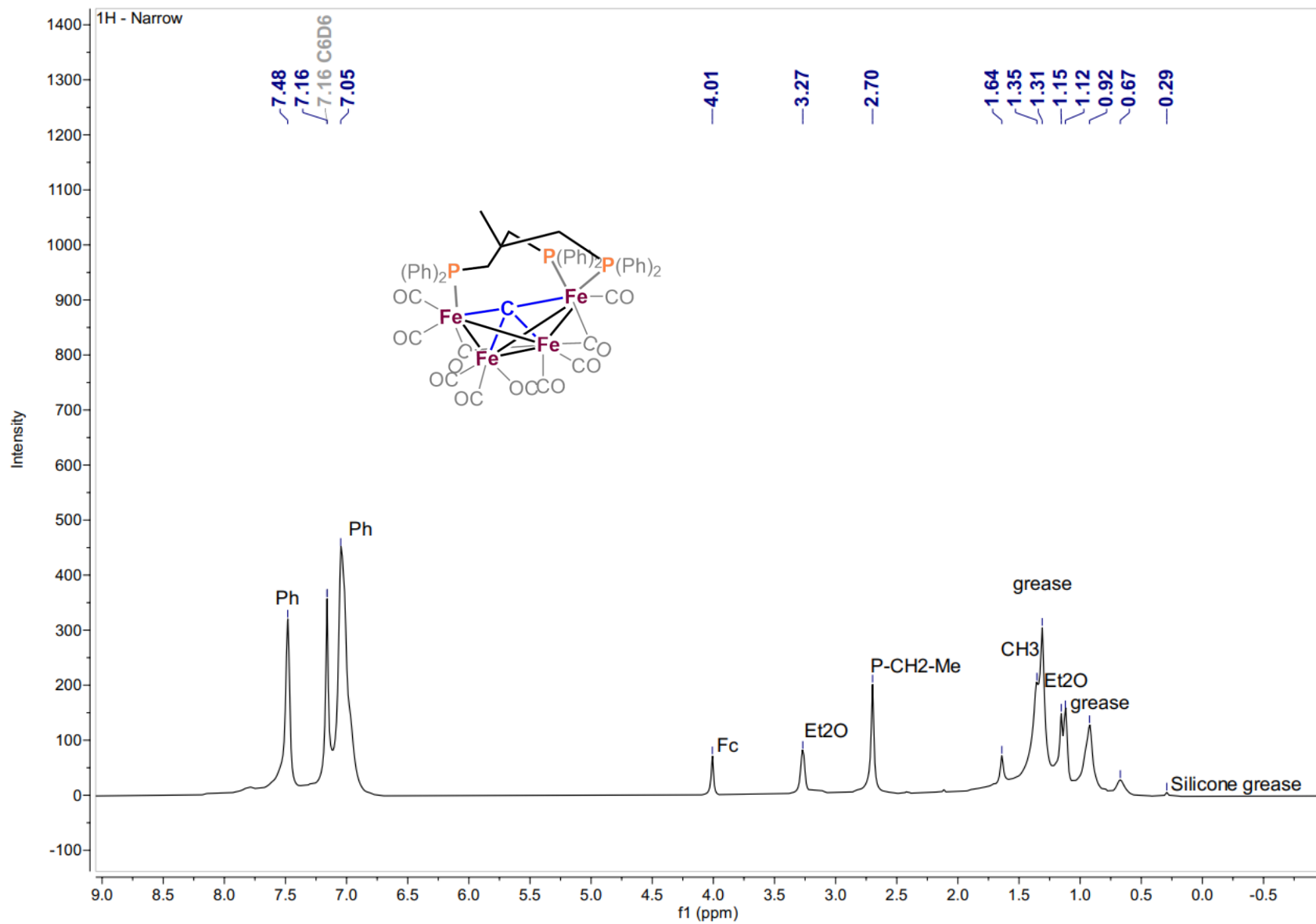


**Figure S27.** <sup>1</sup>H-NMR spectrum of [Fe<sub>4</sub>(μ<sub>4</sub>-C)(κ<sub>3</sub>-Triphos)(CO)<sub>10</sub>] (9) in C<sub>6</sub>D<sub>6</sub> at 25 °C.

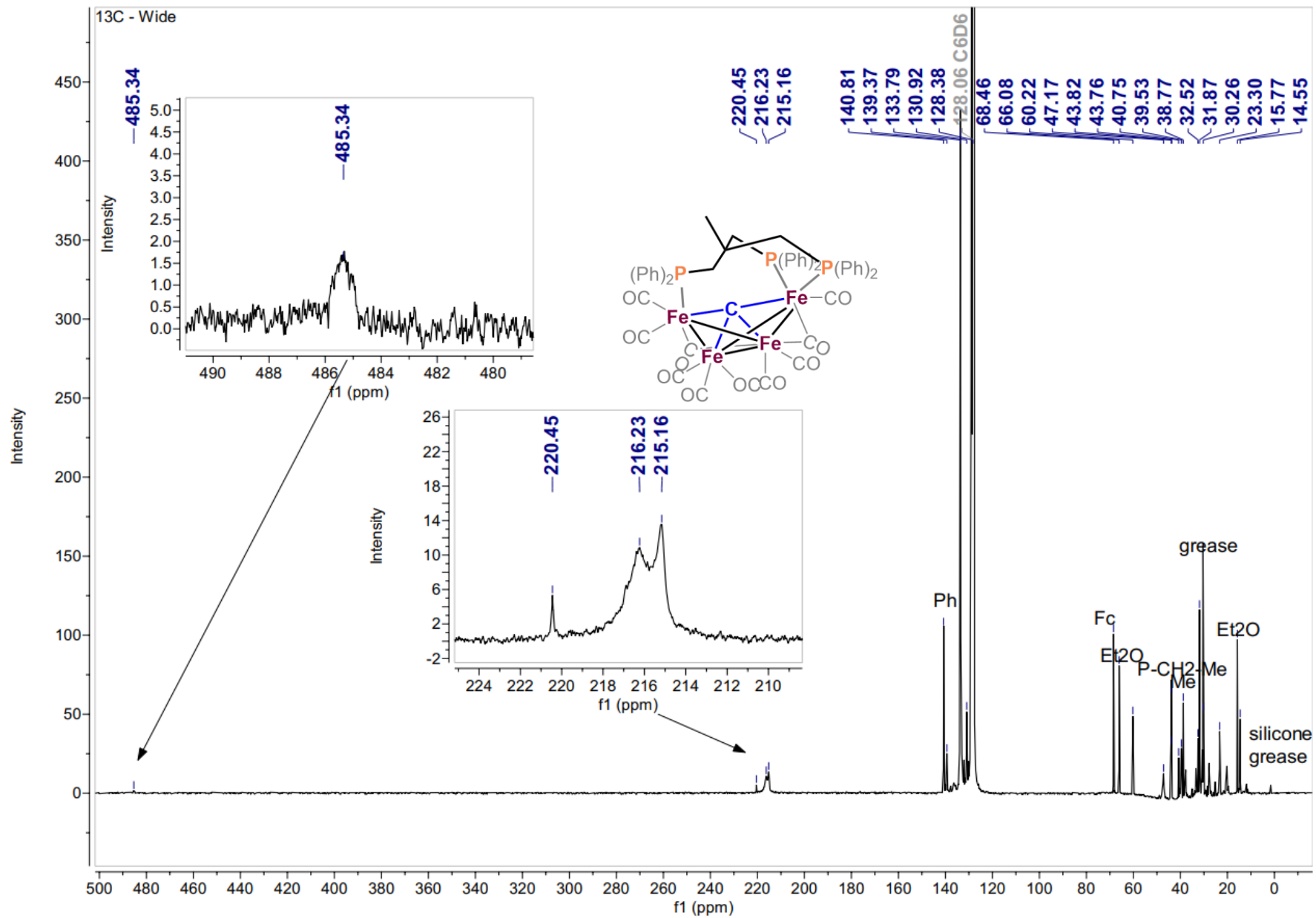


**Figure S28.**  $^{13}\text{C}$  NMR spectrum with carbide region (inset) of  $[\text{Fe}_4(\mu_4\text{-C})(\kappa_3\text{-Triphos})(\text{CO})_{10}]$  (**9**) in  $\text{C}_6\text{D}_6$  at  $25^\circ\text{C}$ .

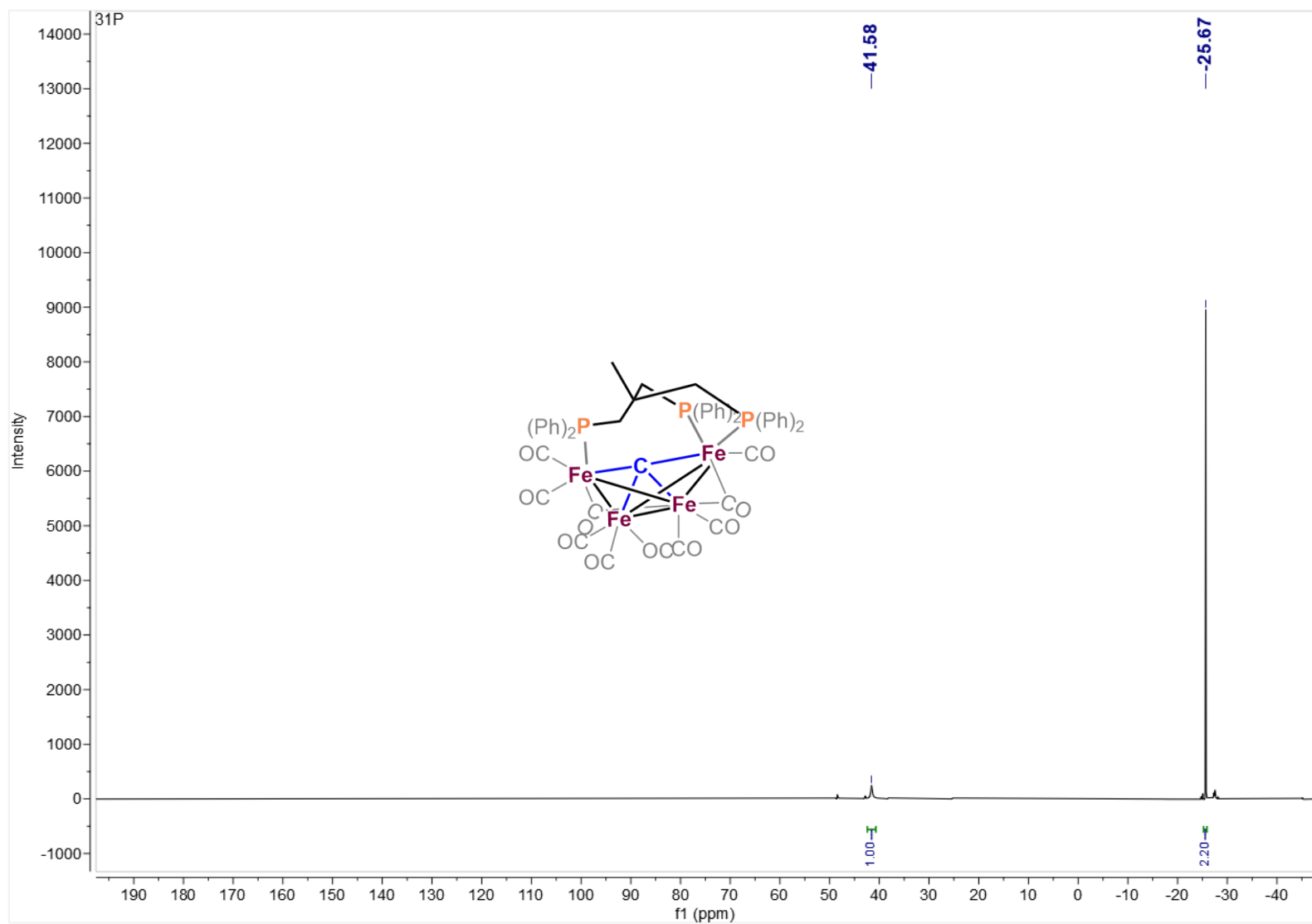


**Figure S29.**  $^{31}\text{P}\{^1\text{H}\}$  NMR spectrum of  $[\text{Fe}_4(\mu_4\text{-C})(\kappa_3\text{-Triphos})(\text{CO})_{10}]$  (**9**) in  $\text{C}_6\text{D}_6$  at  $25^\circ\text{C}$ .

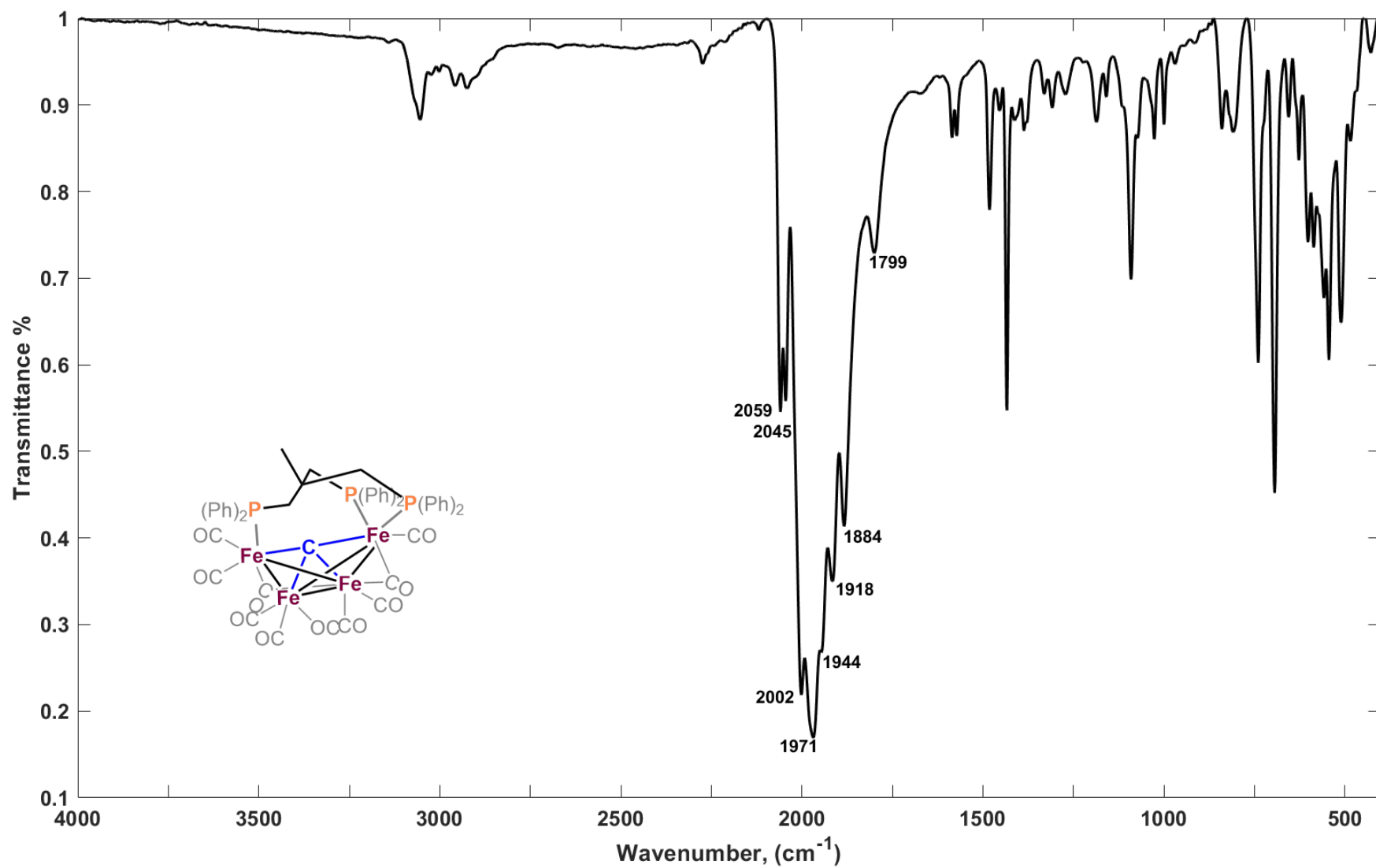


**Figure S30.** IR spectrum of  $[\text{Fe}_4(\mu_4\text{-C})(\kappa_3\text{-Triphos})(\text{CO})_{10}]$  (**9**) in the solid state.

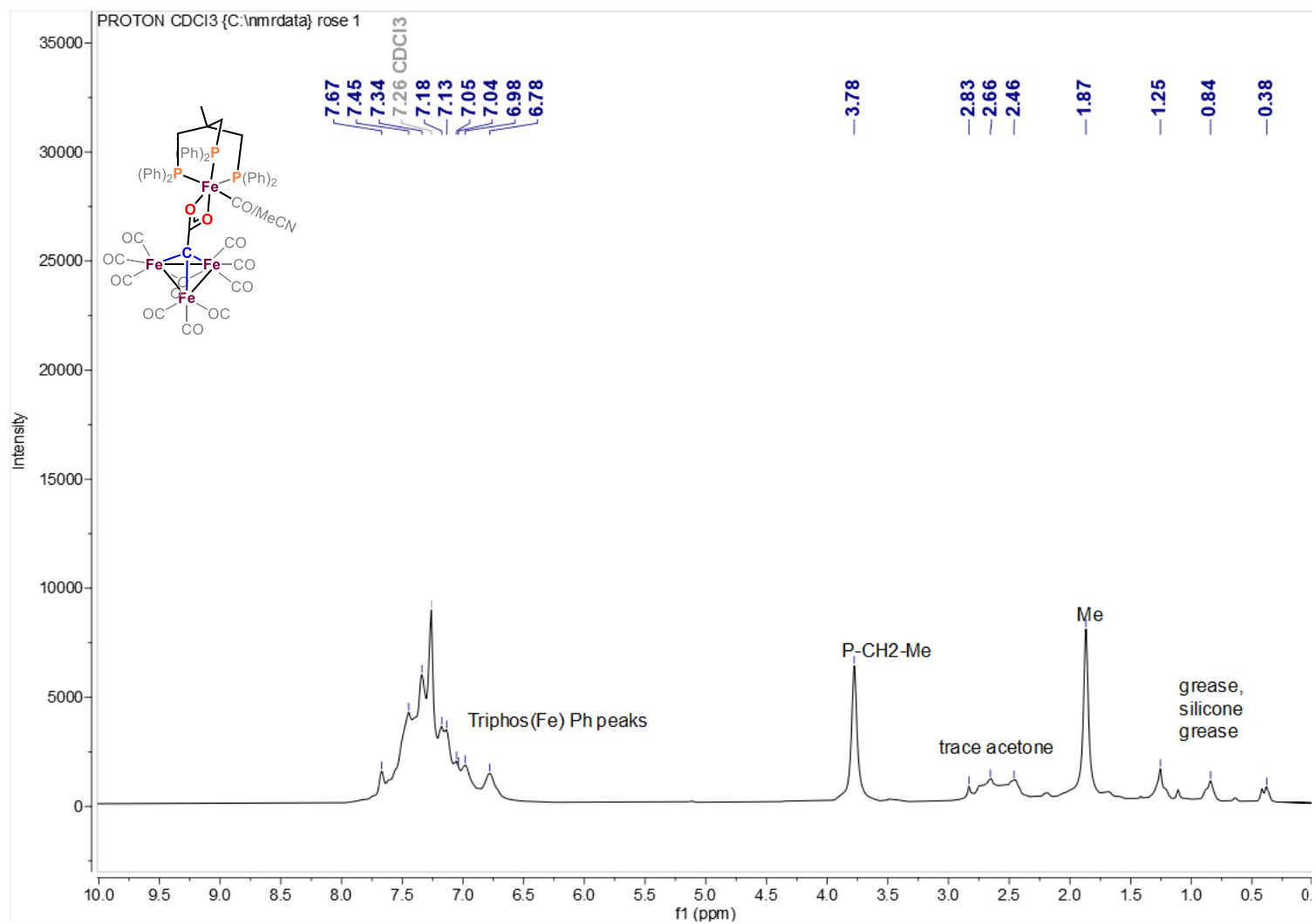


**Figure S31.**  $^1\text{H-NMR}$  spectrum of  $[\text{Fe}_3(\text{CO})_8(\mu_3\text{-CO})(\mu_3\text{-aceto-}\kappa_2\text{-O})\text{Fe}(\text{CO})(\kappa_3\text{-Triphos})]$  (**10**) in  $\text{CDCl}_3$  at  $25^\circ\text{C}$ .

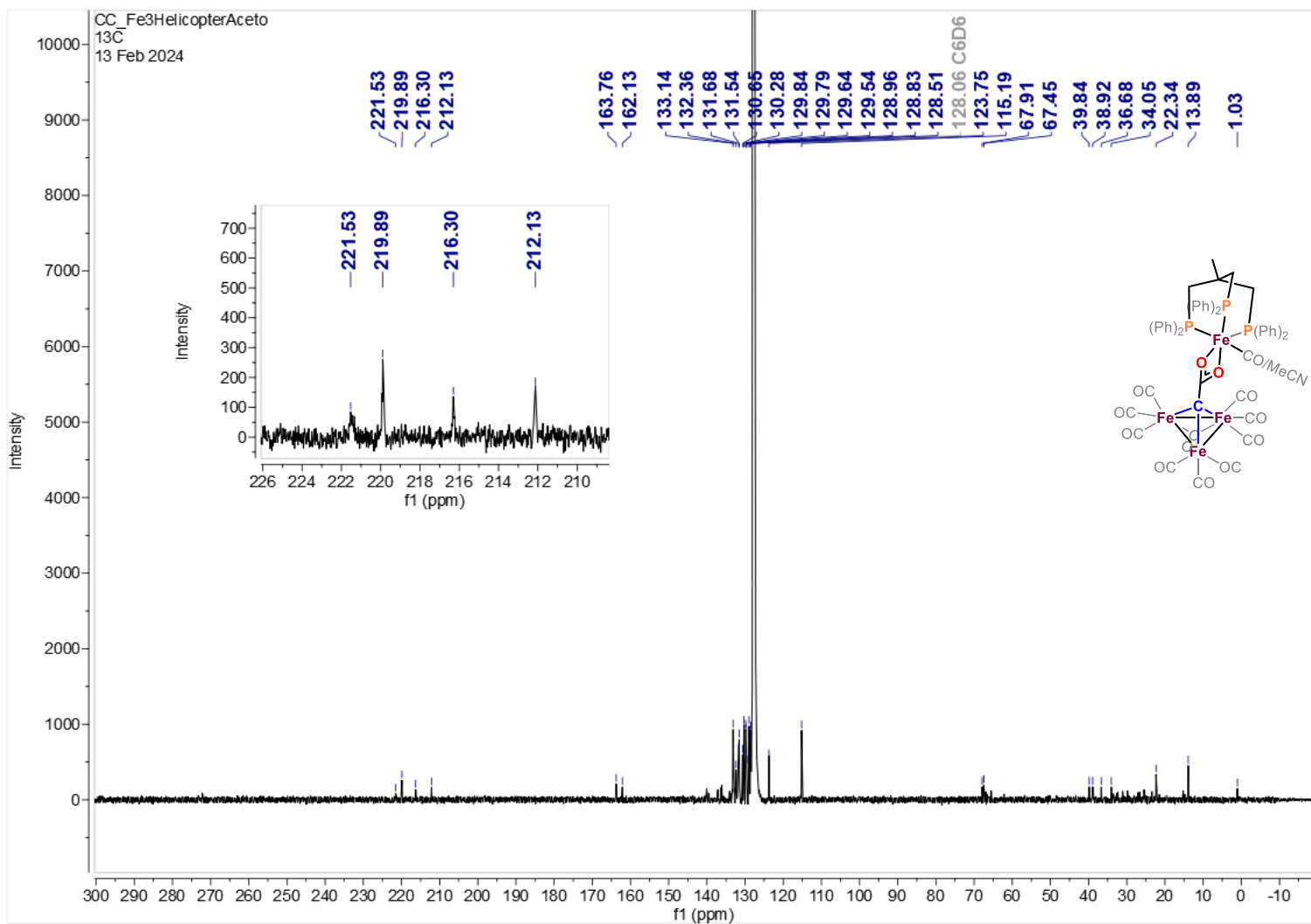


**Figure S32.** <sup>13</sup>C NMR spectrum of [Fe<sub>3</sub>(CO)<sub>8</sub>(μ<sub>3</sub>-CO)(μ<sub>3</sub>-aceto-κ<sub>2</sub>-O)Fe(CO)(κ<sub>3</sub>-Triphos)] (**10**) in C<sub>6</sub>D<sub>6</sub> at 25 °C. (Working on new spectrum but no luck so far)

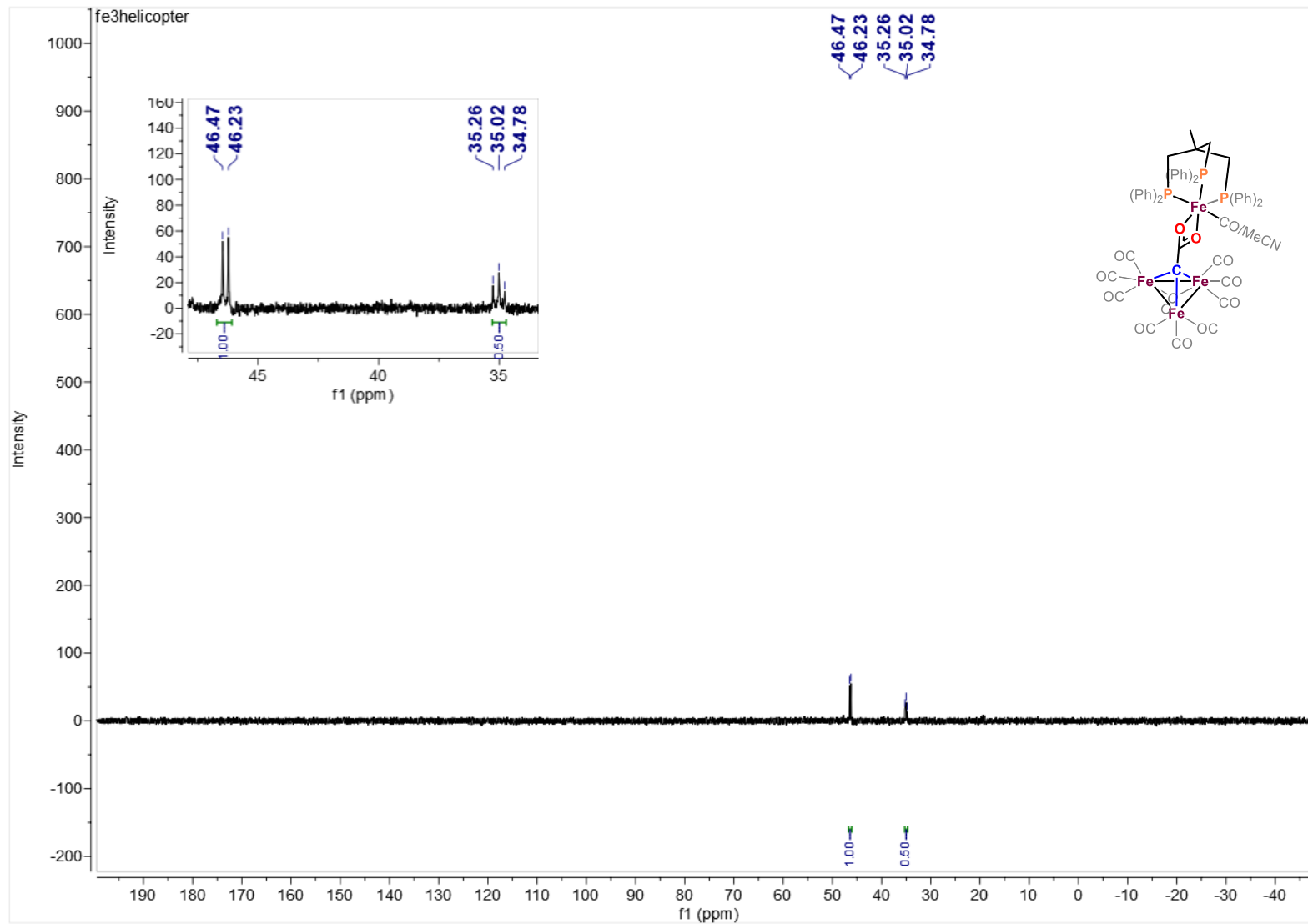


**Figure S33.**  $^{31}\text{P}\{^1\text{H}\}$  NMR spectrum of  $[\text{Fe}_3(\text{CO})_8(\mu_3\text{-CO})(\mu_3\text{-aceto-}\kappa_2\text{-O})\text{Fe}(\text{CO})(\kappa_3\text{-Triphos})]$  (**10**) in  $\text{CDCl}_3$  at  $25^\circ\text{C}$ .

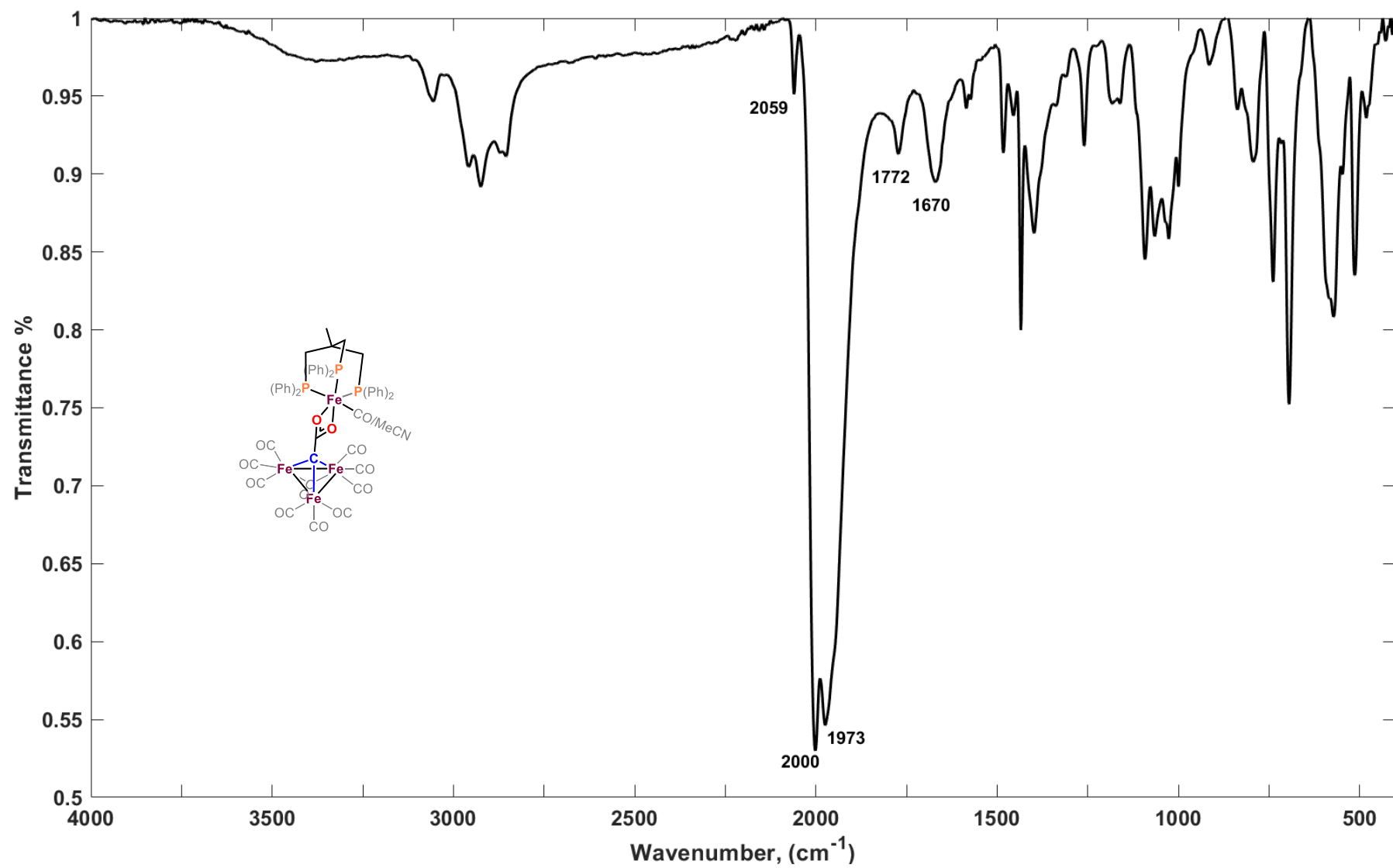


**Figure S34.** IR spectrum of  $[\text{Fe}_3(\text{CO})_8(\mu_3\text{-CO})(\mu_3\text{-aceto-}\kappa_2\text{-O})\text{Fe}(\text{CO})(\kappa_3\text{-Triphos})]$  (**10**) in the solid state.

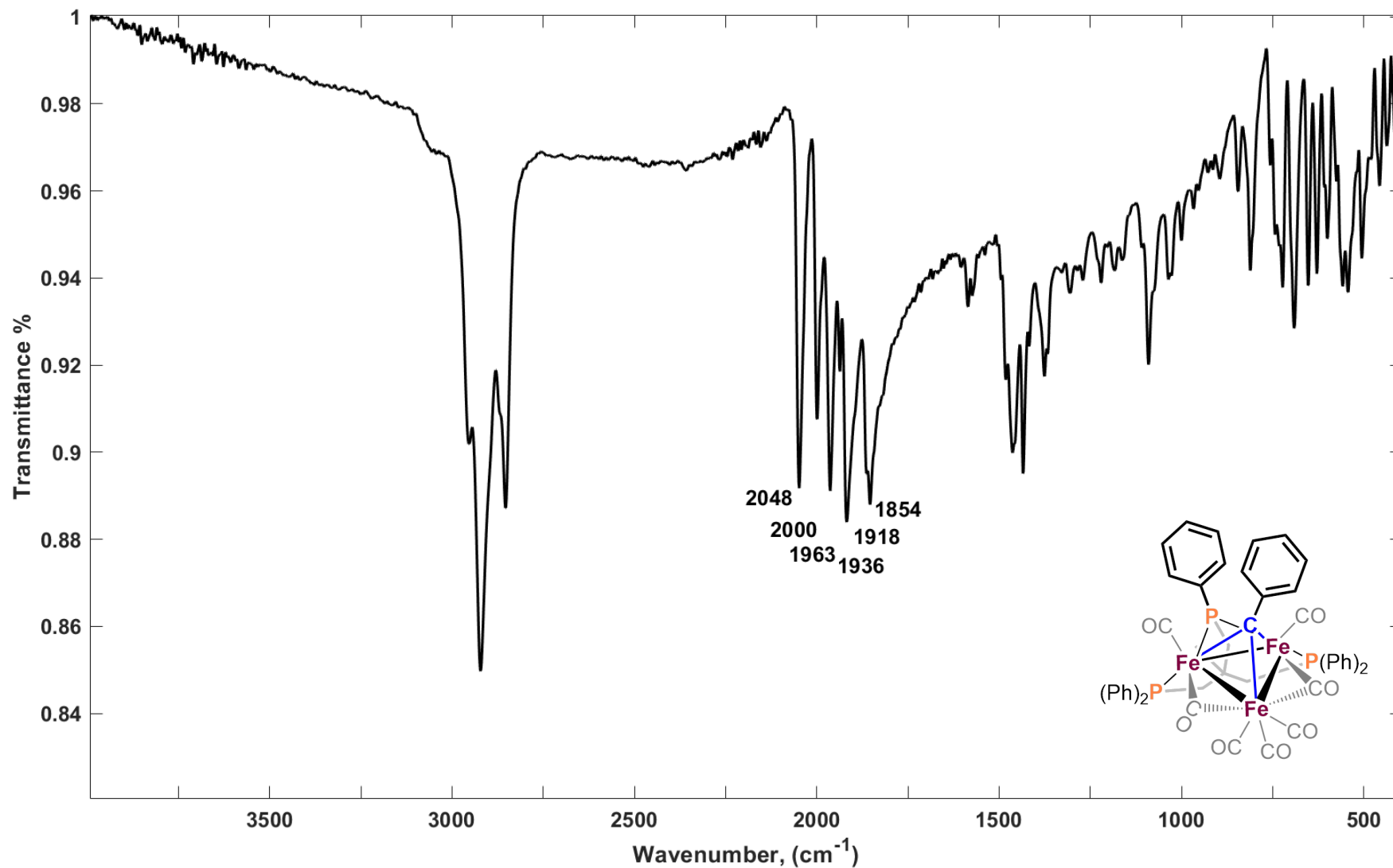


**Figure S35.** IR spectrum of  $[\text{Fe}_3(\mu_3\text{-CPh})\{\text{Triphos}(\text{PPh}_2)_2(\text{PPh})\}(\text{CO})_7]$  (**11**) in the solid state. Some contamination from trace paraffin oil (from crystal handling) is present but does not obscure the  $\nu(\text{CO})$  region.

**Table S1.** IR  $\nu(\text{CO})$  features for all complexes and relevant literature comparisons. Solid state IR data unless otherwise indicated. Literature values obtained as indicated: (a) from Kuppuswamy *et al.* 2017;<sup>1</sup> (b) from Cooke and Mays, 1975;<sup>4</sup> (c) from Bradley *et al.* 1981;<sup>5</sup> and (d) from Taheri *et al.*, 2016.<sup>6</sup>

Metal Cluster	$\nu(\text{CO})$ ( $\text{cm}^{-1}$ )
$[\text{NEt}_4]_2[\text{Fe}_6(\mu_6\text{-C})(\text{CO})_{16}]$ ( <b>1</b> )	Terminal: 2034(w), 1918(s) Bridging: 1742(m)
<sup>a</sup> $[\text{Fe}_6(\mu_6\text{-C})(\text{CO})_{18}]$	Terminal: 1970(s), 1875(m)
$[\text{Fe}_6(\mu_6\text{-C})(\text{CO})_{16}]$ ( <b>2</b> ) dropcast from MeCN	Terminal: 2087(w), 2036(m), 1985(s), 1963(s) Bridging: 1772(w) *may be residual $\text{Fe}_6^{2-}$ in reaction solution
$[\text{Fe}_6(\mu_6\text{-C})(\text{CO})_{16}]$ ( <b>2</b> ) dropcast from DCE	Terminal: 2096(w), 2046(m), 2028(m) 1981(s), 1960(s) Bridging: 1821(m), 1767(w)* may be residual $\text{Fe}_6^{2-}$ in reaction solution
$[\text{Fe}_5(\mu_5\text{-C})(\text{CO})_{15}]$	Terminal: 2098(w), 2050(s), 2031(sh)
$[\text{Fe}_6(\mu_6\text{-C})(\text{CO})_{17}]$ ( <b>3</b> )	Terminal: 2096(w), 2023 (s) Bridging: 1829(m)
$[\text{Fe}_5(\mu_5\text{-C})(\text{CO})_{14}(\text{PPh}_3)]$ ( <b>4</b> )	Terminal: 2079(m), 2005(s), 1987(s), 1959(s)
$\text{NEt}_4[\text{Fe}_5(\mu_5\text{-C})(\mu_2\text{-H})(\text{CO})_{13}(\text{PPh}_3)]$ ( <b>5</b> )	Terminal: 2041(m), 1988(s), 1963(s), 1947(s), 1927(s), 1898(s) Bridging: 1850(s), 1817(s), 1797(s)
<sup>b</sup> $[\text{Fe}_5(\mu_5\text{-C})(\text{CO})_{14}(\text{PMePh}_2)]$	Terminal: 2080(w), 2035(vs), 2026(s), 2010(m)
<sup>b</sup> $[\text{Fe}_5(\mu_5\text{-C})(\text{CO})_{13}(\text{PMePh}_2)_2]$	Terminal: 2061(w), 2031(vs), 2000(m)
<sup>b</sup> $[\text{Fe}_5(\mu_5\text{-C})(\text{CO})_{12}(\text{PMePh}_2)_3]$	Terminal: 2042(m), 2001(s), 1989(s)
$[\text{Fe}_3(\mu_3\text{-CH})(\text{CO})_{10}][\text{Fe}(\text{MeCN})_2(\text{bdpb})_2]$ ( <b>6</b> )	Terminal: 2051(w), 1977(s), 1949(s), 1901(s) Bridging: 1725(m)
$[\text{Fe}_3\{\mu_3\text{-C-P}(\text{Ph}_2)\text{C}_2\text{H}_4(\text{PhP})\text{C}_2\text{H}_4(\text{PPh}_2)\}(\text{CO})_7(\mu_2\text{-CO})]$ ( <b>7</b> )	Terminal: 2061(w), 1963(s) Bridging: 1881(s)
$[\text{Fe}_5(\mu_5\text{-C})(\text{CO})_{14}(\text{Triphos})]$ ( <b>8</b> )	Terminal: 2078(m), 2011(s), 1995(s), 1966(s), 1949(s), 1932(s)
<sup>c</sup> $[\text{Fe}_4(\mu_4\text{-C})(\mu_2\text{-CO})(\text{CO})_{12}]$ in cyclohexane	2062(s) 2051(s), 2040(s), 2035(s), 2015(w), 2000(w), 1990(m), 1901(m)
<sup>d</sup> $[\text{Fe}_4(\mu_4\text{-C})(\text{CO})_{12}]^{2-}$ in MeCN	Terminal: 1969(s), 1945(s)
$[\text{Fe}_4(\mu_4\text{-C})(\mu_2\text{-CO})_2(\text{CO})_8(\kappa_3\text{-Triphos})]$ ( <b>9</b> )	Terminal: 2059(m), 2045(m), 2002(s), 1971(s), 1944(s), 1918(s) Bridging: 1884(m) and 1799(m)
$[\text{Fe}_3(\text{CO})_8(\mu_3\text{-CO})(\mu_3\text{-aceto-}\kappa_2\text{-O})\text{Fe}(\text{CO})(\kappa_3\text{-Triphos})]$ ( <b>10</b> ) dropcast from THF	Terminal: 2059(w), 2000(s), 1973(s) Bridging: 1772(w) aceto $\nu(\text{C=O})$ : 1670(w)
$[\text{Fe}_3(\mu_3\text{-CPh})\{\text{Triphos}(\text{PPh}_2)_2(\text{PPh})\}(\text{CO})_7]$ ( <b>11</b> )	Terminal: 2048(s), 2000(s), 1963(s), 1936(m), 1918(s) Bridging: 1854(s)

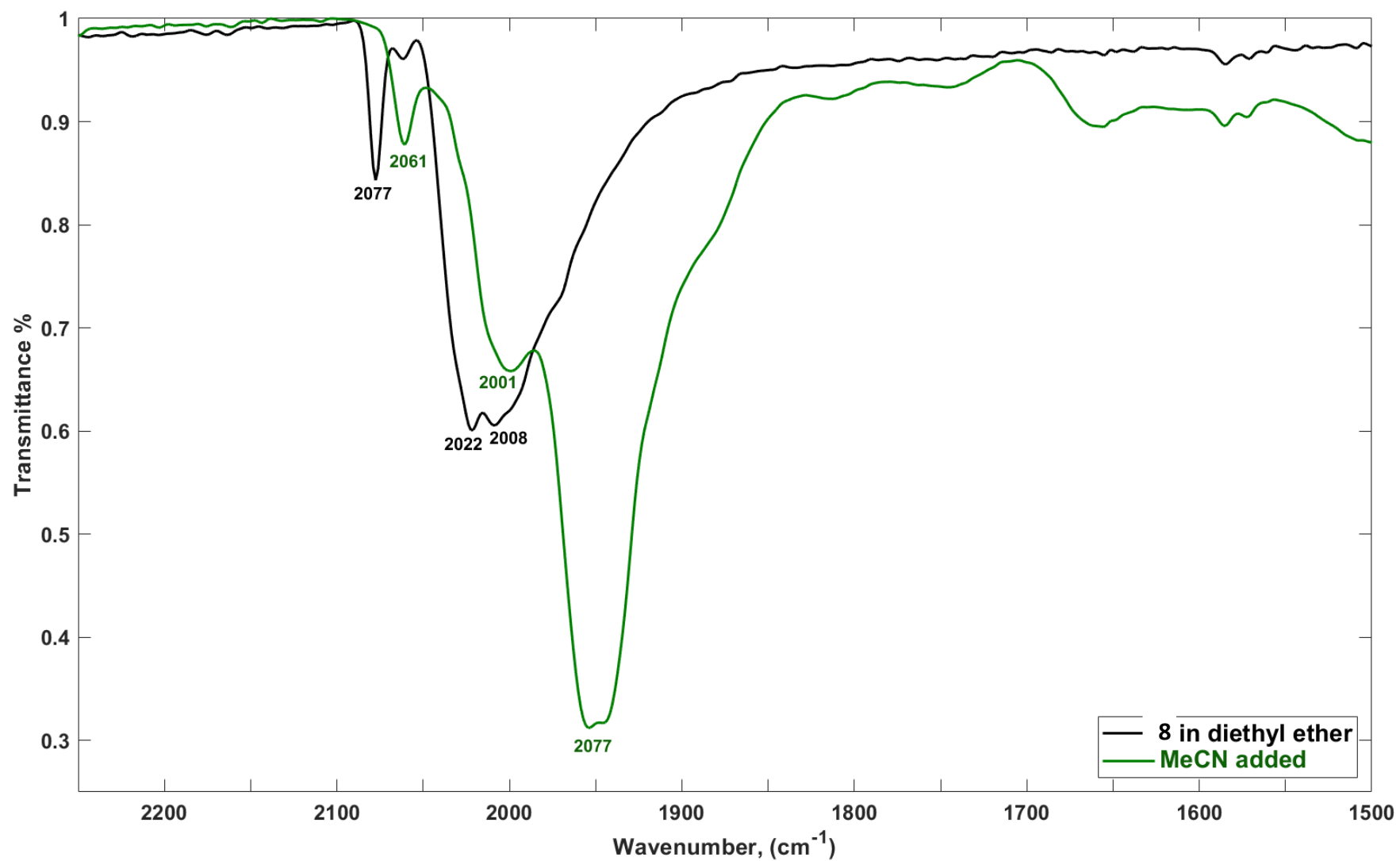


**Figure S36.** Dropcast FT-IR spectra in the  $\nu(\text{CO})$  region for **8** in  $\text{Et}_2\text{O}$ , and of the reaction mixture of **8** with MeCN.

## X-ray Diffraction and Crystal Structure of Compounds 3—11

Details of crystal data, data collection, and structure refinement are listed in **Table S2-S4**. All figures were generated using Mercury for Windows.<sup>7</sup>

### X-ray Diffraction and Crystal Structure Solution of (3) Experimental Details

Dark black plate crystals of compound **3** were grown by slow evaporation of a fluorobenzene solution at  $-20\text{ }^{\circ}\text{C}$  under nitrogen atmosphere. The data crystal had the approximate dimensions  $0.15 \times 0.11 \times 0.07\text{ mm}^3$ .

The data were collected on an XtaLAB Synergy Single source home/near using a  $\mu$ -focus sealed X-ray tube PhotonJet (Cu)  $K\alpha$  radiation source ( $\lambda = 1.54184\text{ \AA}$ ) with collimating mirror monochromators and a Rigaku Oxford Diffraction HyPix 6000E Hybrid Pixel Array Detector. A total of 1796 frames of data were collected using  $\omega$ -scans with a scan width of  $0.5^{\circ}$  at a detector distance of 33.00 mm and beam slit was set to 10.0 mR divergence at 100 percent intensity.

Scans were collected with an exposure time of 0.400 seconds per frame and with an exposure time of 1.440 seconds per frame. The data were collected at an average temperature of 100.0(5) K (min 99.5, max 100.6) using an OxfordCryosystems Cryostream Controller 700 low temperature device.

Data reduction was performed using CrysAlisPro 1.171.42.72a with a per-frame model refinement, 2-cycle 3D peak analysis, and 3D profile fitting used.<sup>8</sup> A CrysAlisPro diffraction orientation matrix type was used.<sup>9</sup> A multi-scan empirical absorption correction using spherical harmonics, implemented in SCALE3 ABSPACK scaling algorithm were applied.

Using Olex2 1.5<sup>10</sup>, the structure was solved with the SHELXT<sup>11</sup> structure solution program using Intrinsic Phasing and refined by full-matrix least-squares on  $F^2$  with anisotropic displacement parameters for the non-H atoms using the SHELXL<sup>12</sup> refinement package using Least Squares minimization. Hydrogens were calculated isotropically in ideal positions. The function  $\sum w(|F_o^2| + |F_c^2|)^2$  was minimized  $w = \frac{1}{[(\sum(F_o^2)) + (0.0722P)^2 + 2.9775P]}$  where  $P = \frac{(|F_o^2| + |F_c^2|)}{3}$ .  $wR(F^2)$  refined to 0.0345, with  $R(F)$  equal to 0.0867 and a goodness of fit on  $F^2$ ,  $S = 1.060$ . Definitions used for  $wR(F^2)$ ,  $R(F)$ , and a goodness of fit on  $F^2$ ,  $S$ , are given in reference 14. Weighting factors were calculated with Olex2 1.5 as 0.0436, 3.4306. Neutral atom scattering factors and values used to calculate the linear absorption coefficient are from the International Tables for X-ray Crystallography.<sup>13</sup>

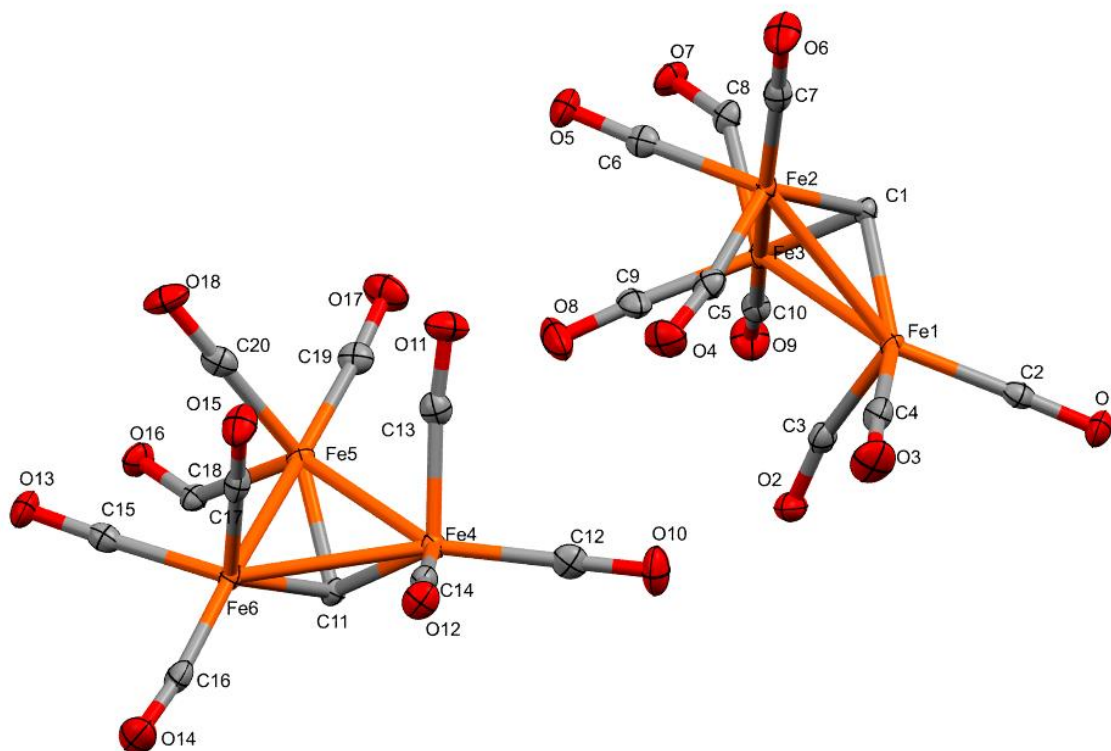


**Figure S37.** Full thermal ellipsoid plot (50% probability) of  $[\text{Fe}_6(\mu_6\text{-C})(\text{CO})_{17}]$  (**3**) with hydrogen atoms omitted for clarity.

### X-ray Diffraction and Crystal Structure Solution of (**4**) Experimental Details

Dark black plate crystals of compound **4** were grown by slow evaporation of a diethyl ether solution at  $-20\text{ }^\circ\text{C}$  under nitrogen atmosphere. The data crystal had the approximate dimensions  $0.32 \times 0.26 \times 0.055\text{ mm}^3$ .

The data were collected on an XtaLAB Synergy Single source home/near using a  $\mu$ -focus sealed X-ray tube PhotonJet (Cu)  $\text{K}\alpha$  radiation source ( $\lambda = 1.54184\text{ \AA}$ ) with collimating mirror monochromators and a Rigaku Oxford Diffraction HyPix 6000E Hybrid Pixel Array Detector. A total of 5206 frames of data were collected using  $\omega$ -scans with a scan width of  $0.5^\circ$  at a detector distance of 33.00 mm and beam slit was set to 10.0 mR divergence at 100 percent intensity. Scans were collected with an exposure time of 4 seconds per frame for frames collected with a detector offset of  $\pm 48.294^\circ$ , and scans were collected with an exposure time of 12 seconds per frame with frames collected with a detector offset of  $\pm 104.518^\circ$ . The data were collected at an average temperature of  $100.0(5)\text{ K}$  (min 99.5, max 100.6) using an OxfordCryosystems Cryostream Controller 700 low temperature device.

Data reduction was performed using CrysAlisPro 1.171.42.72a with a per-frame model refinement, 2-cycle 3D peak analysis, and 3D profile fitting used.<sup>8</sup> A CrysAlisPro diffraction orientation matrix type was used.<sup>9</sup> A multi-scan empirical absorption correction using spherical harmonics, implemented in SCALE3 ABSPACK scaling algorithm were applied.

Using Olex2 1.5<sup>10</sup>, the structure was solved with the SHELXT<sup>11</sup> structure solution program using Intrinsic Phasing and refined by full-matrix least-squares on  $F^2$  with anisotropic displacement parameters for the non-H atoms using the SHELXL<sup>12</sup> refinement package using Least Squares minimization. Hydrogens were calculated isotropically in ideal positions. Absolute structure flack parameter was determined using 2763 quotients and found as 0.014(5).<sup>14</sup> The function  $\sum w(|F_o^2| + |F_c^2|)^2$  was minimized  $w = \frac{1}{[(\Sigma(F_o^2)) + (0.0722P)^2 + 2.9775P]}$  where  $P = \frac{(|F_o^2| + |F_c^2|)}{3}$ .  $wR(F^2)$  refined to 0.0910, with  $R(F)$  equal to 0.0345 and a goodness of fit on  $F^2$ ,  $S$ , = 1.059. Definitions used for  $wR(F^2)$ ,  $R(F)$ , and a goodness of fit on  $F^2$ ,  $S$ , are given in reference 14. The data were checked for secondary extinction effects, but no correction was necessary. Neutral atom scattering factors and values used to calculate the linear absorption coefficient are from the International Tables for X-ray Crystallography.<sup>13</sup>

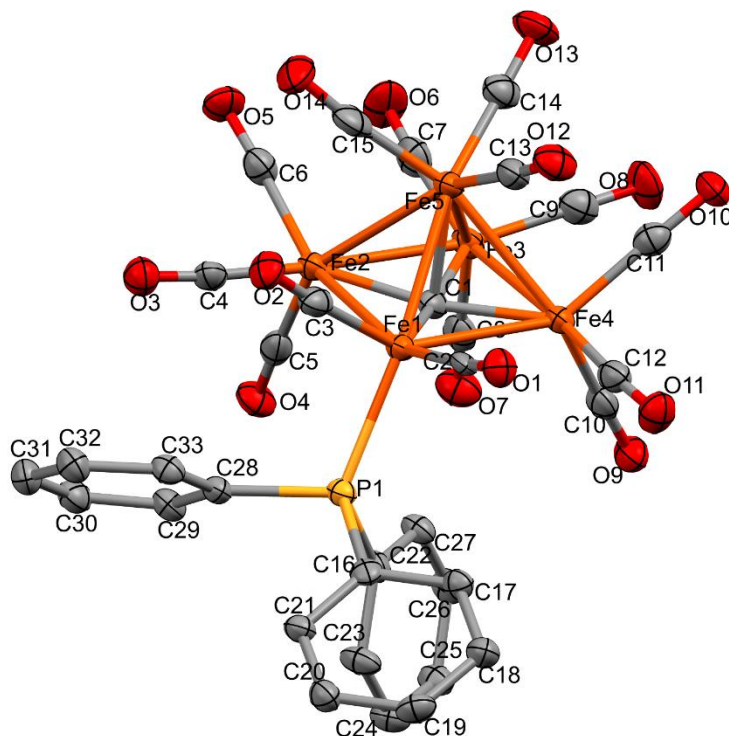


**Figure S38.** Full thermal ellipsoid plot (50% probability) of  $[\text{Fe}_5(\mu_5\text{-C})(\text{CO})_{14}\text{PPh}_3]$  (**4**) with hydrogen atoms omitted for clarity.

## X-ray Diffraction and Crystal Structure Solution of (5) Experimental Details

Crystals of **5** were grown as dark red plates from a vapor diffusion of diethyl ether into fluorobenzene. The data crystal had the approximate dimensions:  $0.12 \times 0.06 \times 0.03$  mm.

The data were collected on an XtaLAB Synergy Single source home/near using a  $\mu$ -focus sealed X-ray tube PhotonJet (Cu)  $K\alpha$  radiation source ( $\lambda = 1.54184 \text{ \AA}$ ) with collimating mirror monochromators and a Rigaku Oxford Diffraction HyPix 6000E Hybrid Pixel Array Detector. A total of 2814 frames of data were collected using  $\omega$ -scans with a scan width of  $0.5^\circ$  at a detector distance of 33.00 mm and beam slit was set to 10.0 mR divergence at 100 percent intensity. Scans were collected with an exposure time of 0.44 seconds per frame for frames collected with a detector offset of  $\pm 48.294^\circ$ , and scans were collected with an exposure time of 1.74 seconds per frame with frames collected with a detector offset of  $\pm 104.518^\circ$ . The data were collected at an average temperature of 100.0(5) K (min 99.8, max 100.2) using an OxfordCryosystems Cryostream Controller 700 low temperature device.

Data reduction was performed using CrysAlisPro 1.171.42.72a with a per-frame model refinement, 2-cycle 3D peak analysis, and 3D profile fitting used.<sup>8</sup> A CrysAlisPro diffraction orientation matrix type was used.<sup>9</sup> A numerical absorption correction based on gaussian integration over a multifaceted crystal model with a multi-scan empirical absorption correction using spherical harmonics, implemented in SCALE3 ABSPACK scaling algorithm were applied.

Using Olex2 1.5<sup>10</sup>, the structure was solved with the SHELXT<sup>11</sup> structure solution program using Intrinsic Phasing and refined by full-matrix least-squares on  $F^2$  with anisotropic displacement parameters for the non-H atoms using the SHELXL<sup>12</sup> refinement package using Least Squares minimization. Hydrogens were refined with isotropic displacement parameters. The hydrogen atom bridging Fe1 and Fe2 was observed in a difference electron density map and refined with an isotropic displacement parameter. The function  $\sum w(|F_o^2| + |F_c^2|)^2$  was minimized  $w = \frac{1}{[(\sum(F_o^2)) + (0.0947P)^2 + 2.0813P]}$  where  $P = \frac{(|F_o^2| + |F_c^2|)}{3}$ .  $wR(F^2)$  refined to 0.1375, with R(F) equal to 0.0459 and a goodness of fit on  $F^2$ ,  $S = 1.137$ . Definitions used for  $wR(F^2)$ , R(F), and the goodness of fit on  $F^2$ , S, are given in reference 14. The data were checked for secondary extinction effects, but no correction was necessary. Neutral atom scattering factors and values used to calculate the linear absorption coefficient are from the International Tables for X-ray Crystallography.<sup>13</sup>

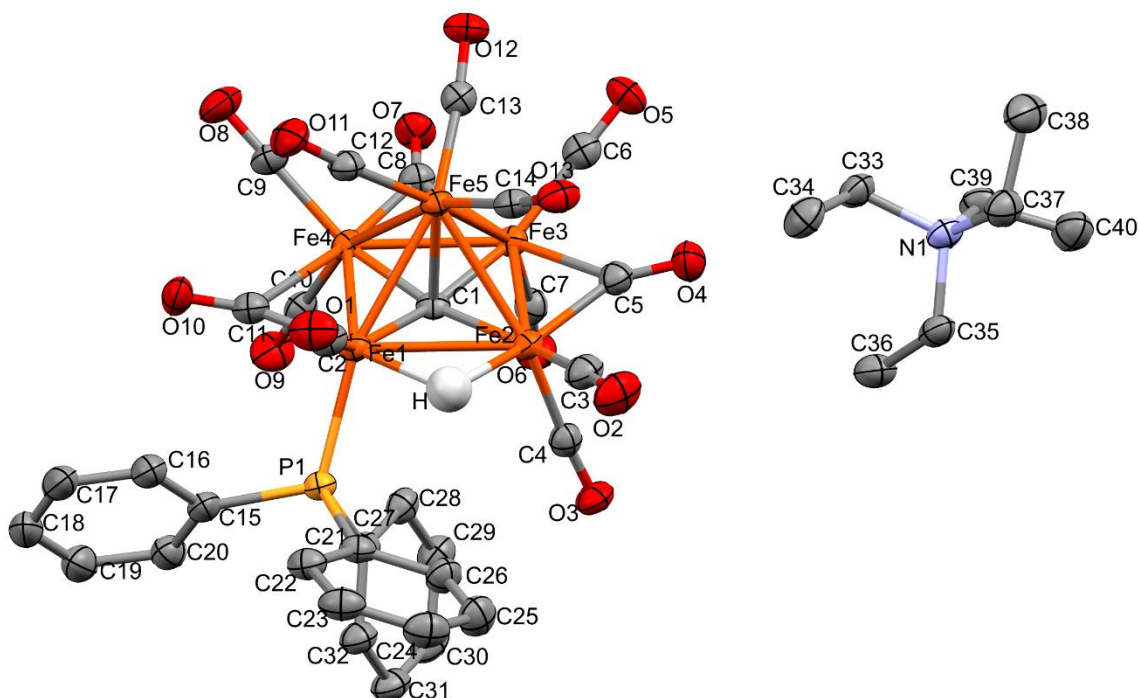


**Figure S39.** Full thermal ellipsoid plot (50% probability) of  $\text{NEt}_4[\text{Fe}_5(\mu_5\text{-C})(\mu_2\text{-H})(\text{CO})_{13}\text{PPh}_3]$  (**5**) with hydrogen atoms omitted for clarity, except the hydride H.

### X-ray Diffraction and Crystal Structure Solution of (**6**) Experimental Details

Compound **6** was purified by fractional crystallization of unreacted phosphine impurities by slow evaporation from diethyl ether at  $-20\text{ }^\circ\text{C}$ . Crystals of **6** were grown as bright red prisms by vapor diffusion of pentane into a saturated solution in diethyl ether at room temperature under inert atmosphere. The data crystal had the approximate dimensions:  $0.243 \times 0.110 \times 0.090\text{ mm}^3$ .

The data were collected on an Agilent Technologies SuperNova Dual Source diffractometer using a  $\mu$ -focus sealed X-ray tube SuperNova (Cu)  $K\alpha$  radiation source ( $\lambda = 1.54184\text{ \AA}$ ) with collimating mirror monochromators and a Rigaku Oxford Diffraction HyPix 6000E Hybrid Pixel Array Detector. A total of 4452 frames of data were collected using  $\omega$ -scans with a scan width of  $0.5^\circ$  at a detector distance of 34.00 mm and beam slit set to 10.0 mR divergence at 100 percent intensity. Scans were collected with an exposure time of 4.0 seconds per frame for frames collected with a detector offset of  $\pm 48.29^\circ$ , and scans were collected with an exposure time of 16.0 seconds per frame with frames collected with a detector offset of  $\pm 104.52^\circ$ . The data were collected at an average temperature of 100.0(5) K using an OxfordCryosystems Cryostream Controller 700 low temperature device.

Data reduction was performed using CrysAlisPro 1.171.42.72a with a per-frame model refinement, 2-cycle 3D peak analysis, and 3D profile fitting used.<sup>8</sup> A CrysAlisPro diffraction orientation matrix type was used.<sup>9</sup> A multiscan empirical absorption correction using spherical harmonics, implemented in SCALE3 ABSPACK scaling algorithm were applied.

Using Olex2 1.5<sup>10</sup>, the structure was solved with the SHELXT<sup>11</sup> structure solution program using Intrinsic Phasing and refined by full-matrix least-squares on  $F^2$  with anisotropic displacement parameters for the non-H atoms using SHELXL<sup>12</sup> refinement package using Least Squares minimization. Bond distances in a disordered solvent diethyl ether molecule were restrained to 1.5 with  $\sigma = 0.02$  for C2A—C1A and C4A—C3A, 2.4 with  $\sigma = 0.04$  for O1A—C1A, C2A—C3A, and O1A—C4A, and 1.45  $\sigma = 0.02$  for O1A—C2A and O1A—C3A. All esds (except the esd in the dihedral angle between two l.s. planes) were estimated using the full covariance matrix. The cell esds were taken into account individually in the estimation of esds in distances, angles and torsion angles; correlations between esds in cell parameters are only used when they are defined by crystal symmetry. An approximate (isotropic) treatment of cell esds is used for estimating esds involving l.s. planes. Hydrogens were calculated in ideal positions isotropically by mixed methods, see .cif file for details.

The function  $\sum w(|F_o^2| + |F_c^2|)^2$  was minimized  $w = \frac{1}{[(\sum(F_o^2)) + (0.0361P)^2 + 3.7934P]}$  where  $P = \frac{(|F_o^2| + |F_c^2|)}{3}$ .  $wR(F^2)$  refined to 0.0800, with R(F) equal to 0.0376 and a goodness of fit on  $F^2$ , S, = 1.099. Definitions used for  $wR(F^2)$ , R(F), and the a goodness of fit on  $F^2$ , S, are given in reference 14. The data were checked for secondary extinction effects, but no correction was necessary. Neutral atom scattering factors and values used to calculate the linear absorption coefficient are from the International Tables for X-ray Crystallography.<sup>13</sup>

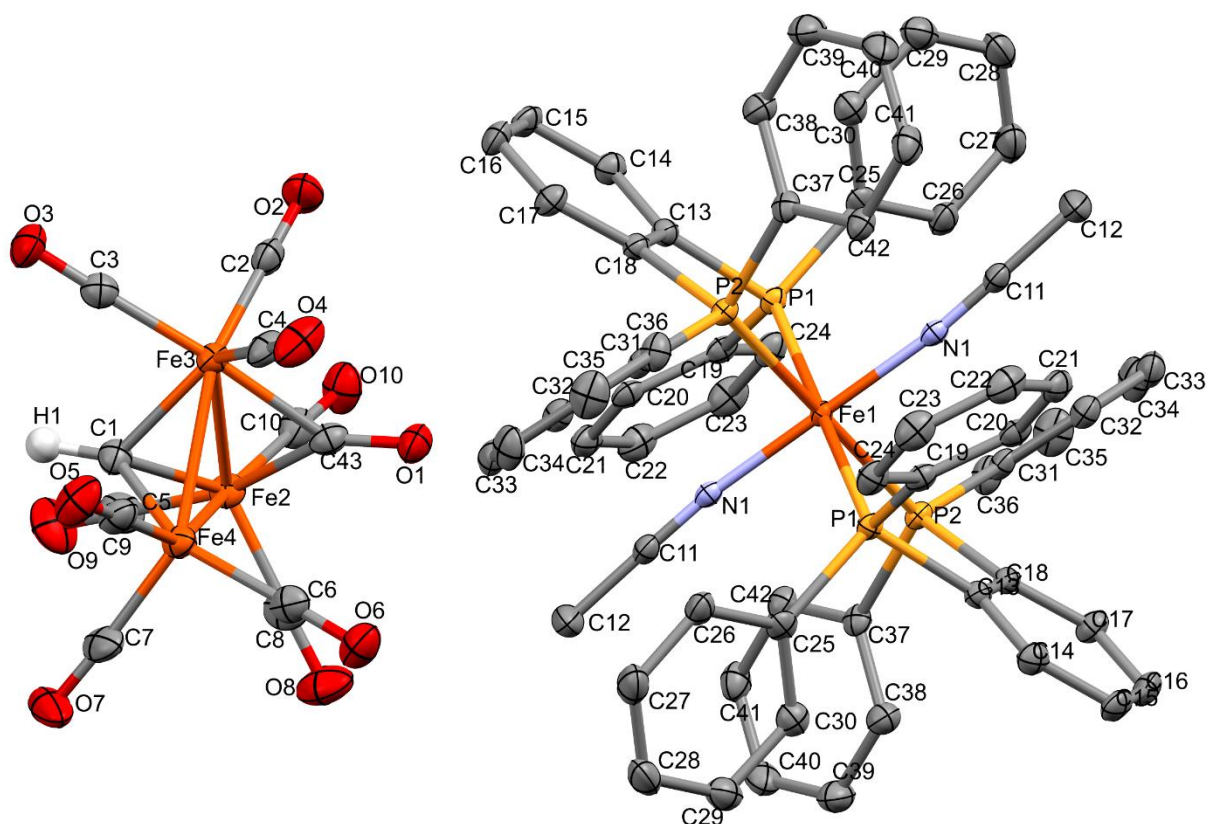


**Figure S40.** Full thermal ellipsoid plot (50% probability) of  $[\text{Fe}_3(\mu_3\text{-CH})(\mu_3\text{-CO})(\text{CO})_9]_2 [(\text{bdpb})_2\text{Fe}(\text{MeCN})_2]$  (**6**) with hydrogen atoms omitted for clarity, except the methyldene hydrogen atom H1. A disordered diethyl ether solvent molecule is omitted for clarity. Shown as a grown structure.

### X-ray Diffraction and Crystal Structure Solution of (**7**) Experimental Details

Crystals of **7** were grown as brown needles by vapor diffusion of pentane into a solution of **7** in toluene at  $-20\text{ }^\circ\text{C}$  under a nitrogen atmosphere. The data crystal had the approximate dimensions:  $0.038 \times 0.054 \times 0.212\text{ mm}^3$ .

The data were collected on an XtaLAB Synergy Single source home/near using a  $\mu$ -focus sealed X-ray tube PhotonJet (Cu)  $\text{K}\alpha$  radiation source ( $\lambda = 1.54184\text{ \AA}$ ) with collimating mirror monochromators and a Rigaku Oxford Diffraction HyPix 6000E Hybrid Pixel Array Detector. A total of 985 frames of data were collected using  $\omega$ -scans with a scan width of  $0.5^\circ$  at a detector distance of 33.00 mm and beam slit was set to 10.0 mR divergence at 100 percent intensity. Scans were collected with an exposure time of 100 seconds per frame for all frames collected (detector offset of  $-55.558^\circ$  and  $+54.308^\circ$ ). The data were collected at an average temperature of 100.02(12) K (min 99.5, max 100.4) using an OxfordCryosystems Cryostream Controller 700 low temperature device. The crystal scattered poorly requiring high scan times, therefore the data collection strategy was set to a lower resolution to make better use of the available instrument time. Data reduction was performed using CrysAlisPro 1.171.42.72a with a per-frame model refinement, 2-cycle 3D peak analysis, and 3D profile fitting used.<sup>8</sup> A CrysAlisPro

diffraction orientation matrix type was used.<sup>9</sup> A multi-scan empirical absorption correction using spherical harmonics, implemented in SCALE3 ABSPACK scaling algorithm were applied.

Using Olex2 1.5<sup>10</sup>, the structure was solved with the SHELXT<sup>11</sup> structure solution program using Intrinsic Phasing and refined by full-matrix least-squares on  $F^2$  with anisotropic displacement parameters for the non-H atoms using the SHELXL<sup>12</sup> refinement package using Least Squares minimization. Hydrogen atoms were not calculated. Three solvent toluene molecules are present, one of which is disordered. The function  $\sum w(|F_o^2| + |F_c^2|)^2$  was minimized  $w = \frac{1}{[(\sum(F_o^2)) + (0.1114P)^2 + 45.3231P]}$  where  $P = \frac{(|F_o^2| + |F_c^2|)}{3}$ .  $wR(F^2)$  refined to 0.2349, with  $R(F)$  equal to 0.0842 and a goodness of fit on  $F^2$ ,  $S$ , = 1.109. Definitions used for  $wR(F^2)$ ,  $R(F)$ , and the a goodness of fit on  $F^2$ ,  $S$ , are given in reference 14. Neutral atom scattering factors and values used to calculate the linear absorption coefficient are from the International Tables for X-ray Crystallography.<sup>13</sup>

Note: The structure of **7** is only satisfactory for determining atom connectivity, and as such no in-depth bond metric analysis is presented. The structure reveals that the linear Triphos stabilizes the Fe cluster via chelation, but the inter-phosphine atom distances appear to favor multiple binding events at a single iron, likely inducing cluster disproportionation and functionalization of the carbide site. Nonetheless, the functionalization of the carbide by P-C coordination from the free linear Triphos arm is notable.

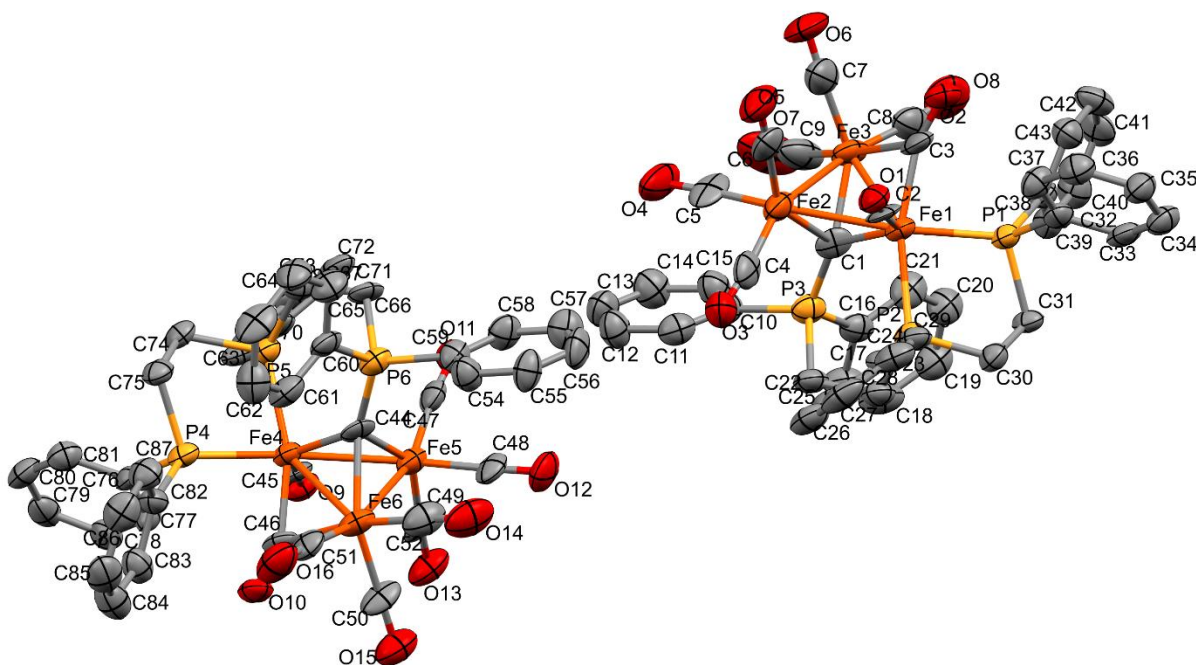


**Figure S41.** Full thermal ellipsoid plot (50% probability) showing the connectivity of  $[\text{Fe}_3\{\mu_3\text{-C-P}(\text{Ph}_2)\text{C}_2\text{H}_4(\text{PhP})\text{C}_2\text{H}_4(\text{PPh}_2)\}]$  (**7**). H atoms omitted. Three toluene solvent molecules, one disordered, are omitted for clarity.

## X-ray Diffraction and Crystal Structure Solution of **8** Experimental Details

Small grey-green needle crystals of **8** were grown by slow evaporation from a solution in pentane under a nitrogen atmosphere at  $-20\text{ }^{\circ}\text{C}$ . The data crystal had the approximate dimensions:  $0.045 \times 0.059 \times 0.136\text{ mm}^3$ .

The data were collected on an XtaLAB Synergy Single source home/near using a  $\mu$ -focus sealed X-ray tube PhotonJet (Cu)  $K\alpha$  radiation source ( $\lambda = 1.54184\text{ \AA}$ ) with collimating mirror monochromators and a Rigaku Oxford Diffraction HyPix 6000E Hybrid Pixel Array Detector. A total of 2732 frames of data were collected using  $\omega$ -scans with a scan width of  $0.5^{\circ}$  at a detector distance of 33.00 mm and beam slit was set to 10.0 mR divergence at 100 percent intensity. Scans were collected with an exposure time of 30 seconds per frame for frames collected with a detector offset of  $\pm 48.570^{\circ}$ , and scans were collected with an exposure time of 40 seconds per frame with frames collected with a detector offset of  $\pm 105.116^{\circ}$ . The data were collected at an average temperature of 100.02(12) K (min 99.5, max 100.4) using an OxfordCryosystems Cryostream Controller 700 low temperature device. The data crystal scattered poorly. Data collection was stopped to make better use of the instrument time. A resolution cutoff of 1.0 angstrom was applied to the data.

Data reduction was performed using CrysAlisPro 1.171.42.72a with a per-frame model refinement, 2-cycle 3D peak analysis, and 3D profile fitting used.<sup>8</sup> Reflections were merged by SHELXL according to the crystal class for the calculation of statistics and refinement. Structure factors included contributions from the .fab file. A CrysAlisPro diffraction orientation matrix type was used.<sup>9</sup> A numerical absorption correction based on gaussian integration over a multifaceted crystal model with an empirical absorption correction using spherical harmonics, implemented in SCALE3 ABSPACK scaling algorithm were applied.

Using Olex2 1.5<sup>10</sup>, the structure was solved with the SHELXT<sup>11</sup> structure solution program using Intrinsic Phasing and refined by full-matrix least-squares on  $F^2$  with anisotropic displacement parameters for the non-H atoms using the SHELXL<sup>12</sup> refinement package using Least Squares minimization. Hydrogens were calculated in ideal position with fixed  $U_{\text{iso}}$  set to 1.2 times for all C(H) groups and all C(H,H) groups, and to 1.5 times for all (C(H,H,H)) groups. An idealized Methyl was refined as rotating group: C19(H19A, H19B, H19C). The function  $\sum w(|F_o^2| + |F_c^2|)^2$  was minimized  $w = \frac{1}{[(\sum(F_o^2)) + (0.1046P)^2 + 4.8603P]}$  where  $P = \frac{(|F_o^2| + |F_c^2|)}{3}$ .  $wR(F^2)$  refined to 0.1826, with  $R(F)$  equal to 0.1983 and a goodness of fit on  $F^2$ ,  $S$ , = 1.066. Definitions used for  $wR(F^2)$ ,  $R(F)$ , and the a goodness of fit on  $F^2$ ,  $S$ , are given in reference 14. The data were checked for secondary extinction effects, but no correction was necessary. Neutral atom scattering factors and values used to calculate the linear absorption coefficient are from the International Tables for X-ray Crystallography.<sup>13</sup> A molecule of n-pentane was disordered. The molecule could not be adequately modeled. Its contribution to the scattering factors was removed using ByPass as utilized in Olex2 1.5<sup>10</sup>.

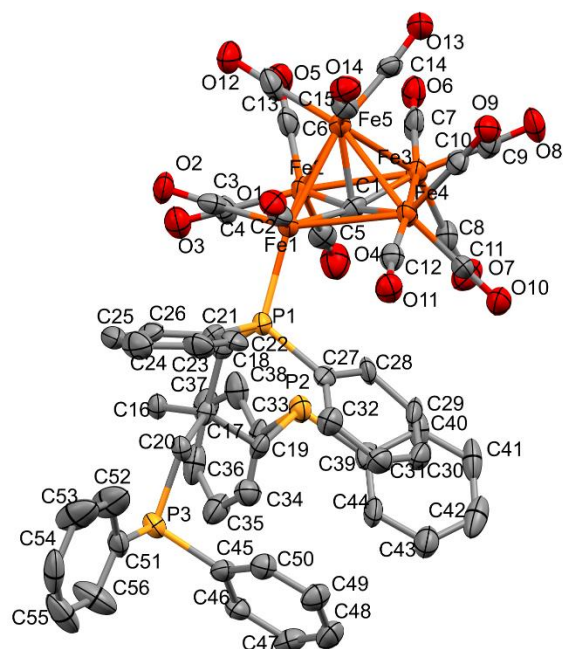


**Figure S42.** Full thermal ellipsoid plot (50% probability) of  $[\text{Fe}_5(\mu_5\text{-C})(\kappa_1\text{-Triphos})(\text{CO})_{14}]$  (**8**) with hydrogen atoms omitted for clarity.

#### X-ray Diffraction and Crystal Structure Solution of (**9**) Experimental Details

Small, metallic, greenish black block crystals of **9** were grown by slow evaporation from a solution in diethyl ether at room temperature under a nitrogen atmosphere. The data crystal had the approximate dimensions:  $0.141 \times 0.227 \times 0.426 \text{ mm}^3$ .

The data were collected on an Agilent Technologies SuperNova Dual Source diffractometer using a  $\mu$ -focus sealed X-ray tube SuperNova (Cu)  $K\alpha$  radiation source ( $\lambda = 1.54184 \text{ \AA}$ ) with collimating mirror monochromators and a CCD plate AtlasS2 Detector. A total of 1053 frames of data were collected using  $\omega$ -scans with a scan width of  $1.0^\circ$  at a detector distance of 54.00 mm. Scans were collected with an exposure time of 30.0 seconds per frame for frames collected with a detector offset of  $\pm 39.84^\circ$ , and scans were collected with an exposure time of 37.5 seconds per frame with frames collected with a detector offset of  $\pm 107.09^\circ$ . The data were collected at an average temperature of 100.02(12) K (min 99.9, max 100.1) using an OxfordCryosystems Cryostream Controller 700 low temperature device.

Data reduction was performed using CrysAlisPro 1.171.42.72a with 3D profile fitting used.<sup>8</sup> A CrysAlisPro diffraction orientation matrix type was used.<sup>9</sup> A multiscan empirical absorption correction using spherical harmonics, implemented in SCALE3 ABSPACK scaling algorithm were applied.

Using Olex2 1.5<sup>10</sup>, the structure was solved with the SHELXT<sup>11</sup> structure solution program using Intrinsic Phasing and refined by full-matrix least-squares on  $F^2$  with anisotropic displacement parameters for the non-H atoms using the SHELXL<sup>12</sup> refinement package using Least Squares minimization. Hydrogens were calculated in ideal position with fixed  $U_{\text{iso}}$  set to 1.2 times for all C(H) groups and all C(H,H) groups, and to 1.5 times for all (C(H,H,H)) groups (methyl hydrogens.) The function  $\sum w(|F_o^2| + |F_c^2|)^2$  was minimized  $w = \frac{1}{[(\sum(F_o^2)) + (0.1259P)^2 + 13.9167P]}$  where  $P = \frac{(|F_o^2| + |F_c^2|)}{3}$ .  $wR(F^2)$  refined to 0.0804, with  $R(F)$  equal to 0.02005 and a goodness of fit on  $F^2$ ,  $S = 1.027$ . Definitions used for  $wR(F^2)$ ,  $R(F)$ , and the a goodness of fit on  $F^2$ ,  $S$ , are given in reference 14. The data were checked for secondary extinction effects, but no correction was necessary. Neutral atom scattering factors and values used to calculate the linear absorption coefficient are from the International Tables for X-ray Crystallography.<sup>13</sup> A toluene solvent molecule is disordered around a crystallographic inversion center.

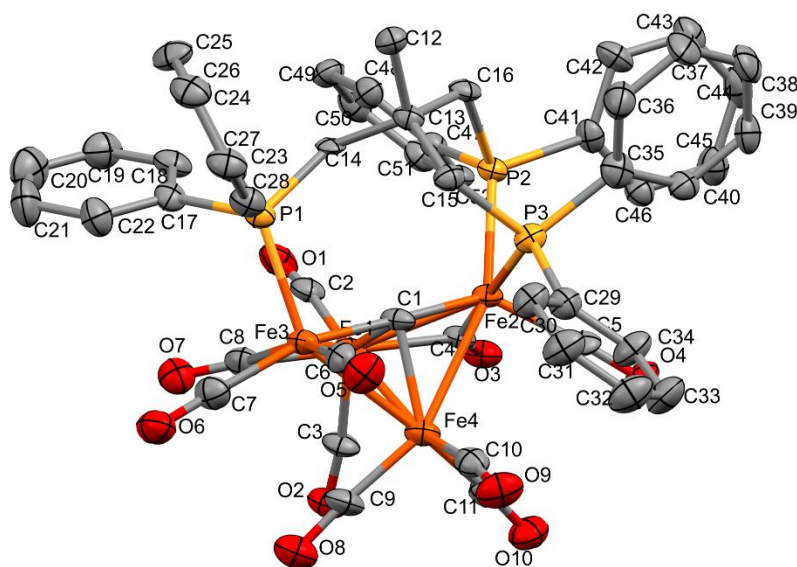


**Figure S43.** Full thermal ellipsoid plot (50% probability) of  $[\text{Fe}_4(\mu_4\text{-C})(\kappa_3\text{-Triphos})(\text{CO})_{10}]$  (**9**) with hydrogen atoms omitted for clarity.

#### X-ray Diffraction and Crystal Structure Solution of (**10**) Experimental Details

Large, clear dark red needle crystals of **10** were grown by vapor diffusion of pentane into toluene at room temperature under nitrogen atmosphere. The sample crystal was cut to a smaller data crystal of the approximate dimensions:  $0.141 \times 0.227 \times 0.426 \text{ mm}^3$ .

The data were collected on an Agilent Technologies SuperNova Dual Source diffractometer using a  $\mu$ -focus sealed X-ray tube SuperNova (Cu)  $K\alpha$  radiation source ( $\lambda = 1.54184 \text{ \AA}$ ) with collimating mirror monochromators and a

Rigaku Oxford Diffraction HyPix 6000E Hybrid Pixel Array Detector. A total of 5414 frames of data were collected using  $\omega$ -scans with a scan width of  $0.5^\circ$  at a detector distance of 34.00 mm and beam slit was set to 10.0 mR divergence at 100 percent intensity. Scans were collected with an exposure time of 1.3 seconds per frame for frames collected with a detector offset of  $\pm 48.449^\circ$ , and scans were collected with an exposure time of 5.2 seconds per frame with frames collected with a detector offset of  $\pm 107.750^\circ$ . The data were collected at an average temperature of 100.0(4) K (min 99.9, max 100.1) using an OxfordCryosystems Cryostream Controller 700 low temperature device.

Data reduction was performed using CrysAlisPro 1.171.42.72a with a per-frame model refinement, 2-cycle 3D peak analysis, and 3D profile fitting used.<sup>8</sup> A CrysAlisPro diffraction orientation matrix type was used.<sup>9</sup> A multiscan empirical absorption correction using spherical harmonics, implemented in SCALE3 ABSPACK scaling algorithm were applied.

Using Olex2 1.5<sup>10</sup>, the structure was solved with the SHELXT<sup>11</sup> structure solution program using Intrinsic Phasing and refined by full-matrix least-squares on  $F^2$  with anisotropic displacement parameters for the non-H atoms using SHELXL<sup>12</sup> refinement package using Least Squares minimization. A CO and MeCN both partially occupy a coordination site (CO: 0.578, MeCN: 0.422) to Fe1. Restrained distances for the CO bond C54-O13 and the nitrile bond N1-C55 were set to 1.14 with  $\sigma = 0.01$ . Restrained distance for the MeCN C55-C56 was set to 1.45 with  $\sigma = 0.01$ . The C-C bonds of a disordered toluene solvent molecule were also restrained (see cif for details). Hydrogens were calculated in ideal positions isotropically. The function  $\sum w(|F_o^2| + |F_c^2|)^2$  was minimized  $w = \frac{1}{[(\sum(F_o^2)) + (0.0455P)^2 + 1.6688P]}$  where  $P = \frac{(|F_o^2| + |F_c^2|)}{3}$ .  $wR(F^2)$  refined to 0.0912, with  $R(F)$  equal to 0.0382 and a goodness of fit on  $F^2$ ,  $S = 1.060$ . Definitions used for  $wR(F^2)$ ,  $R(F)$ , and the a goodness of fit on  $F^2$ ,  $S$ , are given in reference 14. The data were checked for secondary extinction effects, but no correction was necessary. Neutral atom scattering factors and values used to calculate the linear absorption coefficient are from the International Tables for X-ray Crystallography.<sup>13</sup> A toluene solvent molecule is disordered around a crystallographic inversion center.

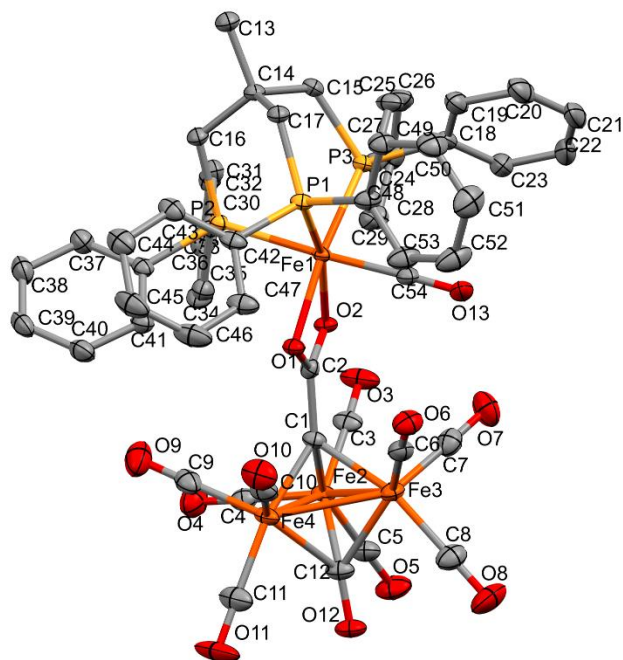


**Figure S44.** Full thermal ellipsoid plot (50% probability) of  $[\text{Fe}_3(\text{CO})_8(\mu_3\text{-CO})(\mu_3\text{-aceto-}\kappa_2\text{-O})\text{Fe}(\text{CO})(\kappa_3\text{-Triphos})]$  (**10**) with hydrogen atoms omitted for clarity. A disordered toluene molecule is omitted for clarity.

#### X-ray Diffraction and Crystal Structure Solution of (**11**) Experimental Details

Crystals **11** were grown as dichromic green and yellow (appearing brown when large enough to be opaque) prisms by cooling a solution of **9** in toluene to  $-20\text{ }^\circ\text{C}$  for over two months. The data crystal had the approximate dimensions:  $0.223 \times 0.103 \times 0.049\text{ mm}^3$ .

The data were collected on an XtaLAB Synergy Single source home/near using a  $\mu$ -focus sealed X-ray tube PhotonJet (Cu)  $K\alpha$  radiation source ( $\lambda = 1.54184\text{ \AA}$ ) with collimating mirror monochromators and a Rigaku Oxford Diffraction HyPix 6000E Hybrid Pixel Array Detector. A total of 5210 frames of data were collected using  $\omega$ -scans with a scan width of  $0.5^\circ$  at a detector distance of 33.00 mm and beam slit was set to 10.0 mR divergence at 100 percent intensity. Scans were collected with an exposure time of 5 seconds per frame for frames collected with a detector offset of  $\pm 48.294^\circ$ , and scans were collected with an exposure time of 12 seconds per frame with frames collected with a detector offset of  $\pm 104.518^\circ$ . The data were collected at an average temperature of  $100.0(4)\text{ K}$  (min 99.7, max 100.3) using an OxfordCryosystems Cryostream Controller 700 low temperature device.

Data reduction was performed using CrysAlisPro 1.171.42.72a with a per-frame model refinement, 2-cycle 3D peak analysis, and 3D profile fitting used.<sup>8</sup> A CrysAlisPro diffraction orientation matrix type was used.<sup>9</sup> A numerical absorption correction based on gaussian integration over a multifaceted crystal model with an empirical absorption correction using spherical harmonics, implemented in SCALE3 ABSPACK scaling algorithm were applied.

Using Olex2 1.5<sup>10</sup>, the structure was solved with the SHELXT<sup>11</sup> structure solution program using Intrinsic Phasing and refined by full-matrix least-squares on  $F^2$  with anisotropic displacement parameters for the non-H atoms using the SHELXL<sup>12</sup> refinement package using Least Squares minimization. There is a disordered toluene molecule residing around an inversion center. Hydrogens were calculated in ideal position with fixed  $U_{iso}$  set to 1.2 times for all C(H) groups and all C(H,H) groups, and to 1.5 times for all (C(H,H,H)) groups (methyl hydrogens.) The function  $\sum w(|F_o^2| + |F_c^2|)^2$  was minimized  $w = \frac{1}{[(\Sigma(F_o^2)) + (0.0349P)^2 + 3.5472P]}$  where  $P = \frac{(|F_o^2| + |F_c^2|)}{3}$ .  $wR(F^2)$  refined to 0.0735, with  $R(F)$  equal to 0.0288 and a goodness of fit on  $F^2$ ,  $S = 1.072$ . Definitions used for  $wR(F^2)$ ,  $R(F)$ , and the a goodness of fit on  $F^2$ ,  $S$ , are given in reference 14.<sup>15</sup> The data were checked for secondary extinction effects, but no correction was necessary. Neutral atom scattering factors and values used to calculate the linear absorption coefficient are from the International Tables for X-ray Crystallography.<sup>13</sup> A toluene solvent molecule is disordered around a crystallographic inversion center.

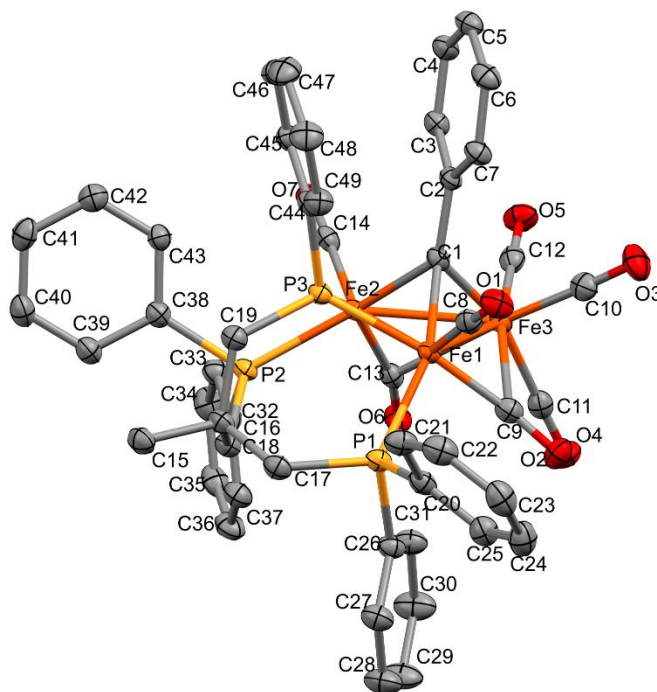


**Figure S45.** Full thermal ellipsoid plot (50% probability) of  $[\text{Fe}_3(\mu_3\text{-CPh})\{\text{Triphos}(\text{PPh}_2)_2(\text{PPh})\}(\text{CO})_7]$  (**11**). One disordered toluene molecule and H atoms are omitted for clarity.

**Table S2.** Summary of Crystal Data Intensity collection and structural refinement parameters for  $\text{Fe}_6\text{C}(\text{CO})_{17}$  (**3**).

<b>3</b>	
<b>Empirical formula</b>	$\text{C}_{36}\text{Fe}_{12}\text{O}_{34}$
<b>FW</b>	1646.56
<b>T (K)</b>	100.15
<b>Crystal system</b>	monoclinic
<b>Space group</b>	P2/c
<b>a (Å)</b>	16.9478(3)
<b>a (Å)</b>	8.96230(10)
<b>c (Å)</b>	17.1515(3)
<b><math>\alpha</math> (°)</b>	90
<b><math>\beta</math> (°)</b>	115.433(2)
<b><math>\gamma</math> (°)</b>	90
<b>Volume (Å<sup>3</sup>)</b>	2352.69(7)
<b>Z</b>	2
<b><math>\rho_{\text{calc}}</math> (g/cm<sup>3</sup>)</b>	2.324
<b><math>\mu</math> (mm<sup>-1</sup>)</b>	29.717
<b>F(000)</b>	1600.0
<b>Crystal size (mm<sup>3</sup>)</b>	0.15 × 0.11 × 0.07
<b>Radiation</b>	Cu K $\alpha$ ( $\lambda = 1.54184$ )
<b>2<math>\theta</math> range for data collection/°</b>	5.774 to 153.618
<b>Index ranges</b>	-21 ≤ h ≤ 13, -11 ≤ k ≤ 9, -20 ≤ l ≤ 21
<b>Reflections collected</b>	15524
<b>GOF on F<sup>2</sup></b>	1.059
<b>Final R indexes [I &gt;= 2<math>\sigma</math> (I)]</b>	R <sub>1</sub> = 0.0345, wR <sub>2</sub> = 0.0867
<b>Final R indexes [all data]</b>	R <sub>1</sub> = 0.0416, wR <sub>2</sub> = 0.0910

**Table S3.** Summary of Crystal Data Intensity collection and structural refinement parameters for [Fe<sub>5</sub>(μ<sub>5</sub>-C)(CO)<sub>14</sub>(PPh<sub>3</sub>)] (**4**), Et<sub>4</sub>N[Fe<sub>5</sub>(μ<sub>5</sub>-C)(μ<sub>2</sub>-H)(CO)<sub>13</sub>PPh<sub>3</sub>] (**5**), [Fe<sub>3</sub>(μ<sub>3</sub>-CH)(μ<sub>3</sub>-CO)(CO)<sub>9</sub>]<sub>2</sub>[(bdpb)<sub>2</sub>Fe(MeCN)<sub>2</sub>] (**6**), and [Fe<sub>3</sub>{μ<sub>3</sub>-C-P(Ph<sub>2</sub>)C<sub>2</sub>H<sub>4</sub>(PhP)C<sub>2</sub>H<sub>4</sub>(PPh<sub>2</sub>)}] (**7**).

	<b>4</b>	<b>5</b>	<b>6</b>	<b>7</b>
<b>Empirical formula</b>	C <sub>33</sub> H <sub>15</sub> Fe <sub>5</sub> O <sub>14</sub> P	C <sub>40</sub> H <sub>36</sub> Fe <sub>5</sub> NO <sub>13</sub> P	C <sub>45</sub> H <sub>33</sub> Fe <sub>3.5</sub> NO <sub>10.5</sub> P <sub>2</sub>	C <sub>107</sub> H <sub>90</sub> Fe <sub>6</sub> O <sub>16</sub> P <sub>6</sub>
<b>FW</b>	945.67	1048.92	1013.14	2152.70
<b>T (K)</b>	100.0(8)	100.0(5)	100.15	100.15
<b>Crystal system</b>	monoclinic	Monoclinic	monoclinic	Triclinic
<b>Space group</b>	Pn	P2 <sub>1</sub> /c	P2 <sub>1</sub> /c	P-1
<b>a (Å)</b>	9.5978(2)	17.1733(3)	12.61041(12)	10.0809(6)
<b>a (Å)</b>	11.8597(2)	12.1213(2)	15.93666(13)	20.0100(11)
<b>c (Å)</b>	14.5875(3)	20.6329(3)	21.4660(2)	25.3574(12)
<b>α (°)</b>	90	90	90	101.231(5)
<b>β (°)</b>	90.663(2)	103.2791(16)	94.5540(8)	99.701(5)
<b>γ (°)</b>	90	90	90	104.279(5)
<b>Volume (Å<sup>3</sup>)</b>	1660.34(6)	4180.17(13)	4300.36(7)	4734.3(5)
<b>Z</b>	2	4	4	2
<b>ρ<sub>calc</sub> (g/cm<sup>3</sup>)</b>	1.892	1.667	1.565	1.510
<b>μ (mm<sup>-1</sup>)</b>	18.203	14.509	10.529	8.695
<b>F(000)</b>	940.0	2128.0	2060.0	2212.0
<b>Crystal size (mm<sup>3</sup>)</b>	1.145 × 0.688 × 0.149	0.32 × 0.26 × 0.055	0.090 × 0.110 × 0.243	0.038 × 0.054 × 0.212
<b>Radiation</b>	Cu Kα (λ = 1.54184)	Cu Kα (λ = 1.54184)	CuKα (λ = 1.54184)	CuKα (λ = 1.54184)
<b>2θ range for data collection/°</b>	7.454 to 153.638	5.288 to 152.98	6.916 to 136.502	9.182 to 103.904
<b>Index ranges</b>	-12 ≤ h ≤ 12, -14 ≤ k ≤ 14, -17 ≤ l ≤ 18	-21 ≤ h ≤ 21, -15 ≤ k ≤ 14, -22 ≤ l ≤ 25	-15 ≤ h ≤ 14, -19 ≤ k ≤ 19, -25 ≤ l ≤ 25	-10 ≤ h ≤ 10, -16 ≤ k ≤ 20, -25 ≤ l ≤ 23
<b>Reflections collected</b>	29237	63765	76437	14550
<b>GOF on F<sup>2</sup></b>	1.137	1.137	1.099	1.109
<b>Final R indexes [I ≥ 2σ (I)]</b>	R <sub>1</sub> = 0.0410, wR <sub>2</sub> = 0.1174	R <sub>1</sub> = 0.0460, wR <sub>2</sub> = 0.1375	R <sub>1</sub> = 0.0376, wR <sub>2</sub> = 0.0800	R <sub>1</sub> = 0.0842, wR <sub>2</sub> = 0.2349
<b>Final R indexes [all data]</b>	R <sub>1</sub> = 0.0427, wR <sub>2</sub> = 0.1226	R <sub>1</sub> = 0.0484, wR <sub>2</sub> = 0.1401	R <sub>1</sub> = 0.0413, wR <sub>2</sub> = 0.0815	R <sub>1</sub> = 0.1148, wR <sub>2</sub> = 0.2546

**Table S4.** Summary of Crystal Data Intensity collection and structural refinement parameters for [Fe<sub>5</sub>(μ<sub>5</sub>-C)(CO)<sub>14</sub>(Triphos)] (**8**), [Fe<sub>4</sub>(μ<sub>4</sub>-C)(μ<sub>2</sub>-CO)<sub>2</sub>(CO)<sub>8</sub>(κ<sub>3</sub>-Triphos)] (**9**), [Fe<sub>3</sub>(CO)<sub>9</sub>(μ<sub>3</sub>-aceto-κ<sub>2</sub>O)Fe(CO)(κ<sub>3</sub>-triphos)] (**10**), [Fe<sub>3</sub>(μ<sub>3</sub>-CPh){Triphos(PPh<sub>2</sub>)<sub>2</sub>(PPh)}(CO)<sub>7</sub>] (**11**).

	<b>8</b>	<b>9</b>	<b>10</b>	<b>11</b>
<b>Empirical formula</b>	C <sub>56</sub> H <sub>37</sub> Fe <sub>5</sub> O <sub>14</sub> P <sub>3</sub>	C <sub>52</sub> H <sub>39</sub> Fe <sub>4</sub> O <sub>10</sub> P <sub>3</sub>	C <sub>61.42</sub> H <sub>48.27</sub> Fe <sub>4</sub> N <sub>0.42</sub> O <sub>12.58</sub> P <sub>3</sub>	C <sub>53.5</sub> H <sub>42.5</sub> Fe <sub>3</sub> O <sub>7</sub> P <sub>3</sub>
<b>FW</b>	1306.01	1140.14	1309.78	1045.82
<b>T (K)</b>	100.15	100.02(12)	100.02(12)	100.0(4)
<b>Crystal system</b>	triclinic	Monoclinic	triclinic	monoclinic
<b>Space group</b>	P-1	P2 <sub>1</sub> /c	P-1	P2 <sub>1</sub> /n
<b>a (Å)</b>	9.4782(8)	10.2347(3)	12.9515(3)	12.22120(10)
<b>a (Å)</b>	15.6679(7)	24.9460(6)	13.3229(3)	19.70640(10)
<b>c (Å)</b>	18.6940(10)	19.6152(6)	19.7999(3)	19.6407(2)
<b>α (°)</b>	85.773(5)	90	107.235(2)	90
<b>β (°)</b>	76.692(7)	104.582(3)	91.498(2)	98.7080(10)
<b>γ (°)</b>	89.678(5)	90	117.671(2)	90
<b>V (Å<sup>3</sup>)</b>	2694.0(3)	4846.7(2)	2835.23(11)	4675.66(7)
<b>Z</b>	2	4	2	4
<b>ρ<sub>calc</sub> (g/cm<sup>3</sup>)</b>	1.610	1.563	1.534	1.486
<b>μ (mm<sup>-1</sup>)</b>	11.949	10.843	9.388	8.770
<b>F(000)</b>	1320.0	2320.0	1339.0	2146.0
<b>Size (mm<sup>3</sup>)</b>	0.029 × 0.044 × 0.168	0.141 × 0.227 × 0.426	0.096 × 0.117 × 0.189	0.223 × 0.103 × 0.049
<b>Radiation</b>	CuKα (λ = 1.54184)	Cu Kα (λ = 1.54184)	CuKα (λ = 1.54184)	CuKα (λ = 1.54184)
<b>2θ range /°</b>	5.656 to 100.862	5.85 to 147	7.75 to 154.04	6.39 to 152.928
<b>Index ranges</b>	-9 ≤ h ≤ 8, -14 ≤ k ≤ 15, -17 ≤ l ≤ 18	-12 ≤ h ≤ 12, -29 ≤ k ≤ 30, -24 ≤ l ≤ 15	-16 ≤ h ≤ 14, -16 ≤ k ≤ 16, -25 ≤ l ≤ 24	-15 ≤ h ≤ 15, -24 ≤ k ≤ 21, -24 ≤ l ≤ 24
<b>N<sub>ref</sub> (all)</b>	16464	24734	52147	88271
<b>GOF on F<sup>2</sup></b>	1.059	1.044	1.060	1.072
<b>Final R indexes [I &gt;= 2σ (I)]</b>	R <sub>1</sub> = 0.0699, wR <sub>2</sub> = 0.1843	R <sub>1</sub> = 0.0804, wR <sub>2</sub> = 0.2005	R <sub>1</sub> = 0.0382, wR <sub>2</sub> = 0.0912	R <sub>1</sub> = 0.0288, wR <sub>2</sub> = 0.0735
<b>Final R indexes [all data]</b>	R <sub>1</sub> = 0.0949, wR <sub>2</sub> = 0.2003	R <sub>1</sub> = 0.1209, wR <sub>2</sub> = 0.2307	R <sub>1</sub> = 0.0432, wR <sub>2</sub> = 0.0936	R <sub>1</sub> = 0.0305, wR <sub>2</sub> = 0.0743

**Table S5.** Bond lengths for Fe<sub>6</sub>C(μ<sub>2</sub>-C)(CO)<sub>16</sub> (**3**).<sup>1</sup><sub>-X,+Y,1/2-Z</sub>; <sup>2</sup><sub>1-X,+Y,3/2-Z</sub>

	<b>Bond (3)</b>	<b>Length (Å)</b>
Fe-(μ <sub>6</sub> -C)	Fe1-C1	1.890(3)
	Fe2-C1	1.9129(5)
	Fe3-C1	1.891(3)
	Fe4-C11	1.899(3)
	Fe5-C11	1.899(3)
	Fe6-C11	1.9099(5)
C-O	C2-O1	1.148(4)
	C3-O2	1.142(4)
	C4-O3	1.134(4)
	C5-O4	1.138(4)
	C6-O5	1.143(4)
	C7-O6	1.136(4)
	C8-O7	1.160(5)
	C9-O8	1.135(4)
	C10-O9	1.132(4)
	C12-O10	1.143(4)
	C13-O11	1.139(4)
	C14-O12	1.149(4)
	C15-O13	1.140(4)
	C16-O14	1.141(4)
	C17-O15	1.130(4)
	C18-O16	1.158(5)
C19-O17	1.139(4)	
C20-O18	1.139(4)	
Fe-CO	Fe1-C2	1.790(3)
	Fe1-C3	1.814(3)
	Fe1-C4	1.814(4)
	Fe2-C5	1.810(3)
	Fe2-C6	1.972(3)
	Fe2-C7	1.811(3)
	Fe3-C8	1.975(3)
	Fe3-C9	1.798(3)
	Fe3-C10	1.793(3)
	Fe4-C12	1.808(3)
	Fe4-C13	1.815(3)
	Fe4-C14	1.785(3)
	Fe6-C15	1.798(3)
	Fe6-C16	1.806(3)
	Fe6-C17	1.815(3)
	Fe5-C18	1.967(3)
Fe5-C19	1.799(3)	
Fe5-C20	1.788(3)	
Fe-Fe	Fe1-Fe2	2.7703(6)
	Fe1-Fe3	2.7178(6)
	Fe1-Fe2 <sup>1</sup>	2.6999(6)
	Fe1-Fe1 <sup>1</sup>	2.6469(9)
	Fe2-Fe3 <sup>1</sup>	2.6224(6)
	Fe3-Fe2	2.6224(6)
	Fe3-Fe3 <sup>1</sup>	2.6116(9)
	Fe6-Fe4	2.7003(6)
	Fe6-Fe5	2.6284(6)
Fe4-Fe6 <sup>2</sup>	2.7699(6)	

Fe4–Fe4 <sup>2</sup>	2.6335(9)
Fe5–Fe4	2.7519(6)
Fe5–Fe5 <sup>2</sup>	2.6032(9)
Fe5–Fe6 <sup>2</sup>	2.6725(7)

**Table S6.** Bond angles for Fe<sub>6</sub>C(CO)<sub>17</sub> (**3**). <sup>1</sup><sub>-X,+Y,1/2-Z</sub>; <sup>2</sup><sub>1-X,+Y,3/2-Z</sub>

	<b>Angle (3)</b>	<b>Degrees</b>
Fe–C1–Fe; Fe–C11–Fe	Fe1–C1– Fe1 <sup>1</sup>	88.89(18)
	Fe1–C1– Fe2 <sup>1</sup>	90.45(9)
	Fe1–C1– Fe2	93.51(9)
	Fe2–C1– Fe1 <sup>1</sup>	90.45(9)
	Fe1 <sup>1</sup> –C1– Fe2 <sup>1</sup>	93.51(9)
	Fe1–C1– Fe3	91.90(2)
	Fe3–C1– Fe1 <sup>1</sup>	178.97(14)
	Fe1–C1– Fe3 <sup>1</sup>	178.97(14)
	Fe1 <sup>1</sup> –C1– Fe3 <sup>1</sup>	91.90(2)
	Fe2–C1– Fe2 <sup>1</sup>	174.4(2)
	Fe2–C1– Fe3	88.83(10)
	Fe2 <sup>1</sup> –C1– Fe3 <sup>1</sup>	88.83(10)
	Fe3–C1– Fe2 <sup>1</sup>	87.15(9)
	Fe2–C1– Fe3 <sup>1</sup>	87.15(9)
	Fe3–C1– Fe3 <sup>1</sup>	87.33(18)
	Fe4–C11– Fe4 <sup>2</sup>	87.78(17)
	Fe4–C11– Fe6	90.29(9)
	Fe4 <sup>2</sup> –C11– Fe6 <sup>2</sup>	90.29(9)
	Fe4 <sup>2</sup> –C11– Fe6	93.30(9)
	Fe4–C11– Fe6 <sup>2</sup>	93.30(9)
	Fe5 <sup>2</sup> –C11– Fe4 <sup>2</sup>	92.85(2)
	Fe5–C11– Fe4	92.85(2)
	Fe5–C11– Fe4 <sup>2</sup>	179.15(13)
	Fe4–C11– Fe5 <sup>2</sup>	179.15(13)
	Fe5 <sup>2</sup> –C11– Fe5	86.52(17)
	Fe5–C11– Fe6	87.26(9)
	Fe5 <sup>2</sup> –C11– Fe6 <sup>2</sup>	87.26(9)
	Fe5 <sup>2</sup> –C11– Fe6	89.11(10)
	Fe5–C11– Fe6 <sup>2</sup>	89.11(10)
	Fe–Fe–Fe	Fe1 <sup>1</sup> –Fe1–Fe3
Fe2 <sup>1</sup> –Fe1–Fe2		88.62(2)
Fe3 <sup>1</sup> –Fe2–Fe1		89.000(18)
Fe3–Fe2–Fe1 <sup>1</sup>		89.682(18)
Fe2 <sup>1</sup> –Fe3–Fe2		92.62(2)
Fe3 <sup>1</sup> –Fe3–Fe1		90.369(14)
Fe4 <sup>2</sup> –Fe4–Fe5		89.682(14)
Fe5 <sup>2</sup> –Fe5–Fe4		90.312(14)
Fe6–Fe5–Fe6 <sup>2</sup>		92.09(2)
Fe5–Fe6–Fe4 <sup>2</sup>		89.398(19)
Fe5 <sup>2</sup> –Fe6–Fe4	89.976(19)	

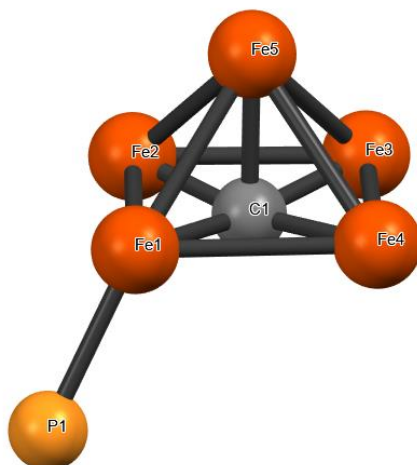


**Figure S46.** Five iron cluster framework and generalized atom numbering guide for **Tables S7-8**.

**Table S7.** Selected bond angles for **4**, **5** and **8**.

	<b>Angle (3)</b>	<b>Degrees</b>	<b>Angle (4)</b>	<b>Length (Å)</b>	<b>Bond (7)</b>	<b>Length (Å)</b>
Fe–C1–Fe	Fe5–C1–Fe1	86.5(3)	Fe5–C1–Fe1	83.88(11)	Fe5–C1–Fe1	84.0(4)
	Fe5–C1–Fe2	85.9(3)	Fe5–C1–Fe2	85.99(11)	Fe5–C1–Fe2	86.0(4)
	Fe5–C1–Fe3	85.1(3)	Fe5–C1–Fe3	83.49(11)	Fe5–C1–Fe3	83.0(4)
	Fe5–C1–Fe4	85.1(3)	Fe5–C1–Fe4	83.99(11)	Fe5–C1–Fe4	85.6(4)
	Fe1–C1–Fe3	171.5(4)	Fe1–C1–Fe3	167.34(17)	Fe1–C1–Fe3	166.9(6)
	Fe2–C1–Fe4	169.7(4)	Fe2–C1–Fe4	168.67(17)	Fe2–C1–Fe4	170.5(6)
	Fe1–C1–Fe2	91.7(3)	Fe1–C1–Fe2	93.44(13)	Fe1–C1–Fe2	92.9(5)
	Fe2–C1–Fe3	87.6(3)	Fe2–C1–Fe3	86.45(12)	Fe2–C1–Fe3	87.6(4)
	Fe3–C1–Fe4	86.8(3)	Fe3–C1–Fe4	87.17(12)	Fe3–C1–Fe4	87.1(4)
	Fe4–C1–Fe1	92.5(3)	Fe4–C1–Fe1	90.75(12)	Fe4–C1–Fe1	90.5(4)
Fe–P–C	Fe1–P1–C16	119.0(2)	Fe1–P1–C21	111.08(10)	Fe1–P1–C18	109.9(3)
	Fe1–P1–C28	111.1(2)	Fe1–P1–C27	119.25(10)	Fe1–P1–C27	110.2(3)
	Fe1–P1–C22	118.0(2)	Fe1–P1–C15	114.75(10)	Fe1–P1–C21	115.3(3)
Fe–Fe–Fe	Fe1–Fe2–Fe3	91.16(5)	Fe1–Fe2–Fe3	89.899(19)	Fe1–Fe2–Fe3	90.48(7)
	Fe2–Fe3–Fe4	91.01(5)	Fe2–Fe3–Fe4	92.00(2)	Fe2–Fe3–Fe4	90.49(6)
	Fe3–Fe4–Fe1	90.39(5)	Fe3–Fe4–Fe1	90.735(19)	Fe3–Fe4–Fe1	91.64(6)
	Fe4–Fe1–Fe2	87.43(4)	Fe4–Fe1–Fe2	87.301(18)	Fe4–Fe1–Fe2	87.18(6)
Fe1–H1–Fe2	–	–	Fe1–H1–Fe2	95.052	–	–

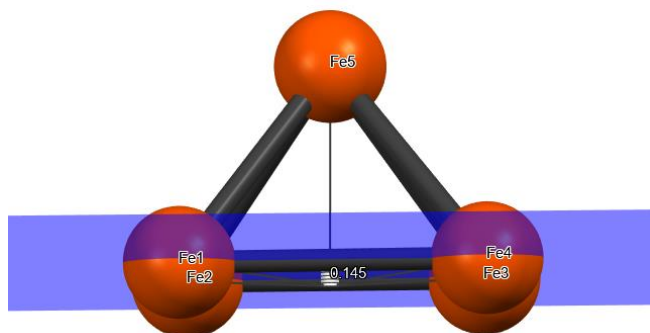


**Figure S47.** Five iron cluster framework with basal 4Fe RMS plane shown (blue), and with distance from plane to center of the interstitial carbide C1 highlighted (compound **4** used in this model).

**Table S8.** Selected bond distances for **4**, **5** and **8**; \*semi-bridging carbonyl.

	<b>Bond (3)</b>	<b>Length (Å)</b>	<b>Bond (4)</b>	<b>Length (Å)</b>	<b>Bond (7)</b>	<b>Length (Å)</b>
Fe-( $\mu_5$ -C)	Fe1-C1	1.888(8)	Fe1-C1	1.859(3)	Fe1-C1	1.897(10)
	Fe2-C1	1.874(8)	Fe2-C1	1.852(3)	Fe2-C1	1.867(10)
	Fe3-C1	1.932(8)	Fe3-C1	1.879(3)	Fe3-C1	1.932(10)
	Fe4-C1	1.899(8)	Fe4-C1	1.857(3)	Fe4-C1	1.876(10)
	Fe5-C1	1.949(7)	Fe5-C1	2.015(3)	Fe5-C1	1.978(10)
( $\mu_5$ -C)-Plane <sub>Fe<sub>4</sub></sub>		0.145		0.183		0.18
Fe-P	Fe1-P1	2.2880(18)	Fe1-P1	2.2245(8)	Fe1-P1	2.261(3)
Fe-H			Fe1-H1	1.82(5)		
			Fe4-H1	1.83(5)		
C-O	C2-O1	1.149(9)	C2-O1	1.152(4)	C2-O1	1.155(13)
	C3-O2	1.140(10)	C3-O2	1.146(4)	C3-O2	1.146(12)
	C4-O3	1.136(10)	C4-O3	1.139(4)	C4-O3	1.150(12)
	C5-O4	1.145(11)	C5-O4*	1.163(4)	C5-O4	1.117(12)
	C6-O5	1.136(10)	C6-O5	1.126(4)	C6-O5	1.164(12)
	C7-O6	1.132(11)	C7-O6	1.152(4)	C7-O6	1.154(12)
	C8-O7	1.140(11)	C8-O7*	1.160(4)	C8-O7	1.108(12)
	C9-O8	1.132(11)	C9-O8	1.141(4)	C9-O8	1.123(12)
	C10-O9	1.141(10)	C10-O9	1.144(4)	C10-O9	1.139(11)
	C11-O10	1.155(10)	C11-O10	1.155(4)	C11-O10	1.150(12)
	C12-O11	1.143(10)	C12-O11	1.150(4)	C12-O11	1.161(11)
	C13-O12	1.168(10)	C13-O12	1.154(4)	C13-O12	1.138(13)
	C14-O13	1.146(10)	C14-O13	1.153(4)	C14-O13	1.152(11)
	C15-O14	1.149(12)			C15-O14	1.134(13)
	Fe-CO	Fe1-C2	1.777(8)	Fe1-C2	1.772(3)	Fe1-C2
Fe1-C3		1.791(9)	Fe1-C11(*)	1.821(3)	Fe1-C3	1.777(13)
Fe2-C4		1.813(8)	Fe2-C3	1.805(4)	Fe2-C4	1.773(12)
Fe2-C5		1.791(9)	Fe2-C4	1.778(3)	Fe2-C5	1.806(14)
Fe2-C6		1.811(9)	Fe2-C5 (*)	1.900(3)	Fe2-C6	1.772(13)
Fe3-C7		1.814(9)	Fe3-C5 (*)	2.054(3)	Fe3-C7	1.789(12)
Fe3-C8		1.813(9)	Fe3-C6	1.822(3)	Fe3-C8	1.822(13)
Fe3-C9		1.809(9)	Fe3-C7	1.779(3)	Fe3-C9	1.814(13)
Fe4-C10		1.801(8)	Fe3-C8 (*)	2.054(3)	Fe4-C10	1.807(12)
Fe4-C11		1.793(8)	Fe4-C8 (*)	1.918(3)	Fe4-C11	1.777(13)
Fe4-C12		1.795(9)	Fe4-C9	1.788(3)	Fe4-C12	1.749(12)
Fe5-C13		1.776(9)	Fe4-C10	1.778(3)	Fe5-C13	1.798(15)
Fe5-C14		1.797(8)	Fe4-C11 (*)	2.359(3)	Fe5-C14	1.773(11)
Fe5-C15		1.796(10)	Fe5-C12	1.783(3)	Fe5-C15	1.811(15)
			Fe5-C13	1.784(3)		
		Fe5-C14	1.790(3)			
Fe-Fe	Fe1-Fe4	2.7362(15)	Fe1-Fe4	2.6450(6)	Fe1-Fe4	2.681(2)
	Fe1-Fe5	2.6285(15)	Fe1-Fe5	2.5923(6)	Fe1-Fe5	2.5937(19)
	Fe1-Fe2	2.6998(15)	Fe1-Fe2	2.7018(6)	Fe1-Fe2	2.728(2)
	Fe4-Fe5	2.6014(16)	Fe4-Fe5	2.5937(6)	Fe4-Fe5	2.619(2)
	Fe4-Fe3	2.6326(16)	Fe4-Fe3	2.5757(6)	Fe4-Fe3	2.624(2)
	Fe5-Fe3	2.6248(16)	Fe5-Fe3	2.5949(6)	Fe5-Fe3	2.590(2)
	Fe5-Fe2	2.6045(16)	Fe5-Fe2	2.6400(6)	Fe5-Fe2	2.623(2)
	Fe3-Fe2	2.6341(16)	Fe3-Fe2	2.5552(6)	Fe3-Fe2	2.628(2)

**Table S9.** Selected bond distances for three iron cluster units in compounds **6**, **7\***, **10** and **11**. \*See crystallographic experimental details and remarks on **7** for the limitations of the data set for structure **7**. The unit cell for **7** contains two iron cluster molecules of equivalent atomic compositions and arrangements, only one of which is tabulated here for general reference.

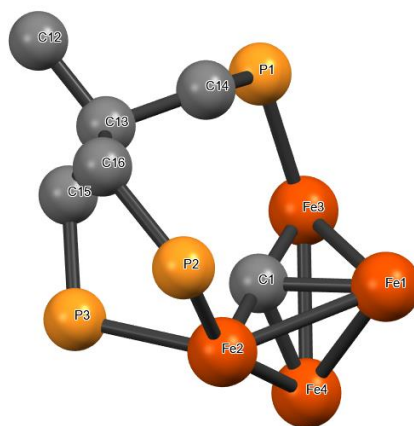
	<b>Bond (5)</b>	<b>Length (Å)</b>	<b>Bond (6)</b>	<b>Length (Å)</b>	<b>Bond (9)</b>	<b>Length (Å)</b>	<b>Bond (10)</b>	<b>Length (Å)</b>
Fe-( $\mu$ 3-C)	Fe1-C1	1.87(1)	Fe1-C1	1.946(13)	Fe2-C1	1.952(2)	Fe1-C1	2.0037(17)
	Fe2-C1	1.880(8)	Fe2-C1	1.933(14)	Fe3-C1	1.952(2)	Fe2-C1	1.9973(17)
	Fe3-C1	1.88(1)	Fe3-C1	1.953(13)	Fe4-C1	1.925(2)	Fe3-C1	1.9046(18)
( $\mu$ 3-C)-R	C1-H1	1.00(3)	C1-P3	1.785(15)	C1-C2	1.457(3)	C1-C2	1.478(2)
Fe-P	Fe1-P1	2.5286(5)	Fe1-P2	2.249(4)	Fe1-P1	2.2229(6)	Fe1-P1	2.2663(5)
	Fe1-P1 <sup>1</sup>	2.3292(6)	Fe1-P1	2.248(4)	Fe1-P2	2.2728(6)	Fe2-P2	2.2334(5)
	Fe1-P2	2.3238(5)	–	–	Fe1-P3	2.2230(7)	Fe1-P3	2.2010(5)
	Fe1-P2 <sup>1</sup>	2.3237(5)	–	–	–	–	Fe2-P3	2.2116(5)
Fe-Fe	Fe2-Fe3	2.5286(5)	Fe1-Fe2	2.591(3)	Fe2-Fe4	2.5715(5)	Fe1-Fe2	2.5907(4)
	Fe3-Fe4	2.5845(5)	Fe1-Fe3	2.578(3)	Fe3-Fe4	2.5698(5)	Fe1-Fe3	2.5900(4)
	Fe4-Fe2	2.5644(6)	Fe2-Fe3	2.550(4)	Fe2-Fe3	2.5355(5)	Fe2-Fe3	2.6059(4)

**Table S10.** Selected bond angles for three iron cluster units in compounds **6** and **7\***. \*See crystallographic experimental details and remarks on **7** for the limitations of the data set for structure **7**. Additionally, the unit cell for **7** contains two iron cluster molecules of equivalent atomic compositions and arrangements, only one of which is tabulated here for general reference.

	<b>Angle (5)</b>	<b>Length (Å)</b>	<b>Angle (6)</b>	<b>Length (Å)</b>
Fe- ( $\mu$ 3-C) – Fe	Fe2-C1-Fe3	79.83(10)	Fe1-C1-Fe2	83.8(5)
	Fe2-C1-Fe4	83.57(11)	Fe2-C1-Fe3	82.0(5)
	Fe3-C1-Fe4	85.11(11)	Fe3-C1-Fe1	82.0(5)
	Fe2-C1-Fe3	79.83(10)	Fe1-C1-Fe2	83.8(5)
Fe-P-C	Fe1-P2-C37	117.55(7)	–	–
	Fe1-P2-C25	117.03(8)	–	–
	Fe1-P2-C18	108.17(7)	–	–
	Fe1-P1-C13	108.77(8)	–	–
	Fe1-P1-C19	118.05(8)	–	–
	Fe1-P1-C25	117.03(8)	–	–
Fe- ( $\mu$ 3-C) – P	–	–	Fe1-C1-P3	134.3(7)
Fe-Fe-Fe	Fe2-Fe3-Fe4	60.190(15)	Fe1-Fe2-Fe3	60.18(8)
	Fe3-Fe2-Fe4	60.986(15)	Fe2-Fe3-Fe1	60.69(8)
	Fe2-Fe4-Fe3	58.824(15)	Fe3-Fe1-Fe2	59.12(9)

**Table S11.** Selected bond angles for three iron cluster units in compounds **10** and **11**.

	Angle (9)	Length (Å)	Angle (10)	Length (Å)
Fe-( $\mu_3$ -C)–Fe	Fe2–C1–Fe3	81.00(9)	Fe1–C1–Fe2	80.71(6)
	Fe3–C1–Fe4	83.02(9)	Fe2–C1–Fe3	83.77(7)
	Fe4–C1–Fe2	83.11(9)	Fe3–C1–Fe1	82.97(7)
	Fe2–C1–Fe3	81.00(9)	Fe1–C1–Fe2	80.71(6)
Fe–P–C	–	–	Fe2–P2–C18	115.07(6)
	–	–	Fe2–P2–C32	115.97(6)
	–	–	Fe2–P2–C38	118.24(6)
	–	–	Fe1–P1–C17	121.63(6)
	–	–	Fe1–P1–C26	118.23(6)
	–	–	Fe1–P1–C20	108.64(6)
Fe–Fe–Fe	Fe3–Fe2–Fe4	60.417(14)	Fe1–Fe2–Fe3	59.787(10)
	Fe2–Fe3–Fe4	60.485(15)	Fe2–Fe3–Fe1	59.8816(10)
	Fe3–Fe4–Fe2	59.099(14)	Fe3–Fe1–Fe2	60.397(10)

**Figure S48.** Simplified four iron cluster framework and atom numbering guide for compound **9**.**Table S12.** Selected bond distances for **9** and literature values for  $\text{Fe}_4(\text{CO})_{13}$ ,  $\text{Fe}_4(\text{CO})_{12}^{2-}$ ,  $\text{Fe}_4(\text{CH})(\text{CO})_{12}$ .

	Bond (8)	Length (Å)
Fe-( $\mu_4$ -C)	Fe1–C1	1.962(7)
	Fe2–C1	1.801(7)
	Fe3–C1	1.813(7)
	Fe4–C1	1.943(7)
Fe–P	Fe3–P1	2.247(2)
	Fe2–P2	2.269(2)
	Fe2–P3	2.2545(19)
Fe–Fe	Fe1–Fe2	2.6016(15)
	Fe1–Fe3	2.6332(15)
	Fe1–Fe4	2.5287(15)
	Fe2–Fe4	2.7028(16)
	Fe3–Fe4	2.6326(16)

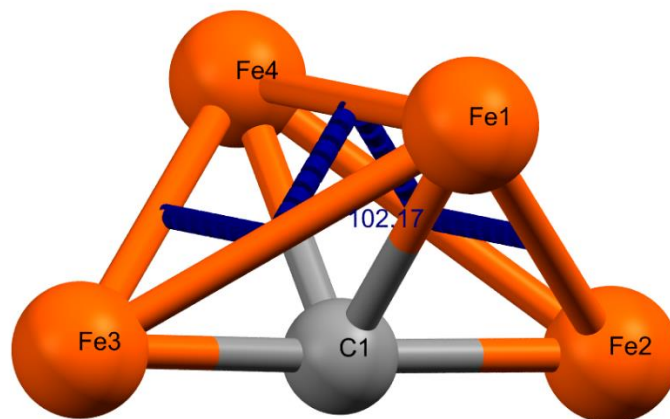


**Figure S49.** Four iron cluster core of **9** with wing to wing torsion highlighted.

**Table S13.** Selected bond angle and torsion for **9**.

	Angle (°)
Fe2-C <sub>carbide</sub> -Fe3	175.3(4)
Wing to wing torsion	102.17

## Computational Methods

Calculations were performed using the ORCA versions 4 and 5 software package.<sup>16,17</sup> We thank the Texas Advanced Computing Center for providing an allocation to run these calculations on the Stampede2 supercomputer (see acknowledgements). Chemcraft was used for optimization and frequency analysis visualizations and structure comparisons.<sup>18</sup> Computational methods (functionals, etc.) are detailed *vide infra*.

## Computational Modeling of 2: Approach and remarks on DFT functional and basis set screening and using $[\text{Fe}_5(\mu_5\text{-C})(\text{CO})_{15}]$ as a benchmark

**Remarks on computational modeling approach, selected methods, and initial screening with  $[\text{Fe}_5(\mu_5\text{-C})(\text{CO})_{15}]$ .** Before attempting to model the geometry of the structurally elusive compound **2**, we compared common DFT methods for geometry optimization by evaluating their suitability for analysis of the known neutral iron cluster,  $[\text{Fe}_5(\mu_5\text{-C})(\text{CO})_{15}]$ . We especially sought to evaluate how the percentage HF contribution affects the convergence, output geometry, calculated single point energies, HOMO-LUMO gap and frequency outputs to inform our functional choice for this and future studies when evaluating iron carbide carbonyl clusters.

Functionals were selected based on their percentage HF exchange and whether they are used for geometry optimization of metal complexes in the literature.<sup>19</sup> Of these functionals, B3LYP is the most popular functional, with accuracy highly variable depending on the system in question (CITATION). According to Kepp et. al ('Chemical Bond Energies...')<sup>20</sup>, hybrid functionals with 10-20% HF is suggested for early transition metals while 0-10% is suggested for late transition metals. Although the suggested %HF decreases as period increases, Fe is midway i.e., neither early or late transition metal. With this in mind, we decided to intentionally vary the percentage HF exchange in our functional selections.

**Table S14.** Hartree Fock exchange (HFX) with selected functionals. †no D4

Functional	Global HFX	Short-Range HFX	Long-Range HFX
B3PW91†	0.200	-	-
BP86	0.000	-	-
B3LYP	0.200	-	-
B3LYP-15	0.150	-	-
ωB97x	-	0.167	1.000
ωB97x-15	-	0.150	1.000

The choice of functional is crucial to accurately representing the electron density. Since functionals vary depending on the metal, ligand and its bond strength, we started with a myriad of functionals. Initially, we screened functionals and basis sets with the known anionic, six-iron cluster and precursor to our target compound **2**, namely  $[\text{Fe}_6(\mu_6\text{-C})(\text{CO})_{16}]^{2-}$  (**1**). However, we found that approaches that proved sufficient for neutral clusters analysis are, in fact, not sufficient for anionic clusters. We continue to explore solutions for this problem (including ranged functionals with solvation models and the counterions included) to identify methods applicable to anionic clusters. However, this report focuses only on the neutral model,  $[\text{Fe}_5(\mu_5\text{-C})(\text{CO})_{15}]$ .

Basis sets were selected based on literature precedent. The Ahlrichs def2 basis set family was selected as the most reasonable basis set choice for a minimal HF exchange approach. Triple-zeta or large basis sets were used to model the Fe orbitals, with larger basis sets tested. In literature and in our study (*vide infra*), geometry variation between basis set choice is minimal.<sup>21</sup> The TZV series with the P polarization basis is sufficient for DFT calculations.

Optimized geometries can be verified in different ways, e.g. comparison with experimental data, calculating single point energy (SPE), or vibrational analysis. Vibrational analysis indicated if the converged geometry is at a minimum instead of a saddlepoint, while SPE determined the energy based on the converged geometry's spatial positions, and differentiated whether the geometry is at local or global minimum.<sup>22</sup> Conventionally, geometries with imaginary frequencies indicate that the final geometry is not at local or global minimum.

**Table S15.** Convergence of optimization and vibrational analyses with selected functionals and basis set combinations on cluster  $[\text{Fe}_5(\mu_5\text{-C})(\text{CO})_{15}]$ . D4 dispersion corrections were applied to all calculations unless specified otherwise.

	ma-def2-TZVP			Grid 2, tightopt			Grid 3, verytightopt		
Functional	Geometry Optimized	Vibrational Analysis	No. imaginary frequencies	Geometry Optimized	Vibrational Analysis	No. imaginary frequencies	Geometry Optimized	Vibrational Analysis	No. imaginary frequencies
B3PW91 <sup>†</sup>	✓	✓	0	✓	✓	2	✓	✓	2
BP86	✓	✓	0	✓	✓	1	✓	✓	1
B3LYP	✓	✓	0	✓	✓	1	✓	✓	1
B3LYP-15	✓	✓	0	-	-	N/A	-	-	N/A
$\omega$ B97x	✓	✓	1	-	-	N/A	-	-	N/A
$\omega$ B97x-15	✓	✓	1	-	-	N/A	-	-	N/A

<sup>†</sup>no D4

**Remarks:** Each successful frequency calculation generated an IR and Raman spectra. Increasing the basis set size did not help resolve imaginary frequencies, instead impeding convergence, and unexpectedly introduced new imaginary frequencies for the functionals B3PW91, BP86, and B3LYP.

**Table S16.** Optimized geometries versus experimental crystal structure geometry RMSD of  $[\text{Fe}_5(\mu_5\text{-C})(\text{CO})_{15}]$  with selected functionals. Ma-def2-TZVP, grid 2, tightopt, D4 applied to all calculations except B3PW91. \*calculations with imaginary frequencies (see details table SX). Experimental crystal structure data used available in CCDC 1552287. Weighted RMSD calculated by minimizing RMSD for iron atoms using Chemcraft's structure comparer tool.<sup>18</sup>

Functional	RMSD - weighted	RMSD - unweighted
B3PW91	0.0196937733211684	0.277776423109345
BP86	0.0457291297063557	0.383227600540954
B3LYP	0.0310725142848452	0.304380725932335
$\omega$ B97x*	0.0760684573893122	0.400790556736424
B3LYP-15	0.0244972042149182	0.303604053065301
$\omega$ B97X-15*	0.0727470945996918	0.399491573766197

**Table S17.** Selected bond lengths (Å) and angles (°) of optimized geometries versus experimental crystal structure geometry of  $[\text{Fe}_5(\mu_5\text{-C})(\text{CO})_{15}]$  with selected functionals. Ma-def2-TZVP, grid 2, tightopt, D4 applied to all except B3PW91. Experimental crystal structure data used available in CCDC 1552287.

	<b>XRD</b>	<b>B3PW91</b>	<b>BP86</b>	<b>B3LYP</b>	<b>*ωB97x</b>	<b>B3LYP-15</b>	<b>*ωB97X-15</b>
<b>axial Fe1–C1</b>	1.948(7)	1.930	1.933	1.930	1.920	1.929	1.927
<b>Fe2–C1</b>	1.875(8)	1.844	1.874	1.858	1.848	1.859	1.854
<b>Fe3–C1</b>	1.897(7)	1.877	1.882	1.893	1.840	1.893	1.848
<b>Fe4–C1</b>	1.865(8)	1.858	1.884	1.875	1.856	1.875	1.863
<b>Fe5–C1</b>	1.893(7)	1.883	1.885	1.902	1.852	1.902	1.859
<b>Fe2-C1-Fe1</b>	88.0(3)	88.445	90.144	90.095	84.136	89.955	84.219
<b>Fe3-C1-Fe1</b>	84.6(3)	85.107	89.837	86.689	87.027	86.503	87.036
<b>Fe2-Fe5-Fe4</b>	89.09(4)	89.544	89.754	89.315	90.663	89.396	90.618
<b>Fe4-Fe3-Fe2</b>	89.61(4)	88.858	89.983	88.774	89.599	88.812	89.602
<b>Fe2–C1–Fe4</b>	175.8(4)	176.831	173.686	179.00	172.003	179.093	172.021
<b>Fe3–C1–Fe5</b>	169.6(5)	169.679	174.147	172.434	173.039	172.112	173.026
<b>Fe1-Fe2</b>	2.6557(16)	2.629	2.615	2.681	2.525	2.678	2.536
<b>Fe1-Fe3</b>	2.5869(15)	2.571	2.641	2.624	2.590	2.619	2.600
<b>Fe1-Fe4</b>	2.6466(16)	2.641	2.637	2.700	2.623	2.686	2.631
<b>Fe1-Fe5</b>	2.5997(14)	2.564	2.606	2.611	2.582	2.605	2.591
<b>Fe2-Fe3</b>	2.6331(15)	2.653	2.659	2.681	2.641	2.676	2.650
<b>Fe3-Fe4</b>	2.6703(15)	2.633	2.659	2.656	2.602	2.661	2.621
<b>Fe4-Fe5</b>	2.6780(15)	2.623	2.654	2.648	2.577	2.650	2.588
<b>Fe5-Fe2</b>	2.6469(15)	2.631	2.653	2.664	2.618	2.659	2.627
<b>Fe2Fe3Fe4Fe5 (rmsplane)-C1</b>	0.119	0.092	0.081	0.057	0.081	0.057	0.117

**Table S18.** All calculated vibrational modes with and without scaling factors applied. Scaling factors detailed below this table. Ma-def2-TZVP, grid 2, tightopt, D4 applied to all except B3PW91. Imaginary frequencies marked with italics.

Mode	Unscaled						Scaled					
	B3PW91	B3LYP	$\omega$ B97x	$\omega$ B97x-15	BP86	B3LYP-15	B3PW91 <sup>A</sup>	B3LYP <sup>B</sup>	$\omega$ B97x <sup>D</sup>	$\omega$ B97x-15	BP86 <sup>C</sup>	B3LYP-15
0	0	0	0	0	0	0	0	0	0	0	0	0
1	0	0	0	0	0	0	0	0	0	0	0	0
2	0	0	0	0	0	0	0	0	0	0	0	0
3	0	0	0	0	0	0	0	0	0	0	0	0
4	0	0	0	0	0	0	0	0	0	0	0	0
5	0	0	0	0	0	0	0	0	0	0	0	0
6	12.69	14.22	<i>-12.05</i>	<i>-8.12</i>	9.16	15.1	12.23316	14.28257	<i>-11.9464</i>	<i>-8.12</i>	9.468692	15.1
7	22.47	24.34	15.35	12.53	18.39	22.24	21.66108	24.4471	15.21799	12.53	19.00974	22.24
8	31.69	33.14	25.31	25.74	27.73	35.06	30.54916	33.28582	25.09233	25.74	28.6645	35.06
9	35.28	33.93	33.79	33.62	34.85	36.18	34.00992	34.07929	33.49941	33.62	36.02445	36.18
10	46.18	43.07	41.21	41.39	37.25	41.4	44.51752	43.25951	40.85559	41.39	38.50533	41.4
11	53.79	52.26	48.31	48.45	39.63	52.36	51.85356	52.48994	47.89453	48.45	40.96553	52.36
12	60.67	60.45	63.7	64.3	57.05	60.46	58.48588	60.71598	63.15218	64.3	58.97259	60.46
13	62.09	65.25	66.16	66.23	62.2	66.13	59.85476	65.5371	65.59102	66.23	64.29614	66.13
14	69.21	71.42	68.97	68.88	67.61	71.56	66.71844	71.73425	68.37686	68.88	69.88846	71.56
15	73.92	73.53	73	73.19	70.55	74.42	71.25888	73.85353	72.3722	73.19	72.92754	74.42
16	75.69	74.73	76.26	76.37	75.67	77.4	72.96516	75.05881	75.60416	76.37	78.22008	77.4
17	80.67	79.39	81.34	81.26	79.41	80	77.76588	79.73932	80.64048	81.26	82.08612	80
18	81.52	81.68	82.85	82.96	81.89	83.37	78.58528	82.03939	82.13749	82.96	84.64969	83.37
19	57.65	86.05	87.09	86.82	83.27	85.73	84.4946	86.42862	86.34103	86.82	86.0762	85.73
20	88.95	87.91	89.72	89.52	84.38	87.86	85.7478	88.2968	88.94841	89.52	87.22361	87.86
21	90.55	89.08	90.64	90.52	87.71	90.81	87.2902	89.47195	89.8605	90.52	90.66583	90.81
22	94.34	93.22	96.22	95.95	88.85	93.98	90.94376	93.63017	95.39251	95.95	91.84425	93.98
23	96.52	95.96	98.19	97.92	94.4	95.23	93.04528	96.38222	97.34557	97.92	97.58128	95.23
24	99.37	97.63	100.03	99.39	94.54	96.87	95.79268	98.05957	99.16974	99.39	97.726	96.87
25	101.13	99.78	102.98	102.44	96.34	101.12	97.48932	100.219	102.0944	102.44	99.58666	101.12

26	103.1	101.56	103.46	102.98	97.9	102.13	99.3884	102.0069	102.5702	102.98	101.1992	102.13
27	104.19	101.83	105.42	104.76	100.32	102.36	100.4392	102.2781	104.5134	104.76	103.7008	102.36
28	107.48	104.96	107.15	106.54	101.33	104.96	103.6107	105.4218	106.2285	106.54	104.7448	104.96
29	108.77	108.29	115.81	115.36	106.16	106.94	104.8543	108.7665	114.814	115.36	109.7376	106.94
30	115.43	113.06	129.14	128.86	119.94	116.85	111.2745	113.5575	128.0294	128.86	123.982	116.85
31	124.74	122.69	132.8	132.19	126.5	126.99	120.2494	123.2298	131.6579	132.19	130.7631	126.99
32	130.22	129.41	137.01	136.22	129.85	129.83	125.5321	129.9794	135.8317	136.22	134.2259	129.83
33	132.61	130.85	144.84	143.92	132.44	131.34	127.836	131.4257	143.5944	143.92	136.9032	131.34
34	142.94	141.14	151.91	151.32	139.7	145.22	137.7942	141.761	150.6036	151.32	144.4079	145.22
35	149.52	145.05	156.98	156.9	142.92	149.69	144.1373	145.6882	155.63	156.9	147.7364	149.69
36	158.53	151.97	162.22	161.6	149.06	155.89	152.8229	152.6387	160.8249	161.6	154.0833	155.89
37	159.93	154.02	163.62	162.89	162.64	157.47	154.1725	154.6977	162.2129	162.89	168.121	157.47
38	166.18	158.97	170.36	169.34	164.33	162.55	160.1975	159.6695	168.8949	169.34	169.8679	162.55
39	190.75	181.26	205.49	204.17	186.37	185.59	183.883	182.0575	203.7228	204.17	192.6507	185.59
40	198.83	190.35	213.28	211.64	188.73	193.46	191.6721	191.1875	211.4458	211.64	195.0902	193.46
41	206.35	194.48	221.62	220.51	206.85	200.19	198.9214	195.3357	219.7141	220.51	213.8208	200.19
42	210.27	198.59	223.23	221.93	208.91	206.98	202.7003	199.4638	221.3102	221.93	215.9503	206.98
43	216.99	205.84	232.68	230.9	210.94	214.5	209.1784	206.7457	230.679	230.9	218.0487	214.5
44	255.12	244.78	272.83	270.78	255.72	254.23	245.9357	245.857	270.4837	270.78	264.3378	254.23
45	404.98	392.92	411.68	409.81	377.03	391.21	390.4007	394.6488	408.1396	409.81	389.7359	391.21
46	410.62	398.54	416.24	413.47	386.45	397.82	395.8377	400.2936	412.6603	413.47	399.4734	397.82
47	413.12	402.04	420.53	417.69	398.05	400.24	398.2477	403.809	416.9134	417.69	411.4643	400.24
48	416.88	405.35	421.85	419.11	403.12	403.34	401.8723	407.1335	418.2221	419.11	416.7051	403.34
49	422.86	410.27	427.17	424.39	404.99	410.2	407.637	412.0752	423.4963	424.39	418.6382	410.2
50	423.87	411.3	428.72	426.32	406.82	411.49	408.6107	413.1097	425.033	426.32	420.5298	411.49
51	426.38	413	431.1	428.59	409.14	412.76	411.0303	414.8172	427.3925	428.59	422.928	412.76
52	431.09	417.38	437.93	434.83	411.91	417.62	415.5708	419.2165	434.1638	434.83	425.7914	417.62
53	434.6	420.03	438.46	436.58	417.36	422.3	418.9544	421.8781	434.6892	436.58	431.425	422.3
54	439.78	426.46	444.42	441.95	422.06	429.44	423.9479	428.3364	440.598	441.95	436.2834	429.44
55	441.28	427.85	448.43	445.55	430.47	431.39	425.3939	429.7325	444.5735	445.55	444.9768	431.39
56	443.48	429.77	450.44	447.79	432.18	432.41	427.5147	431.661	446.5662	447.79	446.7445	432.41

57	456.73	441.63	464.14	461.45	443.7	448.06	440.2877	443.5732	460.1484	461.45	458.6527	448.06
58	457.23	442.89	465.73	463.01	445	448.8	440.7697	444.8387	461.7247	463.01	459.9965	448.8
59	465.59	451.32	471.31	468.82	447.74	457.69	448.8288	453.3058	467.2567	468.82	462.8288	457.69
60	488.11	469.23	481.22	479.02	477.44	476.53	470.538	471.2946	477.0815	479.02	493.5297	476.53
61	490.53	470.05	483.27	481.1	484.03	479.08	472.8709	472.1182	479.1139	481.1	500.3418	479.08
62	500.07	477.16	487.7	485.16	489.72	487.31	482.0675	479.2595	483.5058	485.16	506.2236	487.31
63	503.75	483.55	495.67	492.81	495.97	492.1	485.615	485.6776	491.4072	492.81	512.6842	492.1
64	509.74	488.6	504.03	501.18	500.3	496.15	491.3894	490.7498	499.6953	501.18	517.1601	496.15
65	519.23	498.21	515.11	513.15	510.06	505.53	500.5377	500.4021	510.6801	513.15	527.249	505.53
66	521.06	501.18	518.41	515.37	514.27	508.35	502.3018	503.3852	513.9517	515.37	531.6009	508.35
67	525.2	502.77	522.17	519.11	517.33	512.43	506.2928	504.9822	517.6793	519.11	534.764	512.43
68	530.15	509.68	532.09	529.11	522.26	516.88	511.0646	511.9226	527.514	529.11	539.8602	516.88
69	532.29	511.6	533.45	530.21	523.91	518.2	513.1276	513.851	528.8623	530.21	541.5658	518.2
70	533.8	512.45	539.35	535.53	528.47	518.78	514.5832	514.7048	534.7116	535.53	546.2794	518.78
71	539.13	519.43	546.93	543.3	528.92	525.05	519.7213	521.7155	542.2264	543.3	546.7446	525.05
72	541.19	520.44	550.6	546.58	530.36	527.22	521.7072	522.7299	545.8648	546.58	548.2331	527.22
73	546.7	524.49	556.08	552.7	540.54	535.39	527.0188	526.7978	551.2977	552.7	558.7562	535.39
74	550.85	530.63	566.15	563.14	544	537.91	531.0194	532.9648	561.2811	563.14	562.3328	537.91
75	567.02	549.48	573.84	569.55	545.47	556.62	546.6073	551.8977	568.905	569.55	563.8523	556.62
76	582.26	560.3	588.87	585.23	570.8	568.93	561.2986	562.7653	583.8057	585.23	590.036	568.93
77	585.81	566.5	591.64	587.67	571.5	573.47	564.7208	568.9926	586.5519	587.67	590.7596	573.47
78	588.29	569.28	600.75	596.42	573.5	574.84	567.1116	571.7848	595.5836	596.42	592.827	574.84
79	599.95	579.38	606.71	602.78	575.51	587.22	578.3518	581.9293	601.4923	602.78	594.9047	587.22
80	602.45	581.46	610.86	606.37	583.88	588.19	580.7618	584.0184	605.6066	606.37	603.5568	588.19
81	603.22	586.94	617.61	613.26	590.57	590.83	581.5041	589.5225	612.2986	613.26	610.4722	590.83
82	610.89	591.53	623.95	619.24	593.89	597.02	588.898	594.1327	618.584	619.24	613.9041	597.02
83	614.66	596.08	626.58	621.95	597.07	601.28	592.5322	598.7028	621.1914	621.95	617.1913	601.28
84	617.72	600.9	633.7	628.29	604.05	604.84	595.4821	603.544	628.2502	628.29	624.4065	604.84
85	625.3	607.21	637.1	631.9	604.89	612.06	602.7892	609.8817	631.6209	631.9	625.2748	612.06
86	632.14	614.6	646.94	641.86	610.65	618.1	609.383	617.3042	641.3763	641.86	631.2289	618.1
87	633.24	614.98	647.76	642.77	611.04	618.82	610.4434	617.6859	642.1893	642.77	631.632	618.82

88	638.19	618.97	650.52	645.68	618.4	623.45	615.2152	621.6935	644.9255	645.68	639.2401	623.45
89	639.61	621.68	657.82	652.56	619.8	625.04	616.584	624.4154	652.1627	652.56	640.6873	625.04
90	658.87	636.95	682.81	677.18	644.45	646.98	635.1507	639.7526	676.9378	677.18	666.168	646.98
91	781.59	740.82	845.59	838.72	791.4	762.87	753.4528	744.0796	838.3179	838.72	818.0702	762.87
92	817.28	778.99	852.85	845.08	799.89	809.89	787.8579	782.4176	845.5155	845.08	826.8463	809.89
93	2046.6	2031	2062	2039.87	1964.77	2015.48	1972.922	2039.936	2044.267	2039.87	2030.983	2015.48
94	2059.95	2043.05	2074.59	2052.41	1970.26	2030.66	1985.792	2052.039	2056.749	2052.41	2036.658	2030.66
95	2071.2	2054.4	2085.87	2064.52	1974.19	2040.49	1996.637	2063.439	2067.932	2064.52	2040.72	2040.49
96	2075.53	2059.75	2106.74	2082.47	1977.02	2044.98	2000.811	2068.813	2088.622	2082.47	2043.646	2044.98
97	2081.39	2066.27	2109.99	2085.91	1978.97	2050.58	2006.46	2075.362	2091.844	2085.91	2045.661	2050.58
98	2084.68	2068.55	2113.09	2089.03	1983.05	2052.33	2009.632	2077.652	2094.917	2089.03	2049.879	2052.33
99	2085.41	2069.95	2116.7	2092.3	1994.74	2054.82	2010.335	2079.058	2098.496	2092.3	2061.963	2054.82
100	2095.71	2078.35	2125.05	2101.33	2002.13	2063.84	2020.264	2087.495	2106.775	2101.33	2069.602	2063.84
101	2103.87	2085.43	2135.51	2111.18	2009.93	2072.48	2028.131	2094.606	2117.145	2111.18	2077.665	2072.48
102	2105.37	2088.98	2137.82	2113.17	2010.75	2073.59	2029.577	2098.172	2119.435	2113.17	2078.512	2073.59
103	2115.44	2098.61	2150.73	2126.71	2029.81	2085	2039.284	2107.844	2132.234	2126.71	2098.215	2085
104	2125.94	2109.94	2162.55	2137.61	2031.26	2095.35	2049.406	2119.224	2143.952	2137.61	2099.713	2095.35
105	2135.59	2118.08	2170.78	2146.67	2047.74	2106.03	2058.709	2127.4	2152.111	2146.67	2116.749	2106.03
106	2139.11	2121.79	2171.08	2146.91	2048.01	2109.65	2062.102	2131.126	2152.409	2146.91	2117.028	2109.65
107	2186.64	2170.38	2223.16	2198.09	2088.06	2155.41	2107.921	2179.93	2204.041	2198.09	2158.428	2155.41

**A – scaling factor for B3PW91 with TZVP from NIST.**<sup>23</sup>

**B – scaling factor for B3LYP with def2-TZVP.**<sup>24</sup>

**C – scaling factor for BP86 with def2-TZVP.**<sup>24</sup>

**D – scaling factor for  $\omega$ B97x-D with def2-TZVP.**<sup>24</sup>

**Remarks on scaling factors:** Anharmonic oscillation is the divergence of the harmonic oscillator model.<sup>25</sup> Anharmonic oscillations are not included in idealized conditions, such as a spectroscopic DFT calculations. ORCA automatically set all scaling factors for all calculations to 1.00. Therefore, we scaled the results to more closely approximate to the experimental results. Additionally scaling factors can work to decrease systematic errors.<sup>22</sup>

**Tables S19.** All calculated IR intensities (percent transmittance) for all non-zero, non-imaginary vibrational modes. Ma-def2-TZVP, grid 2, tightopt, D4 applied to all except B3PW91. Imaginary frequencies marked with italic *n/a*.

Mode	B3PW91	B3LYP	$\omega$ B97x	$\omega$ B97x-15	BP86	B3LYP15
6	0.001003	0.001134	<i>n/a</i>	<i>n/a</i>	0.001379	0.00056
7	0.000084	0.000081	0.000295	0.000185	0.000177	0.000157
8	0.000135	0.000148	0.000416	0.000427	0.00014	0.00019
9	0.0003	0.000466	0.00107	0.000964	0.000393	0.000291
10	0.000031	0.000031	0.000335	0.000265	0.000254	0.000041
11	0.000088	0.000053	0.00023	0.000227	0.000026	0.00007
12	0.000228	0.000185	0.000562	0.000466	0.000082	0.000186
13	0.0001	0.000112	0.000136	0.000142	0.000262	0.000139
14	0.000157	0.000203	0.000019	0.000018	0.000217	0.000214
15	0.000145	0.000119	0.000155	0.000136	0.000127	0.000133
16	0.000207	0.000407	0.000012	0.000008	0.00003	0.00015
17	0.000048	0.000211	0.000389	0.000376	0.000098	0.000204
18	0.000273	0.000078	0.00064	0.000563	0.000218	0.000043
19	0.000147	0.000385	0.000122	0.000112	0.000115	0.000369
20	0.000199	0.000188	0.000179	0.000131	0.000036	0.000193
21	0.00045	0.000104	0.000631	0.000593	0.000154	0.000101
22	0.000286	0.000155	0.000095	0.000081	0.000059	0.000087
23	0.000024	0.000107	0.000535	0.000477	0.000085	0.000123
24	0.000057	0.000225	0.000077	0.000089	0.000013	0.000159
25	0.000044	0.000241	0.000596	0.000506	0.00011	0.000184
26	0.000168	0.000232	0.000492	0.000474	0.00011	0.000177
27	0.000325	0.000082	0.000069	0.00015	0.000129	0.00014
28	0.000026	0.000021	0.00026	0.000267	0.000126	0.000058
29	0.000302	0.000135	0.000132	0.000133	0.000018	0.000077
30	0.000039	0.000113	0.000014	0.000012	0.00009	0.000122
31	0.000164	0.000068	0.000102	0.000095	0.000095	0.000062
32	0.00006	0.000119	0.000076	0.000076	0.000116	0.00008
33	0.000043	0.000048	0.000109	0.0001	0.000109	0.000048
34	0.000039	0.000011	0.00007	0.000061	0.000088	0.000013
35	0.000059	0.000126	0.000145	0.000125	0.000344	0.000066
36	0.000089	0.000367	0.000583	0.000369	0.000096	0.000333
37	0.000242	0.000012	0.000361	0.000507	0.000275	0.000008
38	0.000033	0.000046	0.000071	0.000067	0.00018	0.000024
39	0.000321	0.000449	0.0015	0.001287	0.000178	0.000326
40	0.00022	0.000449	0.000338	0.000308	0.000017	0.000214
41	0.004037	0.003925	0.005603	0.004643	0.001074	0.003527
42	0.000061	0.000069	0.005311	0.005548	0.002784	0.000076
43	0.004495	0.004678	0.00296	0.002986	0.001653	0.003858
44	0.000014	0.000017	0.00002	0.000018	0.000042	0.000023

45	0.000548	0.0005	0.000246	0.000236	0.000182	0.000455
46	0.00037	0.00043	0.001224	0.001152	0.000211	0.000377
47	0.000393	0.000255	0.000338	0.000373	0.000222	0.00041
48	0.000361	0.000487	0.000346	0.000292	0.000728	0.000363
49	0.00007	0.000288	0.000447	0.000432	0.000855	0.000301
50	0.000109	0.000036	0.000232	0.000212	0.000852	0.000018
51	0.000208	0.000078	0.000178	0.000156	0.000238	0.000074
52	0.000069	0.000009	0.000512	0.000426	0.000494	0.000021
53	0.000336	0.00037	0.000049	0.000123	0.000677	0.000436
54	0.000255	0.000164	0.000891	0.000882	0.000794	0.000214
55	0.000382	0.000464	0.000332	0.000322	0.000499	0.000401
56	0.000263	0.000396	0.000121	0.000142	0.000033	0.000542
57	0.000111	0.000062	0.00008	0.000048	0.000216	0.000109
58	0.000235	0.000253	0.000137	0.000118	0.000291	0.000374
59	0.000107	0.000139	0.000008	0.000006	0.000364	0.00013
60	0.000682	0.000491	0.000948	0.000832	0.000343	0.000631
61	0.000115	0.000255	0.000549	0.000421	0.00013	0.000082
62	0.000221	0.00026	0.00019	0.000223	0.000132	0.000147
63	0.000767	0.000776	0.002749	0.002677	0.001142	0.000543
64	0.001108	0.001372	0.002291	0.002238	0.000229	0.00081
65	0.000815	0.002068	0.003308	0.002939	0.000374	0.000767
66	0.002487	0.001735	0.001722	0.001842	0.000894	0.002397
67	0.001497	0.001493	0.002851	0.002636	0.000318	0.001072
68	0.000614	0.001453	0.000773	0.000831	0.000481	0.000812
69	0.000599	0.000872	0.001916	0.001789	0.000108	0.000488
70	0.000237	0.000038	0.0006	0.000547	0.000159	0.000226
71	0.000394	0.000359	0.001229	0.001207	0.000151	0.000229
72	0.000322	0.000647	0.000231	0.000218	0.000251	0.000623
73	0.000498	0.000433	0.000634	0.000585	0.000565	0.000361
74	0.000264	0.000267	0.001078	0.001077	0.000065	0.000294
75	0.001437	0.001265	0.000091	0.000132	0.000186	0.001496
76	0.00726	0.008586	0.017647	0.017488	0.009401	0.008616
77	0.004799	0.008985	0.020323	0.02023	0.012995	0.001822
78	0.014516	0.008503	0.001029	0.000979	0.010165	0.01557
79	0.000777	0.000679	0.000697	0.000529	0.003854	0.00008
80	0.002211	0.003069	0.005204	0.005121	0.000411	0.002876
81	0.002211	0.001782	0.004095	0.003985	0.001121	0.002377
82	0.000585	0.000596	0.002812	0.002382	0.000089	0.000822
83	0.002951	0.002783	0.000455	0.000483	0.000855	0.00282
84	0.00404	0.005963	0.004911	0.004209	0.004771	0.005157
85	0.009897	0.010348	0.014956	0.014996	0.00015	0.007628
86	0.009839	0.01205	0.007107	0.006539	0.004753	0.01052
87	0.007459	0.009299	0.006799	0.007098	0.002186	0.007372

<b>88</b>	0.000877	0.000606	0.002993	0.002874	0.003018	0.001155
<b>89</b>	0.014903	0.013202	0.012714	0.012619	0.010547	0.012332
<b>90</b>	0.009738	0.010048	0.012814	0.012533	0.009762	0.010595
<b>91</b>	0.017651	0.017476	0.017368	0.017411	0.016336	0.01785
<b>92</b>	0.017487	0.016745	0.015431	0.01557	0.016583	0.016805
<b>93</b>	0.003172	0.00401	0.002962	0.002909	0.001771	0.003699
<b>94</b>	0.002032	0.002075	0.005651	0.005146	0.001079	0.001698
<b>95</b>	0.003301	0.00707	0.021081	0.019932	0.00315	0.001532
<b>96</b>	0.007292	0.004674	0.001672	0.001671	0.009676	0.006009
<b>97</b>	0.003069	0.00295	0.010912	0.010387	0.005851	0.00166
<b>98</b>	0.001589	0.003326	0.004339	0.00434	0.001269	0.002898
<b>99</b>	0.003384	0.002922	0.004804	0.004456	0.001234	0.003668
<b>100</b>	0.008853	0.009175	0.00108	0.00103	0.000895	0.009151
<b>101</b>	0.002644	0.002819	0.006564	0.005689	0.002204	0.002926
<b>102</b>	0.003416	0.00272	0.003942	0.004265	0.002686	0.002853
<b>103</b>	0.002802	0.004695	0.017507	0.015294	0.031835	0.004253
<b>104</b>	0.083831	0.082829	0.078946	0.080243	0.058645	0.083508
<b>105</b>	0.099411	0.100944	0.096053	0.092745	0.077623	0.095489
<b>106</b>	0.100913	0.104743	0.099227	0.103154	0.07377	0.097767
<b>107</b>	0.001621	0.001651	0.001931	0.00181	0.00063	0.001401

**Tables S20.** All calculated Raman activities (percent transmittance) for all non-zero, non-imaginary vibrational modes. Ma-def2-TZVP, grid 2, tightopt, D4 applied to all except B3PW91. Imaginary frequencies marked with italic n/a.

Mode	B3LYP	$\omega$ B97x	$\omega$ B97x-15	BP86	B3LYP-15
6	0.176216	<i>n/a</i>	<i>n/a</i>	0.282479	0.153701
7	0.15143	0.327633	0.311422	0.048147	0.148803
8	1.098139	0.586018	0.538247	0.335468	0.628628
9	0.24546	0.467652	0.477965	0.384555	0.730725
10	0.240574	0.327215	0.319558	0.35146	0.266207
11	0.139844	0.259801	0.260735	0.178802	0.132593
12	0.745729	0.71403	0.718055	0.188485	0.608219
13	0.717204	0.928776	1.029093	0.664048	0.471862
14	3.946659	1.146151	0.916158	1.697577	4.115721
15	1.444325	4.453615	4.65963	1.032351	1.137706
16	2.080132	4.204025	4.338117	4.936166	3.392228
17	4.189826	2.239847	2.100564	2.142669	4.995783
18	7.866597	3.681069	4.070464	7.79089	7.868537
19	1.3018	2.442249	2.662015	3.655069	1.030279
20	4.578563	2.353711	3.179623	5.824298	4.17209
21	1.202415	6.886012	6.272332	7.200418	1.02143
22	2.931583	4.913799	3.945683	1.953026	4.587912
23	5.460906	3.02724	3.4519	2.55086	4.327806
24	4.05861	5.809498	6.016242	2.184414	3.406827
25	3.636349	5.285242	5.786496	4.470192	1.935859
26	1.612097	2.298231	2.296194	3.425992	1.474873
27	6.496945	2.244195	1.926735	0.8814	7.638364
28	2.424875	2.835662	2.904103	1.717589	1.877443
29	4.014709	1.783638	1.86767	4.757107	4.015397
30	2.277886	1.666881	1.600766	0.382866	1.897154
31	5.191049	0.560808	0.468501	6.842987	4.761109
32	2.640287	6.837587	6.937011	1.485066	2.91108
33	2.298961	2.982003	2.920186	1.522134	2.317425
34	1.640047	1.598534	1.751783	2.942624	1.698485
35	1.089328	0.263971	0.093883	0.968785	0.82187
36	2.133042	5.18157	5.011703	4.103099	1.741839
37	3.286286	1.163344	1.163897	2.25735	4.200441
38	2.106432	4.164112	4.146477	2.522436	1.800815
39	6.987468	6.322767	6.304474	5.406282	6.248668
40	13.99118	14.93679	15.2361	10.87297	13.61914
41	6.636256	4.874733	5.807128	3.270568	5.712667
42	10.21458	9.328082	8.570398	3.666059	8.022838
43	4.07371	13.962	13.23717	3.680481	3.895836
44	85.07911	94.90086	94.76561	66.0122	79.19778

45	1.808944	0.812575	0.67953	0.693276	1.563165
46	1.597282	5.747291	5.6597	0.667735	0.995937
47	0.816692	1.506938	0.892403	0.158822	0.852664
48	2.045345	1.275931	1.564889	0.833549	1.377114
49	0.725942	1.837671	1.932899	0.302694	0.594647
50	1.060933	2.422956	1.898661	0.256543	0.778895
51	1.050036	1.924796	1.858885	0.90459	0.895233
52	0.192534	0.584824	1.721632	0.073979	0.121103
53	0.707166	4.183473	2.603457	0.134169	0.663408
54	0.351931	0.894006	0.816191	0.205318	0.307281
55	1.349383	1.12919	1.143171	0.938786	1.099444
56	0.33805	0.705884	0.648292	0.332428	0.185546
57	2.243756	0.52383	0.524658	1.865836	2.272203
58	0.80436	1.082442	1.028035	2.566517	1.032995
59	1.420946	1.047671	1.089897	3.131426	1.804154
60	1.661444	2.480045	2.239959	3.414046	1.230876
61	1.677395	1.961045	1.873745	2.237543	2.097112
62	0.726806	0.757521	0.770885	2.501376	1.140547
63	5.425952	3.080748	3.447258	0.718751	4.588246
64	3.99396	1.647872	1.518829	14.50381	6.923542
65	2.665139	4.285767	3.872356	0.839257	1.764116
66	1.99863	2.35302	2.292575	2.620212	1.604973
67	1.808681	2.531307	2.410009	3.28371	1.486455
68	4.65987	4.307396	4.323187	3.49683	5.818867
69	2.591588	5.693706	5.171446	8.615971	1.859736
70	7.081344	10.53438	9.903068	1.664543	6.346016
71	5.690785	3.438903	3.426238	1.947479	4.764932
72	2.019178	10.20209	9.372644	2.418296	2.168409
73	8.140445	2.288217	2.218973	3.451039	8.103469
74	6.03957	1.85048	1.822295	9.264881	6.684491
75	1.590793	5.951283	5.831222	13.64835	1.885365
76	1.276807	2.176986	1.937711	1.004718	0.850717
77	1.695156	1.373705	1.203992	0.765835	3.788998
78	4.281062	3.13681	3.189707	1.418891	1.384161
79	2.4314	5.671647	5.166149	5.116602	6.252385
80	2.297356	9.151519	9.369318	1.285327	0.490137
81	9.645964	3.034958	2.793024	0.233937	4.39766
82	1.76862	5.324238	4.79582	0.123889	1.203358
83	1.747947	2.165875	1.954954	0.04306	1.000432
84	1.145386	2.541083	2.396659	0.830512	0.833727
85	1.740757	2.975213	2.695267	0.306845	1.219805
86	0.901855	2.445679	2.303852	0.347396	0.887629
87	1.690532	2.773657	2.764713	0.729679	1.019474

<b>88</b>	4.26694	8.683048	8.332621	2.482381	3.479266
<b>89</b>	5.522798	10.23958	9.995895	3.479361	4.366286
<b>90</b>	2.415568	3.892849	3.549763	0.999575	1.917227
<b>91</b>	1.440025	3.02591	2.720665	0.425921	0.962455
<b>92</b>	1.342922	5.194031	4.602348	0.261823	0.895333
<b>93</b>	67.58339	69.04511	68.32742	32.70585	59.19881
<b>94</b>	47.08043	78.22052	75.98881	36.14453	33.87955
<b>95</b>	66.05136	154.3699	150.178	12.54721	16.78463
<b>96</b>	79.45079	40.46625	39.91858	7.486209	103.7986
<b>97</b>	64.88878	33.37196	33.84537	23.44197	52.82144
<b>98</b>	38.08242	87.4798	75.69418	87.64904	34.97893
<b>99</b>	24.20481	90.57292	87.09747	103.6886	33.39237
<b>100</b>	149.3812	96.56172	107.4773	86.02111	139.8359
<b>101</b>	120.3289	160.8581	160.3295	161.2308	121.6342
<b>102</b>	186.6225	193.452	194.1098	137.3209	176.7241
<b>103</b>	295.6031	270.0561	277.1899	149.7212	264.9425
<b>104</b>	114.1699	132.4205	131.8485	102.6217	99.81054
<b>105</b>	13.61649	50.24018	63.06752	3.954801	10.29737
<b>106</b>	5.979238	36.1524	13.33951	18.67216	3.546323
<b>107</b>	380.5656	407.5174	416.0725	402.3156	381.5516

**Table S21.** Calculated  $\nu(\text{CO})$  vibrational mode frequencies versus experimental  $\nu(\text{CO})$  ( $\text{cm}^{-1}$ ). Scaling factors are tabulated in **Table S15**. Ma-def2-TZVP, grid 2, tightopt, D4 applied to all except B3PW91. Experimental data from Kuppuswamy *et al.*, of a solid crystalline sample (details in reference). Full experimental FT-IR spectrum plotted in **Figure S18** of Kuppuswamy *et al.*<sup>1</sup>

Mode	Calculated $\nu(\text{CO})$ Frequencies ( $\text{cm}^{-1}$ ); Unscaled						Calculated $\nu(\text{CO})$ Frequencies ( $\text{cm}^{-1}$ ); Scaled						FT-IR Data ( $\text{cm}^{-1}$ )
	B3PW91	B3LYP	$\omega\text{B97x}$	$\omega\text{B97x-15}$	BP86	B3LYP-15	B3PW91	B3LYP	$\omega\text{B97x}$	$\omega\text{B97x-15}$	BP86	B3LYP-15	
93	2046.6	2031	2062	2039.87	1964.77	2015.48	1972.922	2039.936	2044.267	2039.87	2030.983	2015.48	1945, 1975, 2015, 2100
94	2059.95	2043.05	2074.59	2052.41	1970.26	2030.66	1985.792	2052.039	2056.749	2052.41	2036.658	2030.66	
95	2071.2	2054.4	2085.87	2064.52	1974.19	2040.49	1996.637	2063.439	2067.932	2064.52	2040.72	2040.49	
96	2075.53	2059.75	2106.74	2082.47	1977.02	2044.98	2000.811	2068.813	2088.622	2082.47	2043.646	2044.98	
97	2081.39	2066.27	2109.99	2085.91	1978.97	2050.58	2006.46	2075.362	2091.844	2085.91	2045.661	2050.58	
98	2084.68	2068.55	2113.09	2089.03	1983.05	2052.33	2009.632	2077.652	2094.917	2089.03	2049.879	2052.33	
99	2085.41	2069.95	2116.7	2092.3	1994.74	2054.82	2010.335	2079.058	2098.496	2092.3	2061.963	2054.82	
100	2095.71	2078.35	2125.05	2101.33	2002.13	2063.84	2020.264	2087.495	2106.775	2101.33	2069.602	2063.84	
101	2103.87	2085.43	2135.51	2111.18	2009.93	2072.48	2028.131	2094.606	2117.145	2111.18	2077.665	2072.48	
102	2105.37	2088.98	2137.82	2113.17	2010.75	2073.59	2029.577	2098.172	2119.435	2113.17	2078.512	2073.59	
103	2115.44	2098.61	2150.73	2126.71	2029.81	2085	2039.284	2107.844	2132.234	2126.71	2098.215	2085	
104	2125.94	2109.94	2162.55	2137.61	2031.26	2095.35	2049.406	2119.224	2143.952	2137.61	2099.713	2095.35	
105	2135.59	2118.08	2170.78	2146.67	2047.74	2106.03	2058.709	2127.4	2152.111	2146.67	2116.749	2106.03	
106	2139.11	2121.79	2171.08	2146.91	2048.01	2109.65	2062.102	2131.126	2152.409	2146.91	2117.028	2109.65	
107	2186.64	2170.38	2223.16	2198.09	2088.06	2155.41	2107.921	2179.93	2204.041	2198.09	2158.428	2155.41	

**Figures S50-S60 show plotted IR intensities and Raman activities** (no Raman calculated for B3PW91) for each listed functional. Ma-def2-TZVP, grid 2, tightopt, D4 applied to all except B3PW91. Plots were generated in Chemcraft 18.0, with Lorentzian line broadening applied.

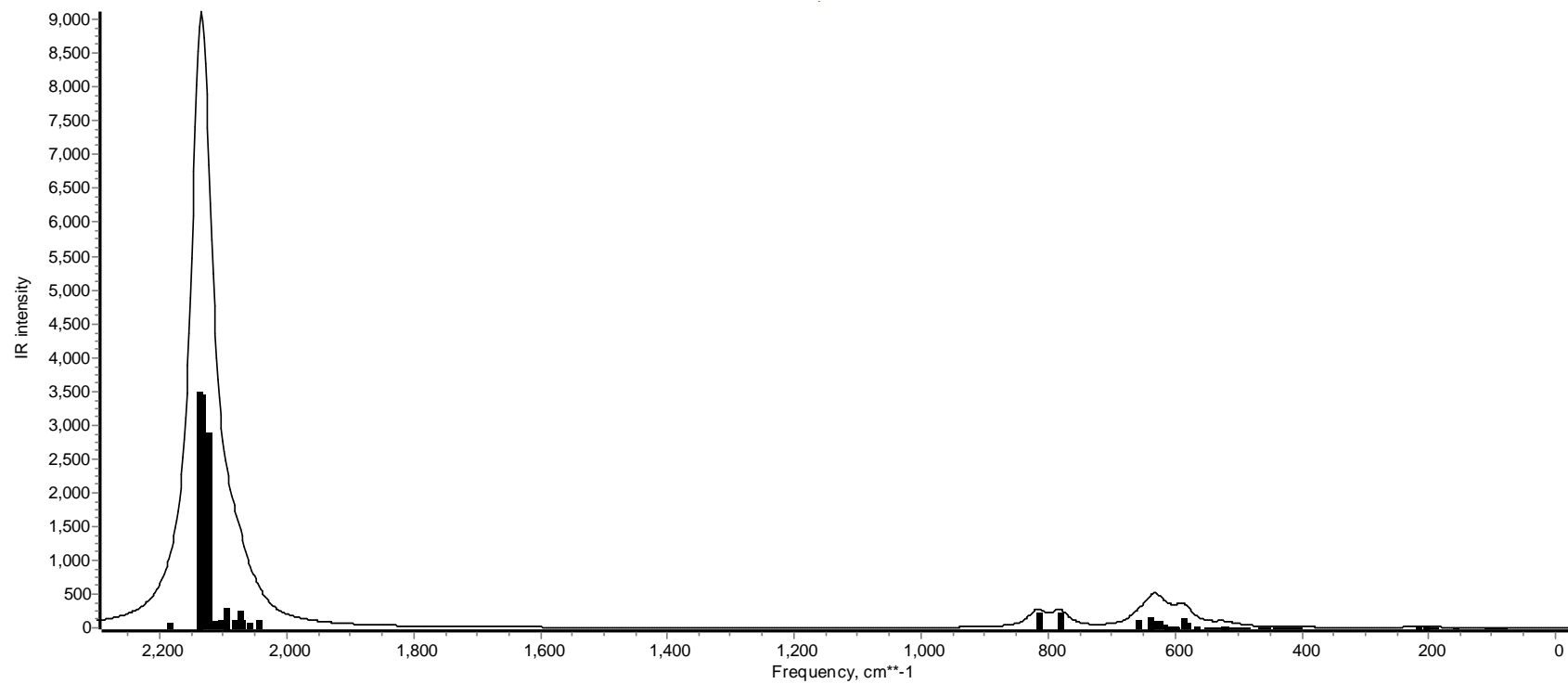


**Figure S50.** B3PW91 IR intensities.

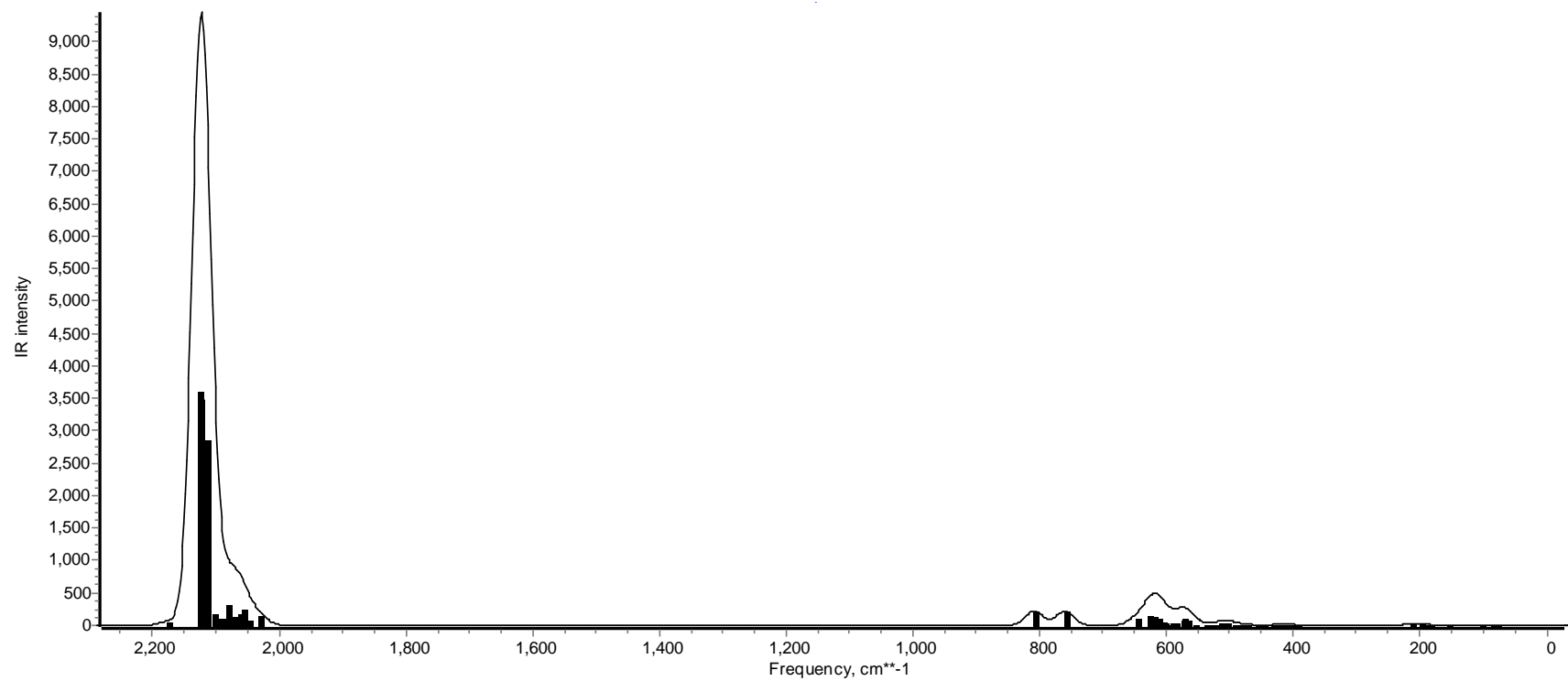


**Figure S51.** B3LYP IR intensities.

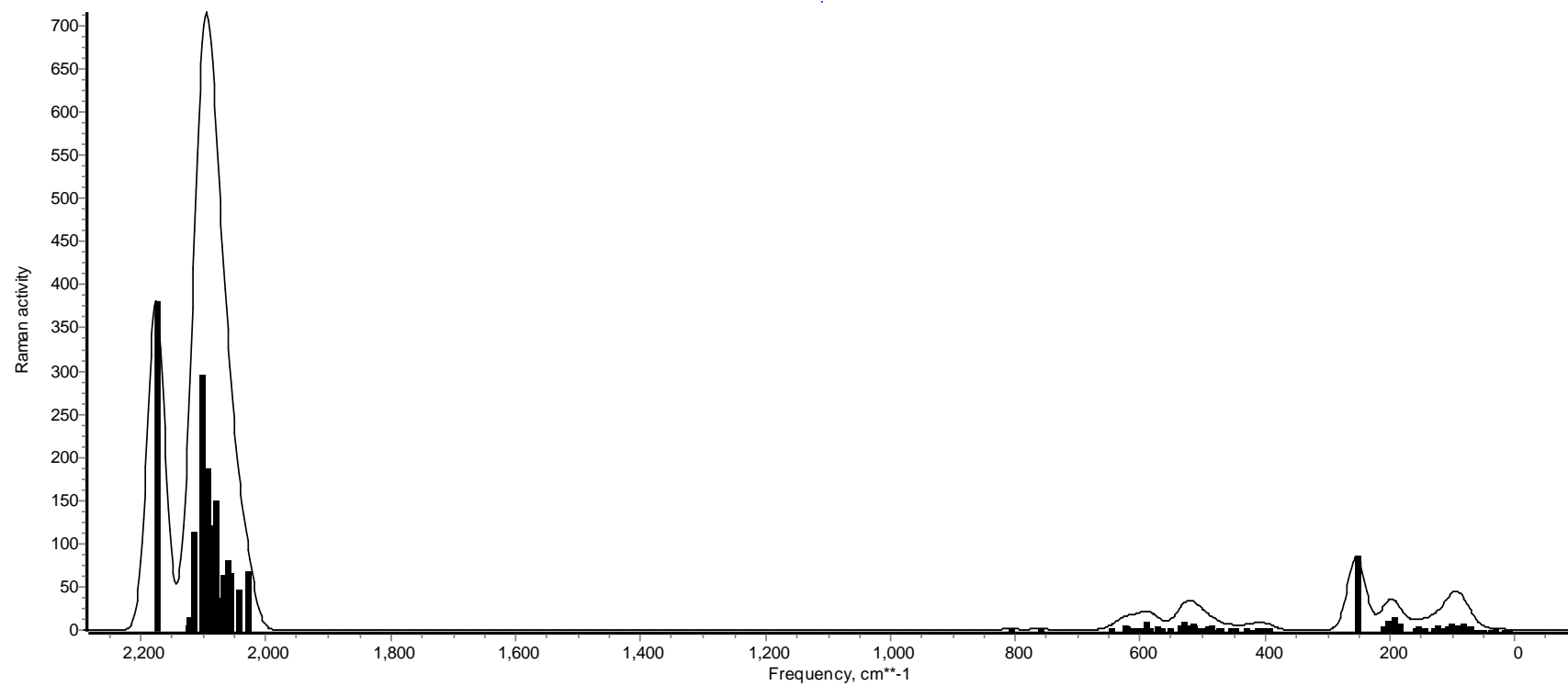


**Figure S52.** B3LYP Raman activities.

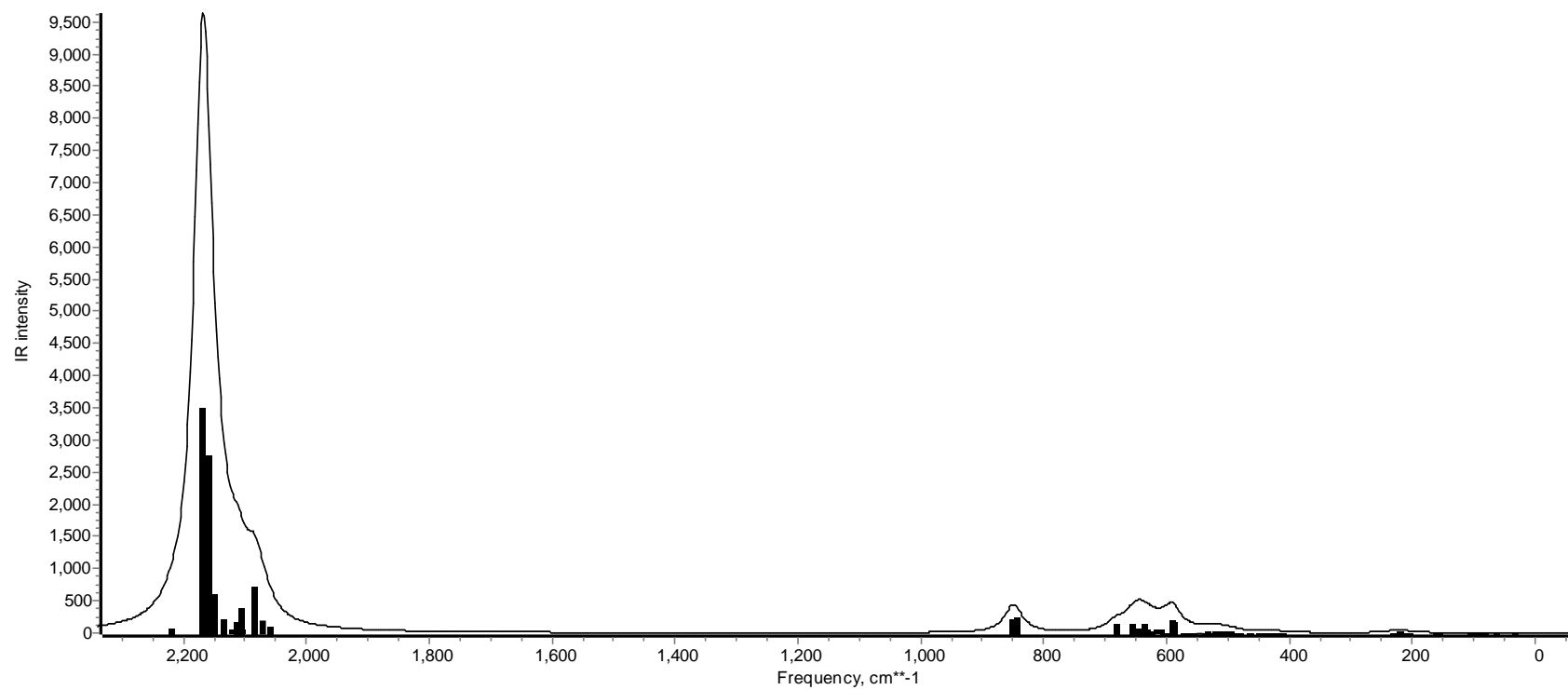


**Figure S53.** ωB97x IR intensities

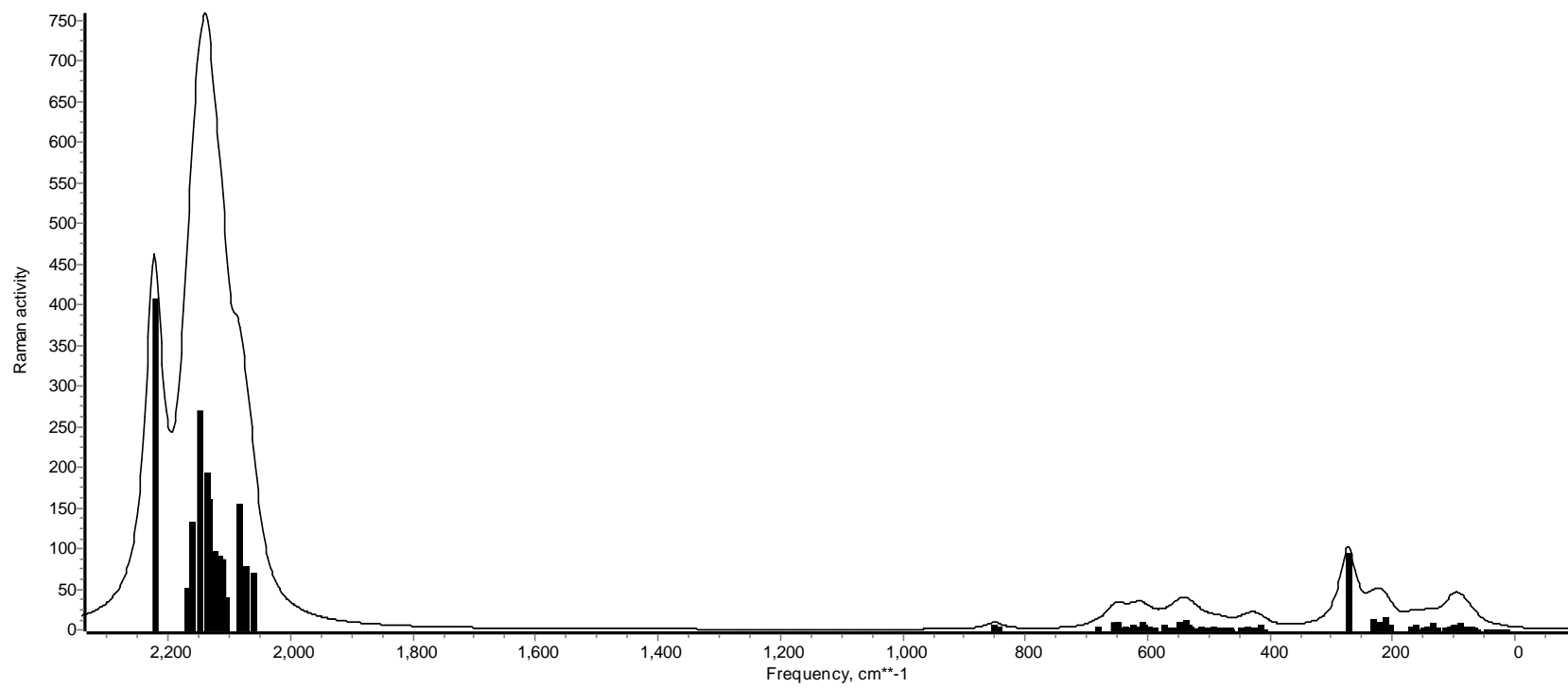


**Figure S54.**  $\omega$ B97x Raman activities.

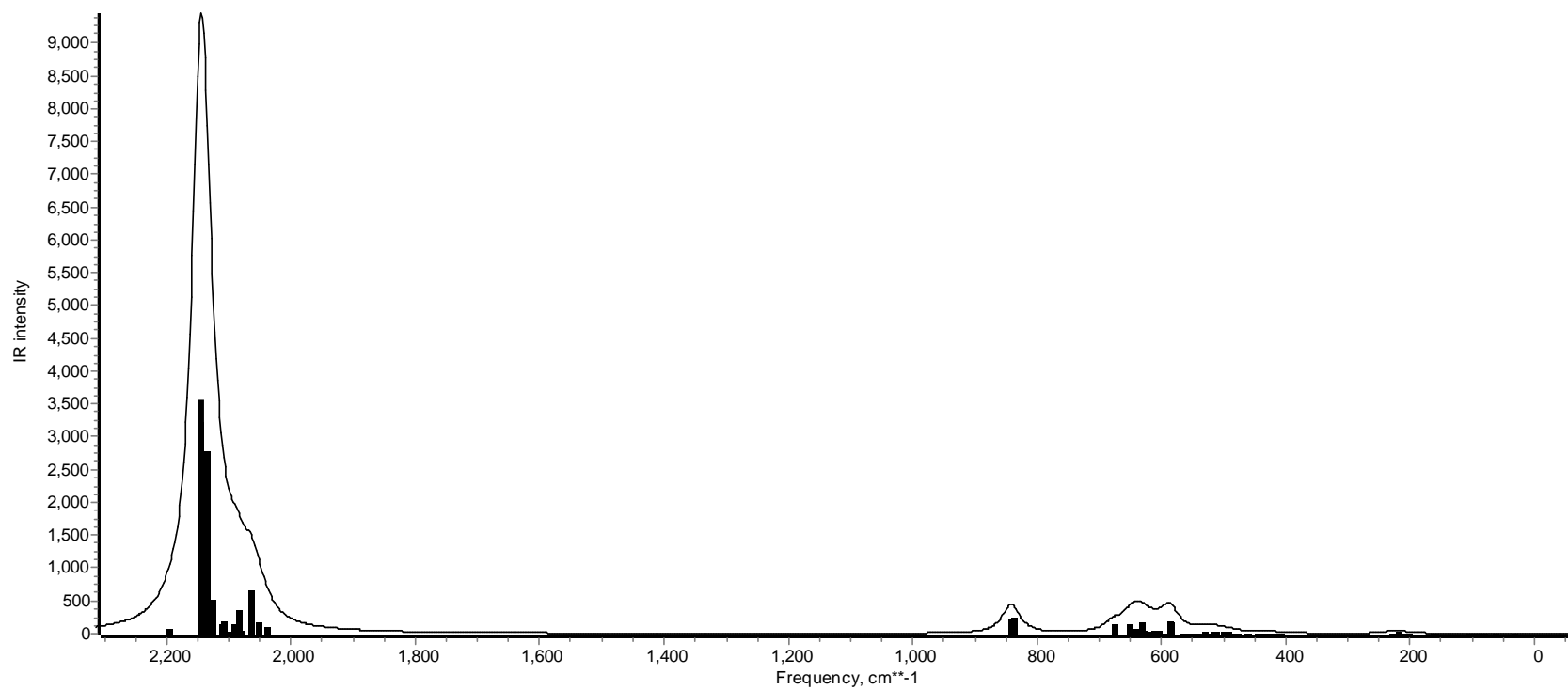


**Figure S55.** ωB97x-15 IR intensities

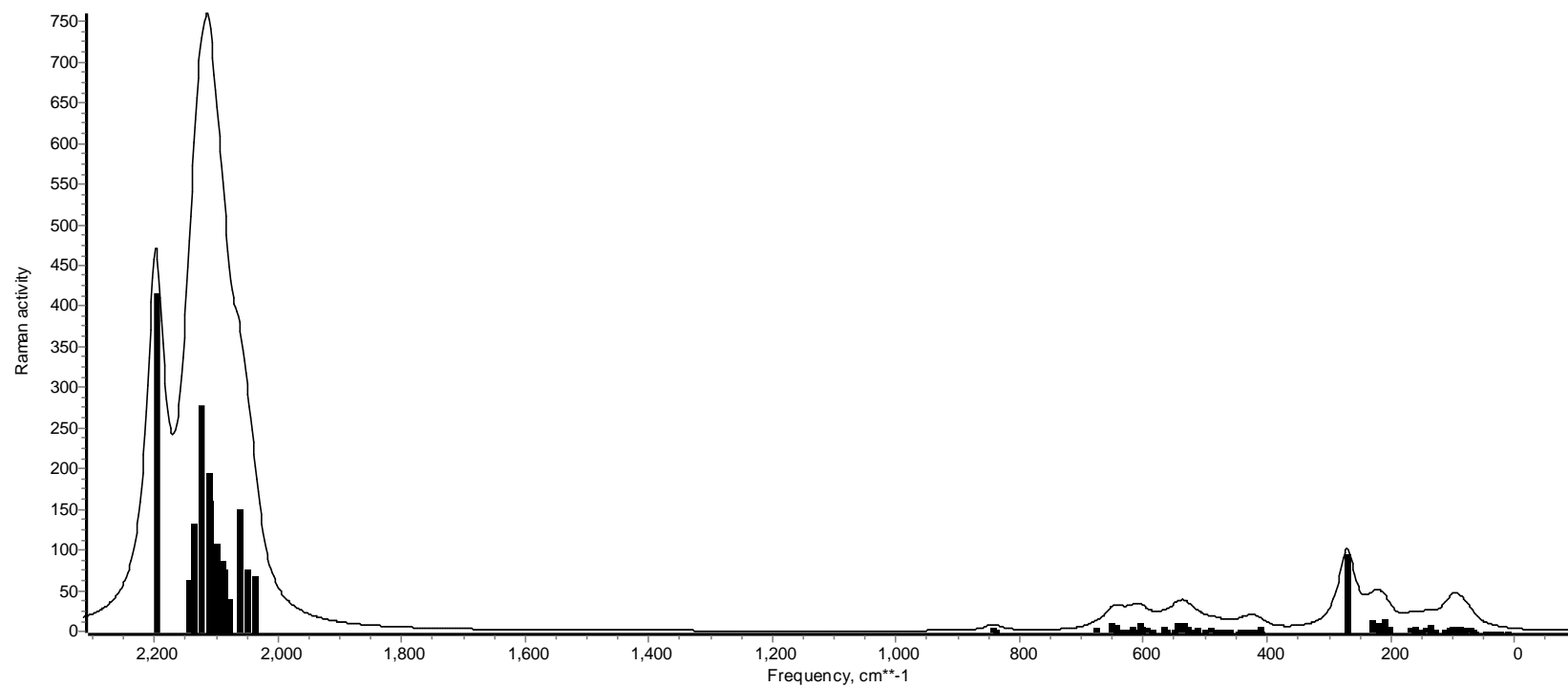


**Figure S56.** ωB97x-15 Raman activities.

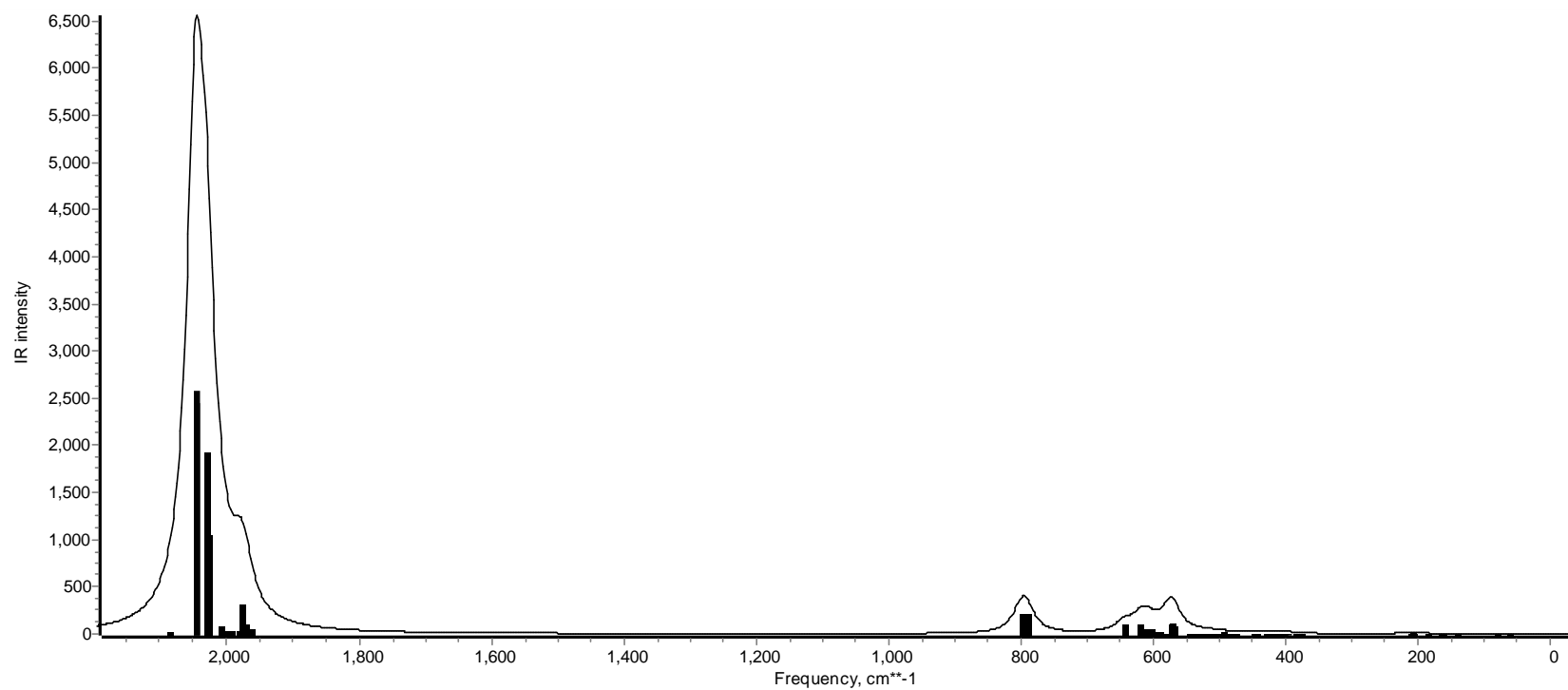


**Figure S57.** BP86 Raman activities.

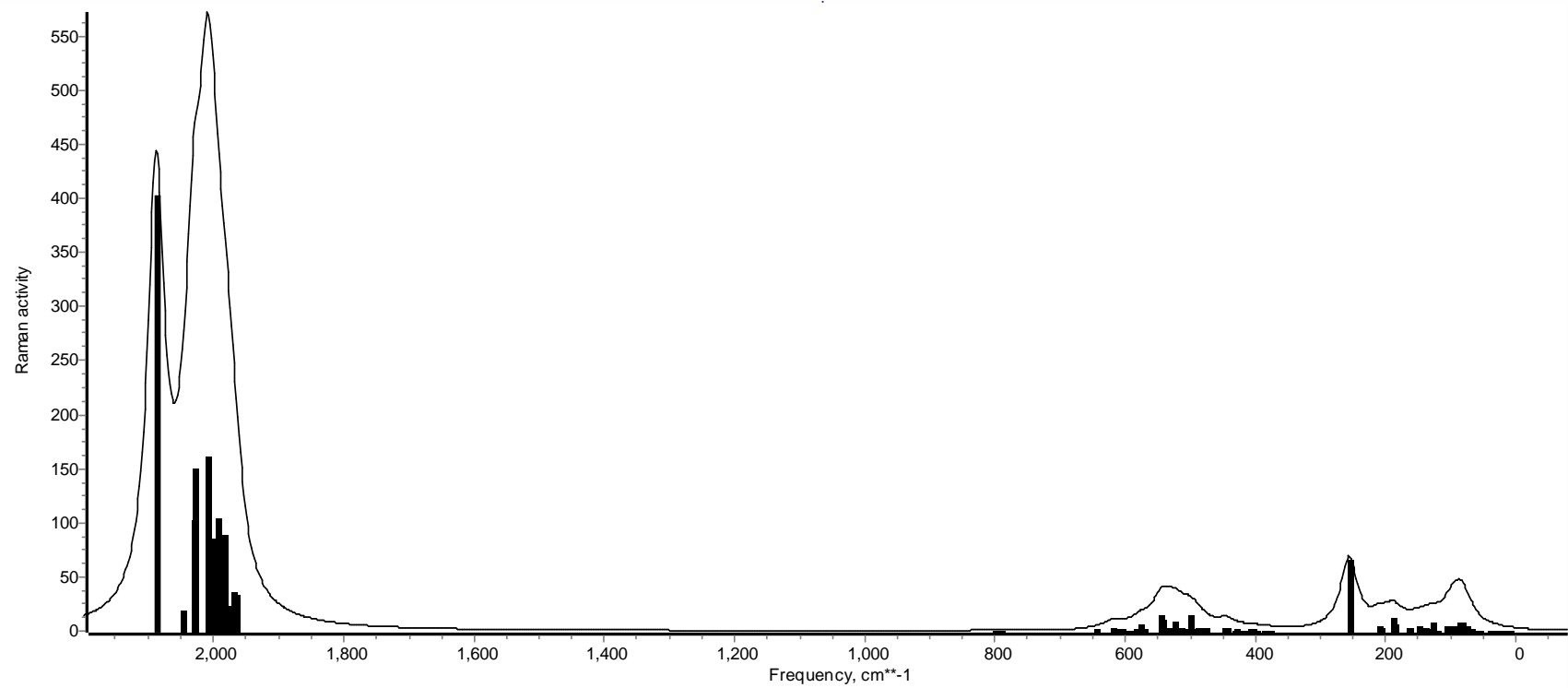


**Figure S58.** BP86 Raman activities.

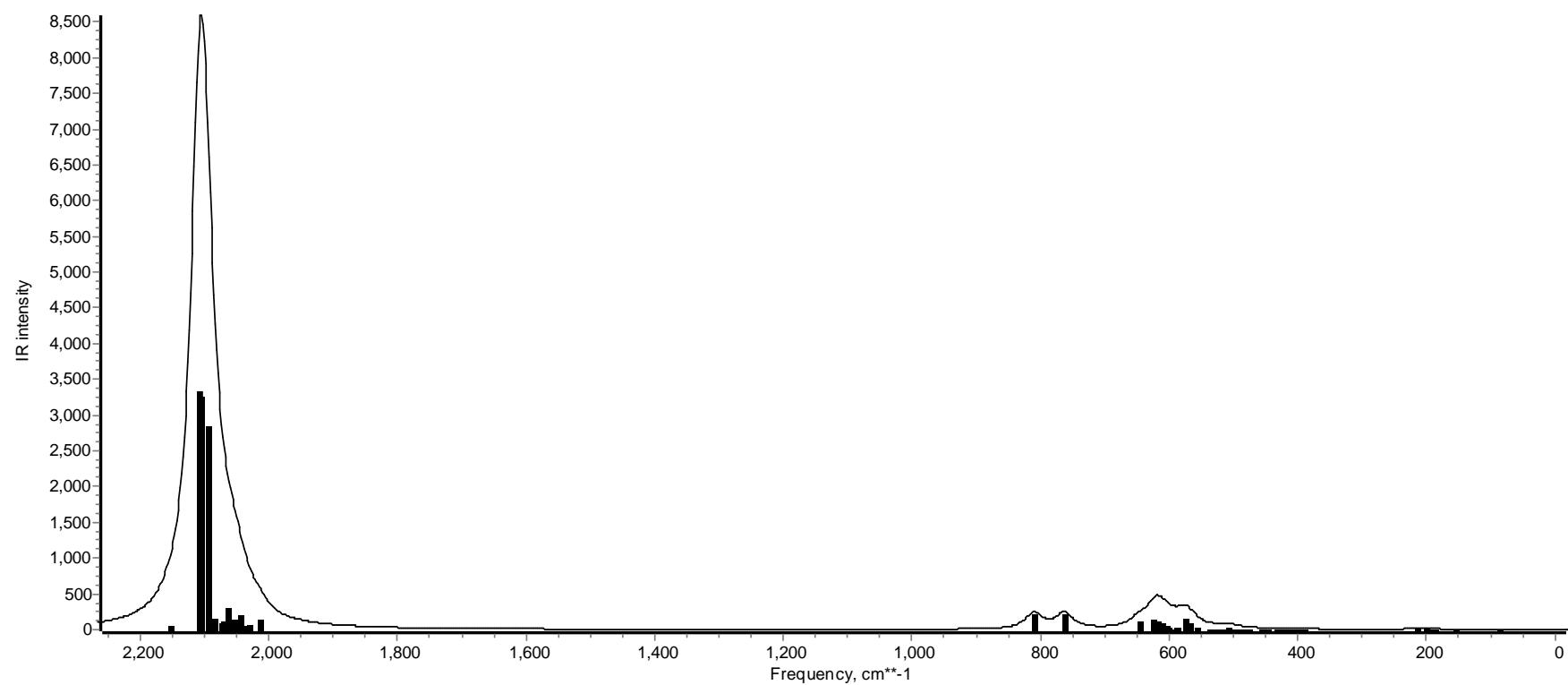


**Figure S59.** B3LYP IR intensities.

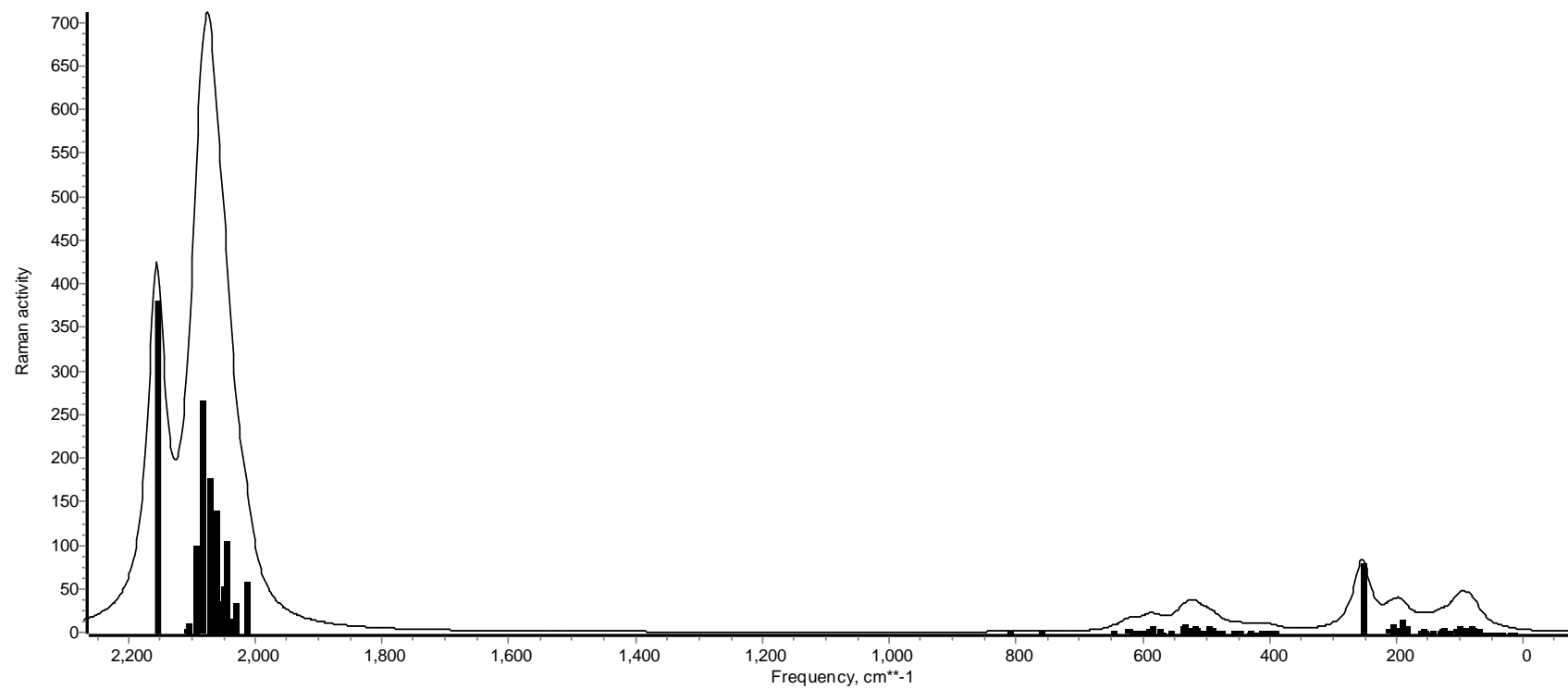


**Figure S60.** B3LYP-15 Raman activities.

**Tables S22.** Results of screening of functionals using  $[\text{Fe}_5(\mu_5\text{-C})(\text{CO})_{15}]$  – calculated single point energies and HOMO-LUMO gaps. ma-def2-TZVP, grid 2, tightopt, D4 applied to all except B3PW91.

	Final Single Point Energy Eh	HOMO-LUMO gap (eV)
<b>B3PW91</b>	-8057.042434878665	2.887967108
<b>BP86</b>	-8059.282600540992	1.611198836
<b>B3LYP</b>	-8056.662814392064	2.751092760
$\omega$ <b>B97x</b>	-8057.871214051423	7.240734644
<b>B3LYP-15</b>	-8054.999929988311	2.441968984
$\omega$ <b>B97X-15</b>	-8049.809906818548	7.088077568

#### Remarks on HOMO-LUMO gaps and SPE:

HOMO-LUMO gap was very large for  $\omega$ B97X-15 and  $\omega$ B97x, but on scale with reported calculated HOMO-LUMO gaps with these functionals when applied to Fe carbonyl carbide clusters in the literature.<sup>26</sup> The lowest SPE was BP86. Based on these results, no functionals were eliminated entirely but BP86, B3LYP, B3LYP-15, and B3PW91 were preferred.

#### Remarks on computational method screening with $\text{Fe}_5(\mu_5\text{-C})(\text{CO})_{15}$ .

All applied methods gave reasonable output geometries with low RMSD values (**Table S24**), and core Fe-carbide and Fe-Fe bond lengths consistent with experimental values (**Table S25**). Interestingly, significant variation was observed in the  $\text{Fe}_4$ -plane-carbide displacement varying with functional. However, this variation was not disproportionate to the variation observed among published crystal data sets (0.119<sup>27</sup> versus 0.09 Å, for 1552287 versus the originally published structure by Bryae *et al.*<sup>28</sup>). The vibrational analysis of  $\text{Fe}_5(\mu_5\text{-C})(\text{CO})_{15}$  that was conducted show the calculated IR  $\nu(\text{CO})$  energies occupy a reasonable range for a neutral cluster with terminally bound carbonyl ligands, varying depending on the applied functional and whether or not a scaling factor is applied. The calculated spectra all had no imaginary modes calculated, with the exception of  $\omega$ B97-x and  $\omega$ B97-x-15, which each had one small ( $< 20 \text{ cm}^{-1}$ ) imaginary mode that could not be resolved by increasing grid size or reoptimizing the geometry from distorted coordinated, or to a tighter level of convergence criteria (**Table S12**). The calculated final single point energy was lowest for BP86, varying between functionals used and particularly between  $\omega$ B97-x and  $\omega$ B97-x-15 (Table SX). The calculated HOMO-LUMO gaps varied drastically by functional used, with very large gaps ( $\sim 7 \text{ eV}$ ) calculated for  $\omega$ B97-x and  $\omega$ B97-x-15, and smaller less variable energy gaps for the other functionals (from 1.6 to 2.9 eV). The high HOMO-LUMO value is comparable to reports on iron carbide carbonyl cluster modeling in other studies using  $\omega$ B97-x and  $\omega$ B97-x-15.<sup>26</sup>

From these results, we concluded that all but  $\omega$ B97-x and  $\omega$ B97-x-15 were reasonable functionals for the geometry optimization of the structurally ambiguous compound **2** and proceeded to apply these methodologies. Of these, only the BP86 ma-def2-TZVP-D4 approach gave a converged geometry with only three small (less than  $100 \text{ cm}^{-1}$ ) calculated imaginary frequencies, the details of which are discussed *vide infra*.

We went on to test C-PCM for DCE with BP86 ma-def2-TZVP-D4. Results were distinct from gas phase only in that four of the carbonyls were bridging, as observed in the experimental results for the dianion, rather than all terminal. This was also indicated by the calculated IR. This does not fit experimental results with the five iron neutral cluster.

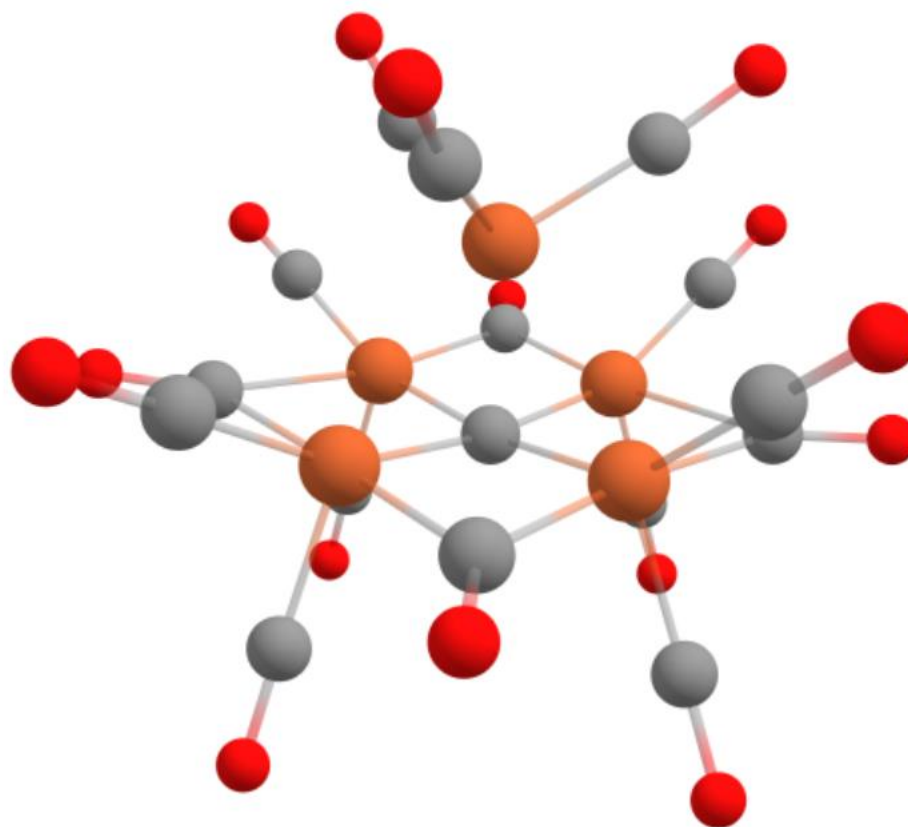


**Figure S61.** Optimized geometry of five-iron neutral cluster with C-PCM for DCE, BP86 ma-def2-TZVP-D4.

**Table S23.** Full IR frequencies for five-iron neutral cluster with C-PCM for DCE, BP86 ma-def2-TZVP-D4, with and without scaling factors. Scaling factor for BP86 with def2-TZVP.<sup>24</sup>

DCE	With Scaling Factor
0	0
0	0
0	0
0	0
0	0
0	0
21.3	22.01781
38.8	40.10756
39.44	40.76913
45.47	47.00234
46.75	48.32548
50.34	52.03646
60.72	62.76626

71.11	73.50641
73.6	76.08032
77.94	80.56658
79.67	82.35488
86.19	89.0946
87.19	90.1283
90.86	93.92198
92.07	95.17276
95.46	98.677
96.27	99.5143
98.5	101.8195
99.01	102.3466
100.59	103.9799
101.57	104.9929
103.5	106.988
106.54	110.1304
109.3	112.9834
123.38	127.5379
135.47	140.0353
160.6	166.0122
164.05	169.5785
170.1	175.8324
173.07	178.9025
192.14	198.6151
201.26	208.0425
202.01	208.8177
204.84	211.7431
215.41	222.6693
232.9	240.7487
257.68	266.3638
258.26	266.9634
272.09	281.2594
356.66	368.6794
385.99	398.9979
394.61	407.9084
397.17	410.5546
405.45	419.1137
407.65	421.3878
408.33	422.0907
410.58	424.4165
414.26	428.2206
415.14	429.1302
416.28	430.3086
421.68	435.8906
435.44	450.1143
439.91	454.735
440.9	455.7583
458.76	474.2202
461.3	476.8458
467.32	483.0687
470.48	486.3352
486.11	502.4919
486.89	503.2982

495.38	512.0743
498.88	515.6923
504.83	521.8428
507.67	524.7785
522.48	540.0876
529.06	546.8893
530.96	548.8534
534.69	552.7091
536.39	554.4663
548.88	567.3773
550.9	569.4653
554.48	573.166
555.57	574.2927
570.43	589.6535
575.04	594.4188
579.78	599.3186
582.09	601.7064
591.8	611.7437
594.74	614.7827
602.6	622.9076
603.12	623.4451
609.12	629.6473
610.19	630.7534
613.98	634.6711
636.05	657.4849
850.75	879.4203
853.37	882.1286
1872.26	1935.355
1884.12	1947.615
1885.14	1948.669
1907.82	1972.114
1960.82	2026.9
1971.37	2037.805
1996.38	2063.658
2003.01	2070.511
2008.25	2075.928
2010.17	2077.913
2016	2083.939
2035.34	2103.931
2044.26	2113.152
2045.32	2114.247
2097.34	2168.02

### Remarks on DFT Modeled Geometry of **2**.

All functionals tested on  $[\text{Fe}_5(\mu_5\text{-C})(\text{CO})_{15}]$  were applied to the modeling of **2**. The chosen starting geometry was the crystal data of **1**. Ultimately, the only dataset which converged to an optimized geometry was the one performed with BP86. This result was unsatisfactory, as the frequency analysis afforded three small ( $<100 \text{ cm}^{-1}$ ) imaginary modes, visualized as breathing modes involving all the molecule's atoms, which could not be eliminated with increasing the grid size or by displacing the atoms and reconverging. With this persistent result, a set of trial calculations were performed this time with a C-

PCM correction. We had initially judged such a correction to be an unnecessary added computational cost given:

1) the success of the gas phase calculations with  $[\text{Fe}_5(\mu_5\text{-C})(\text{CO})_{15}]$ , and

2) the fact that the tested clusters are all neutral, not charged, unlike other computationally modeled iron-carbonyl-carbide clusters in the literature that were conducted with a C-PCM correction.<sup>26,29</sup>

A range of dielectric constants were tested on **2**, with no other modifications to the calculation parameters, but this had no significant impact on results, all of which gave essentially equivalent geometries to the gas phase result, apart from small reductions in the magnitude of the imaginary frequencies (**Table S22**.) We have preliminary results that suggest that the application of C-PCM allows for convergence with a wider range of functionals and basis sets when modeling cluster **2**. We will continue to explore this in future studies.

**Table S24.** RMSD values of gas-phase versus solvated models of **2** by tested dielectric constant.

Solvent / dielectric constant	RMSD of structure coordinates compared with the gas-phase result
Acetonitrile (36.6)	0.0217554032585826
Dichloroethane (9.08)	0.0117467667068557
Tetrahydrofuran (7.25)	0.0178716128334861
Toluene (2.4)	0.0114888118646329

**Tables S25.** Full calculated IR frequencies of **2**, with and without scaling factors. Scaling factor for BP86 with def2-TZVP.<sup>24</sup>

No scaling factor					Scaling Factor Applied				
Gas-Phase	MeCN	DCE	THF	Toluene	Gas-Phase	MeCN	DCE	THF	Toluene
0	0	0	0	0	0	0	0	0	0
0	0	0	0	0	0	0	0	0	0
0	0	0	0	0	0	0	0	0	0
0	0	0	0	0	0	0	0	0	0
0	0	0	0	0	0	0	0	0	0
0	0	0	0	0	0	0	0	0	0
-77.23	-65.48	-57.63	-64.73	-63.27	-79.8327	-67.6867	-59.5721	-66.9114	-65.4022
-77.22	-65.23	-56.76	-64.72	-63.26	-79.8223	-67.4283	-58.6728	-66.9011	-65.3919
-18.92	-41.12	-33.74	-39.23	-34.67	-19.5576	-42.5057	-34.877	-40.5521	-35.8384
14.27	-17.83	16.75	-15.43	-8.99	14.7509	-18.4309	17.31448	-15.95	-9.29296
29.97	21.73	33.59	23.81	27.21	30.97999	22.4623	34.72198	24.6124	28.12698
30	21.87	33.78	23.81	27.21	31.011	22.60702	34.91839	24.6124	28.12698
45.56	36.6	45.62	37.35	38.82	47.09537	37.83342	47.15739	38.6087	40.12823
48.39	49.48	53.19	49.49	49.38	50.02074	51.14748	54.9825	51.15781	51.04411
54.77	57.95	66.95	58.33	58.72	56.61575	59.90292	69.20622	60.29572	60.69886
54.78	58.05	67.02	58.33	58.73	56.62609	60.00629	69.27857	60.29572	60.7092
61.79	61.66	67.16	61.89	62.37	63.87232	63.73794	69.42329	63.97569	64.47187
67.81	65.14	70.84	65.61	66.55	70.0952	67.33522	73.22731	67.82106	68.79274
67.81	65.17	70.9	65.61	66.56	70.0952	67.36623	73.28933	67.82106	68.80307
68.98	68.78	71.51	68.76	68.57	71.30463	71.09789	73.91989	71.07721	70.88081
69.5	71.46	80.26	71.44	71.27	71.84215	73.8682	82.96476	73.84753	73.6718
72.68	71.53	80.42	71.44	71.28	75.12932	73.94056	83.13015	73.84753	73.68214
72.7	72.42	82.07	72.3	71.87	75.14999	74.86055	84.83576	74.73651	74.29202
83.51	85.21	93.34	85.09	84.74	86.32429	88.08158	96.48556	87.95753	87.59574
86	90.26	94.08	90.27	90.36	88.8982	93.30176	97.2505	93.3121	93.40513
86.84	90.71	96.01	90.71	90.72	89.76651	93.76693	99.24554	93.76693	93.77726

90.35	92.04	98.45	91.86	91.38	93.3948	95.14175	101.7678	94.95568	94.45951
91.92	96.87	101.23	96.7	96.19	95.0177	100.1345	104.6415	99.95879	99.4316
91.92	96.94	101.25	96.7	96.19	95.0177	100.2069	104.6621	99.95879	99.4316
99.28	100.02	102.96	100.01	99.97	102.6257	103.3907	106.4298	103.3803	103.339
99.29	102.57	104.46	102.46	102.09	102.6361	106.0266	107.9803	105.9129	105.5304
101.25	102.62	104.55	102.46	102.1	104.6621	106.0783	108.0733	105.9129	105.5408
121.79	115.79	118.47	116.06	116.73	125.8943	119.6921	122.4624	119.9712	120.6638
133.43	132.88	135.05	132.92	133.07	137.9266	137.3581	139.6012	137.3994	137.5545
137.05	132.88	135.06	132.92	133.07	141.6686	137.3581	139.6115	137.3994	137.5545
137.06	135.1	136.71	135.05	134.89	141.6789	139.6529	141.3171	139.6012	139.4358
146.75	143.21	144.7	143.13	143.01	151.6955	148.0362	149.5764	147.9535	147.8294
165.16	169.66	172.05	169.95	169.6	170.7259	175.3775	177.8481	175.6773	175.3155
170.88	169.66	172.79	169.95	170.55	176.6387	175.3775	178.613	175.6773	176.2975
170.89	170.3	172.8	170.12	170.55	176.649	176.0391	178.6234	175.853	176.2975
174.78	174.48	176.65	174.65	175.01	180.6701	180.36	182.6031	180.5357	180.9078
186.17	188.33	189.88	188.22	187.82	192.4439	194.6767	196.279	194.563	194.1495
186.18	188.35	190.11	188.22	187.82	192.4543	194.6974	196.5167	194.563	194.1495
192.52	195.01	197.02	195.03	194.98	199.0079	201.5818	203.6596	201.6025	201.5508
200.58	206.21	209.68	206.42	206.79	207.3395	213.1593	216.7462	213.3764	213.7588
200.58	212.24	214.39	212.11	211.49	207.3395	219.3925	221.6149	219.2581	218.6172
201.22	212.25	214.59	212.11	211.49	208.0011	219.4028	221.8217	219.2581	218.6172
208.37	216.77	220.43	216.68	216.4	215.3921	224.0751	227.8585	223.9821	223.6927
232.26	236.79	237.77	236.56	235.98	240.0872	244.7698	245.7828	244.5321	243.9325
269.18	270.14	273.81	270.3	270.6	278.2514	279.2437	283.0374	279.4091	279.7192
339.38	341.27	343.05	341.04	340.45	350.8171	352.7708	354.6108	352.533	351.9232
339.39	341.28	343.14	341.04	340.45	350.8274	352.7811	354.7038	352.533	351.9232
368.33	370.71	374.18	370.6	370.27	380.7427	383.2029	386.7899	383.0892	382.7481
370.17	373.84	375.54	373.47	372.53	382.6447	386.4384	388.1957	386.0559	385.0843
392.42	389.76	395.36	389.95	390.09	405.6446	402.8949	408.6836	403.0913	403.236
392.42	389.78	395.46	389.95	390.09	405.6446	402.9156	408.787	403.0913	403.236
398.51	396.08	401.8	396.34	396.93	411.9398	409.4279	415.3407	409.6967	410.3065
403.03	400.95	405.25	401.09	401.43	416.6121	414.462	418.9069	414.6067	414.9582
403.04	400.96	405.29	401.09	401.43	416.6224	414.4724	418.9483	414.6067	414.9582
405.36	404.66	411.27	404.77	404.87	419.0206	418.297	425.1298	418.4107	418.5141
414.82	413.27	415.28	413.17	412.93	428.7994	427.1972	429.2749	427.0938	426.8457
434.36	433.4	437.19	433.48	433.77	448.9979	448.0056	451.9233	448.0883	448.388
434.37	433.41	437.26	433.48	433.77	449.0083	448.0159	451.9957	448.0883	448.388
447.2	449.26	451.93	448.93	447.88	462.2706	464.4001	467.16	464.0589	462.9736
447.2	449.28	451.96	449.13	448.83	462.2706	464.4207	467.1911	464.2657	463.9556
449.99	449.29	453.54	449.13	448.85	465.1547	464.4311	468.8243	464.2657	463.9762
453.94	456.43	459.94	456.37	456.24	469.2378	471.8117	475.44	471.7497	471.6153
458.14	460.33	464.47	459.86	458.86	473.5793	475.8431	480.1226	475.3573	474.3236
458.33	460.36	464.92	459.86	458.89	473.7757	475.8741	480.5878	475.3573	474.3546
458.33	462.12	466.99	461.99	461.8	473.7757	477.6934	482.7276	477.5591	477.3627
462.58	465.64	468.93	465.2	465.02	478.1689	481.3321	484.7329	480.8772	480.6912
468.9	465.78	470.85	466.07	466.74	484.7019	481.4768	486.7176	481.7766	482.4691
471.27	472.05	476.68	471.85	471.46	487.1518	487.9581	492.7441	487.7513	487.3482
482.46	486.78	489.56	486.51	485.9	498.7189	503.1845	506.0582	502.9054	502.2748
483.18	487.19	489.99	486.79	486.05	499.4632	503.6083	506.5027	503.1948	502.4299
495.79	501.27	503.6	500.91	500.07	512.4981	518.1628	520.5713	517.7907	516.9224
521.45	519.5	525.65	519.8	520.4	539.0229	537.0072	543.3644	537.3173	537.9375
521.46	519.5	525.73	519.8	520.4	539.0332	537.0072	543.4471	537.3173	537.9375
525.52	521.77	527	522.09	522.79	543.23	539.3536	544.7599	539.6844	540.408
528.06	529.16	533.97	529.07	528.89	545.8556	546.9927	551.9648	546.8997	546.7136
544.15	542.76	547.47	543.28	544.29	562.4879	561.051	565.9197	561.5885	562.6326
544.16	542.76	547.5	543.28	544.29	562.4982	561.051	565.9508	561.5885	562.6326
552.92	553.36	557.56	553.47	553.76	571.5534	572.0082	576.3498	572.1219	572.4217
556.73	557.75	561.21	558.17	558.58	575.4918	576.5462	580.1228	576.9803	577.4041
556.73	557.76	561.28	558.17	558.58	575.4918	576.5565	580.1951	576.9803	577.4041

557.42	558.87	562.96	559	559.51	576.2051	577.7039	581.9318	577.8383	578.3655
557.42	558.88	563.03	559	559.51	576.2051	577.7143	582.0041	577.8383	578.3655
568.07	565.44	569.12	566.48	568.11	587.214	584.4953	588.2993	585.5704	587.2553
573.32	569.85	574.81	570.64	572.3	592.6409	589.0539	594.1811	589.8706	591.5865
576.91	577.56	581.35	577.8	578.28	596.3519	597.0238	600.9415	597.2719	597.768
576.97	577.56	581.42	577.8	578.28	596.4139	597.0238	601.0139	597.2719	597.768
576.98	578.87	581.85	579.02	579.34	596.4242	598.3779	601.4583	598.533	598.8638
593.03	587.53	590.75	588.57	590.7	613.0151	607.3298	610.6583	608.4048	610.6066
619.85	616.97	620.62	618	620.11	640.7389	637.7619	641.5349	638.8266	641.0077
621.11	618.43	620.64	619.05	620.28	642.0414	639.2711	641.5556	639.912	641.1834
621.11	618.44	621.22	619.05	620.29	642.0414	639.2814	642.1551	639.912	641.1938
625.21	620.32	622.46	621.25	623.19	646.2796	641.2248	643.4369	642.1861	644.1915
647.33	647.06	649.76	647.17	647.4	669.145	668.8659	671.6569	668.9796	669.2174
769.55	777.29	784.2	778.3	780.06	795.4838	803.4847	810.6275	804.5287	806.348
769.55	777.29	784.24	778.3	780.06	795.4838	803.4847	810.6689	804.5287	806.348
811.42	809.48	818.07	811.29	814.96	838.7649	836.7595	845.639	838.6305	842.4242
1888.88	1860.49	1872.57	1867.97	1883.74	1952.535	1923.189	1935.676	1930.921	1947.222
1888.88	1860.49	1872.59	1867.97	1883.74	1952.535	1923.189	1935.696	1930.921	1947.222
1894.85	1869.34	1881.08	1876.91	1892.14	1958.706	1932.337	1944.472	1940.162	1955.905
1895.44	1879.88	1889.21	1884.84	1896	1959.316	1943.232	1952.876	1948.359	1959.895
1973.87	1970.45	1973.53	1973.33	1980.03	2040.389	2036.854	2040.038	2039.831	2046.757
1984.53	1978.7	1982.91	1982.48	1990.1	2051.409	2045.382	2049.734	2049.29	2057.166
1984.53	1978.7	1982.95	1982.48	1990.1	2051.409	2045.382	2049.775	2049.29	2057.166
1997.62	1987.28	1992.83	1991.79	2001.84	2064.94	2054.251	2059.988	2058.913	2069.302
2000.36	1987.29	1992.87	1991.79	2001.84	2067.772	2054.262	2060.03	2058.913	2069.302
2000.37	1987.79	1994.55	1993.75	2002.47	2067.782	2054.779	2061.766	2060.939	2069.953
2008.06	1991.11	1995.63	1994.66	2006.56	2075.732	2058.21	2062.883	2061.88	2074.181
2016.9	1998.75	2006.61	2006.83	2019.46	2084.87	2066.108	2074.233	2074.46	2087.516
2026.99	1998.75	2006.69	2006.83	2023.3	2095.3	2066.108	2074.315	2074.46	2091.485
2026.99	2005.85	2010.62	2010.13	2023.3	2095.3	2073.447	2078.378	2077.871	2091.485
2030.92	2011.63	2017.11	2018.1	2031.24	2099.362	2079.422	2085.087	2086.11	2099.693
2072.43	2086.7	2081.24	2087.36	2088.89	2142.271	2157.022	2151.378	2157.704	2159.286

**Table S26.** Full coordinates of gas-phase modeled geometry of **2**, given in 12-digit standard format, in Angstroms.

Fe	8.786777000000	2.928929000000	6.096250000000
Fe	10.119780000000	1.595914000000	4.395807000000
C	7.849094000000	1.991243000000	7.299766000000
O	7.250014000000	1.392162000000	8.079905000000
C	10.289722000000	1.425981000000	6.237749000000
O	10.810738000000	0.904968000000	7.146494000000
C	11.814332000000	1.562356000000	3.898548000000
O	12.915748000000	1.495910000000	3.557691000000
C	8.786774000000	2.928924000000	4.216575000000
Fe	7.453764000000	4.261931000000	4.395809000000
C	9.724468000000	3.866616000000	7.299759000000
O	10.323552000000	4.465699000000	8.079894000000
C	7.283833000000	4.431871000000	6.237752000000
O	6.762819000000	4.952888000000	7.146497000000
C	5.759208000000	4.295495000000	3.898559000000
O	4.657790000000	4.361945000000	3.557710000000
Fe	8.786774000000	2.928922000000	2.336900000000
Fe	7.453765000000	1.595917000000	4.037339000000
C	9.724466000000	1.991239000000	1.133388000000
O	10.323550000000	1.392159000000	0.353252000000
C	7.283833000000	1.425983000000	2.195394000000
O	6.762818000000	0.904966000000	1.286650000000
C	5.759210000000	1.562354000000	4.534591000000
O	4.657793000000	1.495903000000	4.875443000000
Fe	10.119781000000	4.261933000000	4.037344000000
C	7.849092000000	3.866613000000	1.133386000000
O	7.250013000000	4.465696000000	0.353248000000
C	10.289723000000	4.431872000000	2.195405000000
O	10.810738000000	4.952885000000	1.286658000000
C	11.814334000000	4.295493000000	4.534602000000
O	12.915751000000	4.361939000000	4.875458000000
C	7.420203000000	-0.098637000000	4.534594000000
O	7.353754000000	-1.200054000000	4.875447000000
C	10.153342000000	5.956487000000	4.534599000000
O	10.219789000000	7.057904000000	4.875452000000
C	10.153343000000	-0.098641000000	3.898556000000
O	10.219793000000	-1.200059000000	3.557706000000
C	7.420204000000	5.956483000000	3.898549000000
O	7.353757000000	7.057900000000	3.557693000000

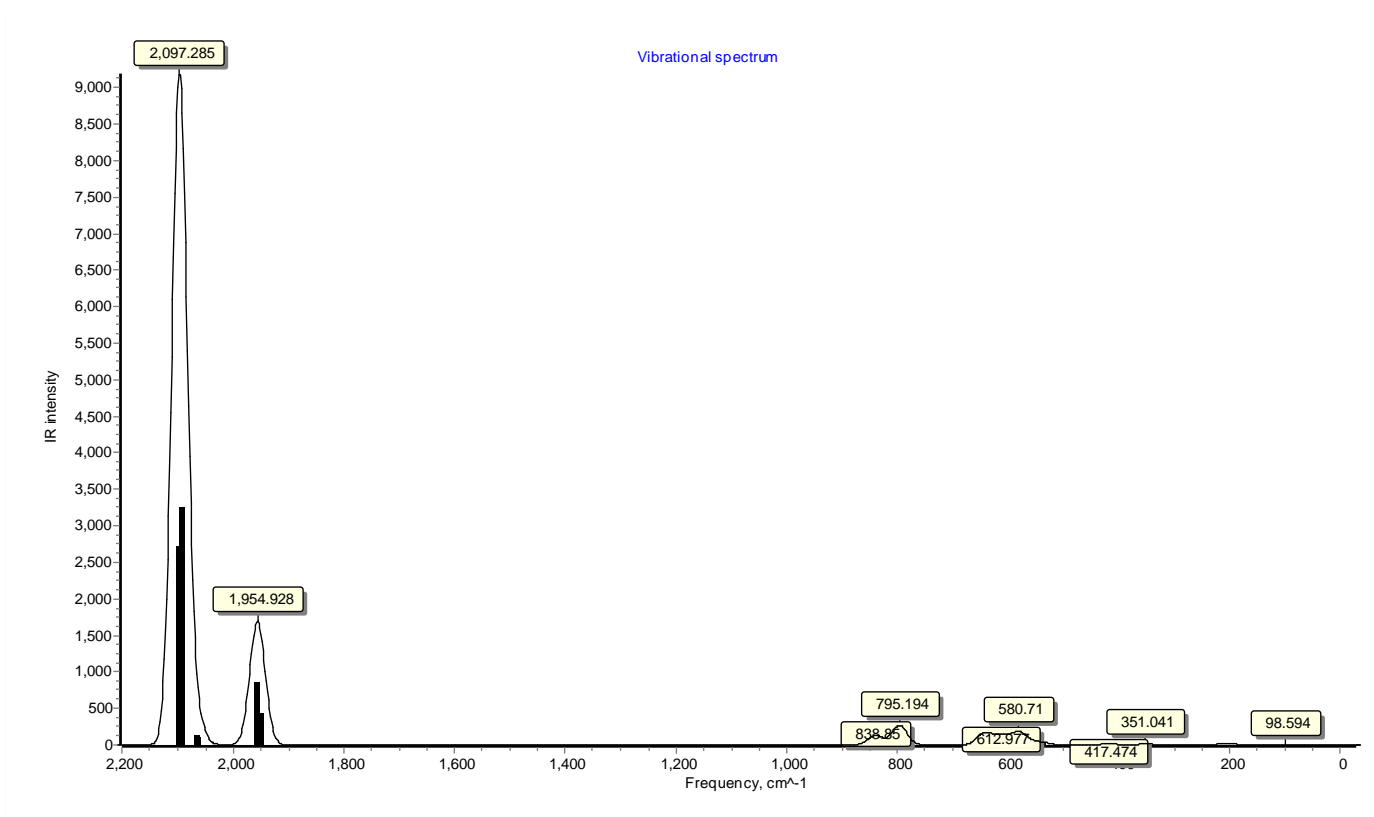
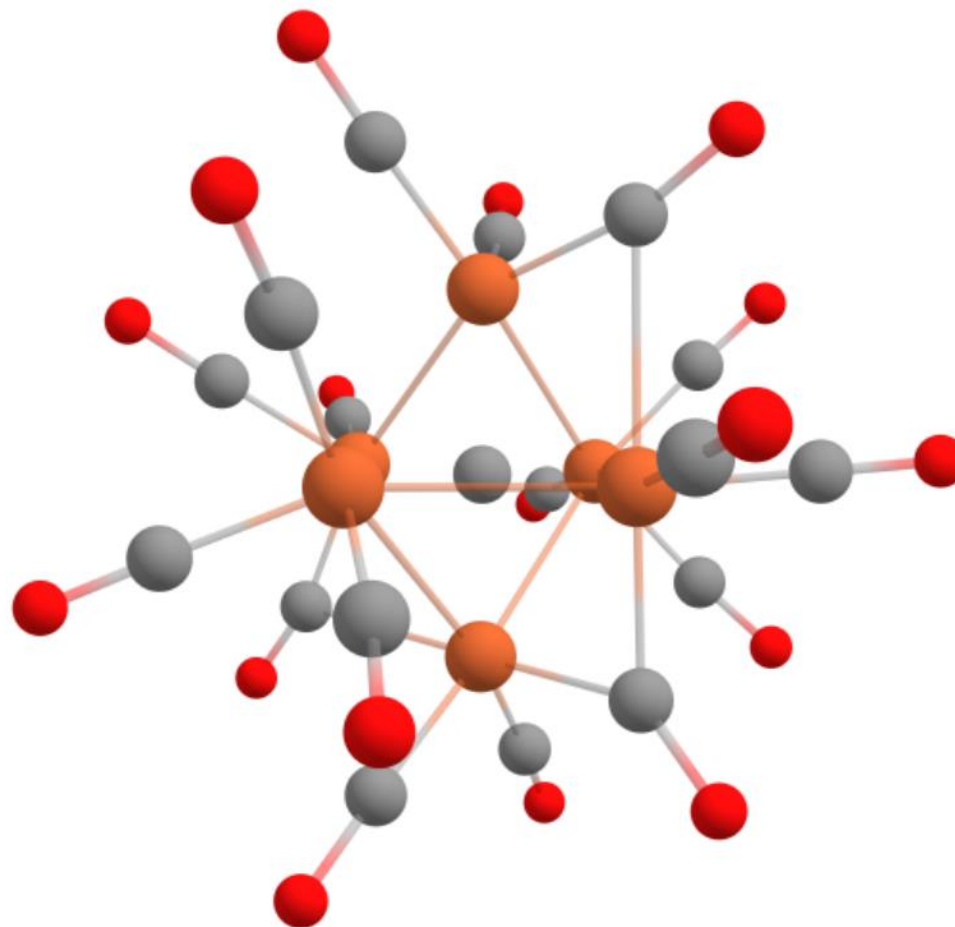


Figure S62. IR activities of gas phase model of **2** with scaling factor.



**Figure S63.** Optimized gas-phase geometry of **3**, BP86 ma-def2-TZVP-D4.

RMSD value of gas-phase versus crystal structure (core A) **3**, unweighted: 3.96958539990249; weighted: 1.52554956383366.

**Table S27.** Full coordinates of gas-phase modeled geometry of **3**, given in 12-digit standard format, in Angstroms.

Fe	-1.604759000000	0.576040000000	2.574704000000
Fe	0.042676000000	1.986483000000	4.190714000000
Fe	-2.088918000000	3.286019000000	5.165049000000
O	-1.841447000000	5.926771000000	3.872337000000
O	0.429950000000	-1.468140000000	3.071074000000
O	-0.686181000000	1.506618000000	-0.058410000000
O	1.409400000000	4.504702000000	4.806434000000
O	2.239016000000	1.361467000000	2.333270000000
O	-4.485342000000	4.495975000000	6.339354000000
O	-3.056957000000	-1.631605000000	1.284886000000
O	1.371934000000	0.803281000000	6.524793000000
O	-0.582412000000	4.391659000000	7.431399000000
C	-1.841452000000	4.749301000000	3.872330000000
C	-1.841452000000	1.934261000000	3.872325000000
C	0.768665000000	1.186695000000	5.610548000000
C	0.811468000000	3.536219000000	4.585570000000
C	-3.556076000000	4.002558000000	5.848591000000
C	-2.527396000000	-0.733919000000	1.790515000000
C	-1.078078000000	1.335992000000	1.025771000000
C	-1.148885000000	3.965479000000	6.513051000000
C	1.356161000000	1.577432000000	3.050624000000
C	-0.339565000000	-0.612054000000	2.906566000000
Fe	-2.078136000000	0.576038000000	5.169948000000
Fe	-3.725579000000	1.986469000000	3.553937000000
Fe	-1.593997000000	3.286027000000	2.579611000000
O	-4.112846000000	-1.468144000000	4.673589000000
O	-2.996711000000	1.506617000000	7.803061000000
O	-5.092297000000	4.504692000000	2.938230000000
O	-5.921912000000	1.361477000000	5.411396000000
O	0.802434000000	4.495963000000	1.405300000000
O	-0.625947000000	-1.631608000000	6.459777000000

O	-5.054862000000	0.803267000000	1.219872000000
O	-3.100473000000	4.391688000000	0.313252000000
C	-4.451585000000	1.186683000000	2.134110000000
C	-4.494362000000	3.536209000000	3.159086000000
C	-0.126835000000	4.002553000000	1.896068000000
C	-1.155507000000	-0.733923000000	5.954144000000
C	-2.604817000000	1.336000000000	6.718877000000
C	-2.534015000000	3.965497000000	1.231603000000
C	-5.039059000000	1.577430000000	4.694036000000
C	-3.343333000000	-0.612055000000	4.838092000000

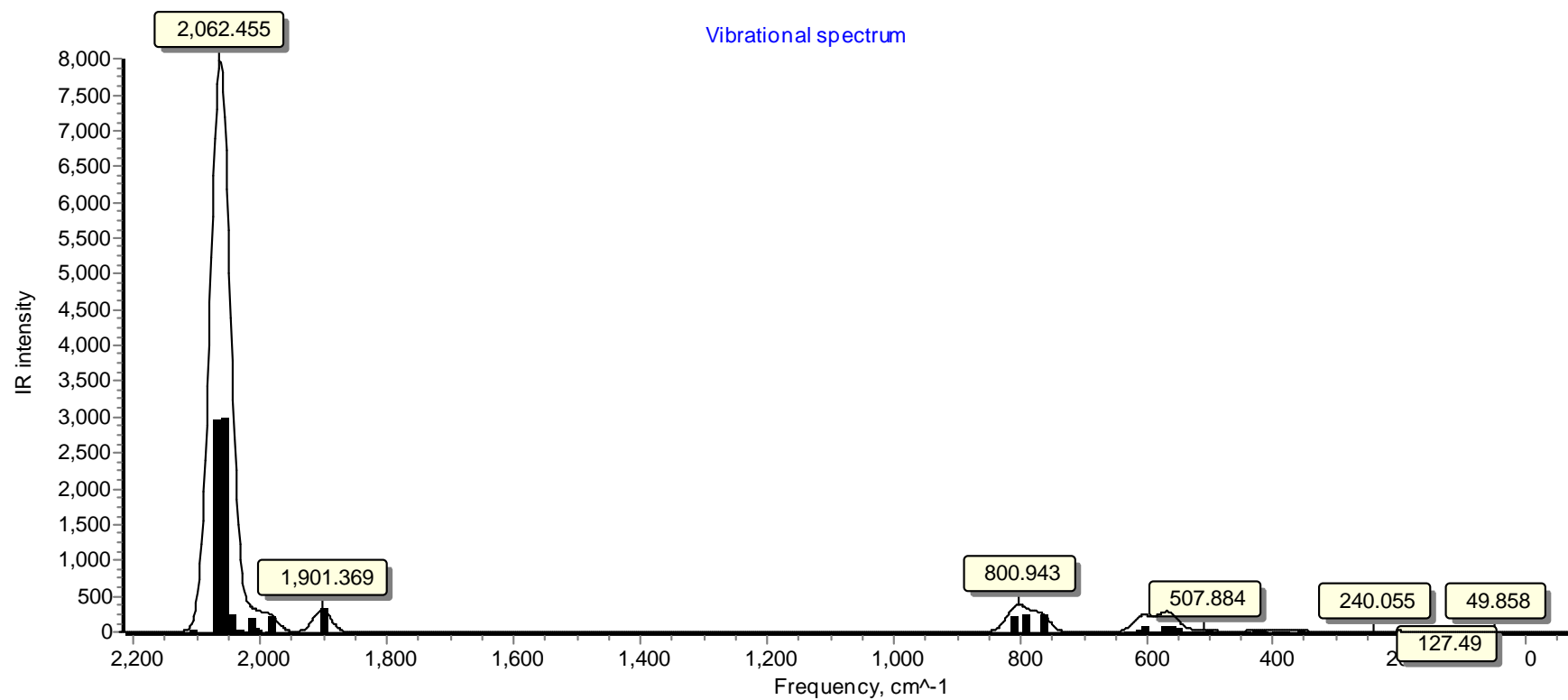


**Figure S64.** IR activities of gas phase model of **3** without scaling factor. Experimental values: 2096(w), 2023 (s), 1829(m).

## Supporting Information References

- 1 S. Kuppuswamy, J. D. Wofford, C. Joseph, Z. L. Xie, A. K. Ali, V. M. Lynch, P. A. Lindahl and M. J. Rose, *Inorg. Chem.*, 2017, **56**, 5998–6012.
- 2 G. R. Fulmer, A. J. M. Miller, N. H. Sherden, H. E. Gottlieb, A. Nudelman, B. M. Stoltz, J. E. Bercaw and K. I. Goldberg, *Organometallics*, 2010, **29**, 2176–2179.
- 3 Y. Jeannin and A. Gourdon, *J. Organomet. Chem.*, 1990, **388**, 195–202.
- 4 C. G. Cooke and M. J. Mays, *J. Organomet. Chem.*, 1975, **88**, 231–236.
- 5 J. S. Bradley, G. B. Ansell, M. E. Leonowicz and E. W. Hill, *J. Am. Chem. Soc.*, 1981, **103**, 4968–4970.
- 6 A. Taheri and L. A. Berben, *Inorg. Chem.*, 2016, **55**, 378–385.
- 7 C. F. Macrae, I. Sovago, S. J. Cottrell, P. T. A. Galek, P. McCabe, E. Pidcock, M. Platings, G. P. Shields, J. S. Stevens, M. Towler and P. A. Wood, *J. Appl. Crystallogr.*, 2020, **53**, 226–235.
- 8 2022.
- 9 W. A. Paciorek, M. Meyer and G. Chapuis, *Acta Crystallogr. Sect. A Found. Crystallogr.*, 1999, **55**, 543–557.
- 10 O. V. Dolomanov, L. J. Bourhis, R. J. Gildea, J. A. K. Howard and H. Puschmann, *J. Appl. Crystallogr.*, 2009, **42**, 339–341.
- 11 G. M. Sheldrick, *Acta Crystallogr. Sect. A Found. Adv.*, 2015, **71**, 3–8.
- 12 G. M. Sheldrick, *Acta Crystallogr. Sect. C Struct. Chem.*, 2015, **71**, 3–8.
- 13 E. Prince, Ed., *International Tables for Crystallography*, International Union of Crystallography, Chester, England, 2006, vol. C.
- 14 S. Parsons, H. D. Flack and T. Wagner, *Acta Crystallogr. Sect. B Struct. Sci. Cryst. Eng. Mater.*, 2013, **69**, 249–259.
- 15  $R_w(F^2) = \{w(|F_o|^2 - |F_c|^2)^2/w(|F_o|^4)\}^{1/2}$  where  $w$  is the weight given each reflection.  
 $R(F) = (|F_o| - |F_c|)/|F_o|$  for reflections with  $F_o > 4(F_o)$ .  
 $S = [w(|F_o|^2 - |F_c|^2)^2/(n - p)]^{1/2}$ , where  $n$  is the number of reflections and  $p$  is the number of refined parameters.
- 16 F. Neese, *WIREs Comput. Mol. Sci.*, 2018, **8**, 1–15.
- 17 F. Neese, 2022, 1–15.
- 18 ChemCraft, <https://www.chemcraftprog.com>.
- 19 V. Vennelakanti, A. Nandy and H. J. Kulik, *Top. Catal.*, 2022, **65**, 296–311.
- 20 K. A. Moltved and K. P. Kepp, *J. Chem. Theory Comput.*, 2018, **14**, 3479–3492.
- 21 A. Jaoul, G. Nocton and C. Clavaguéra, *ChemPhysChem*, 2017, **18**, 2688–2696.
- 22 J. B. Foresman and Ae. Frisch, *Exploring Chemistry With Electronic Structure Methods: A Guide*

- to *Using Gaussian*, Gaussian, Inc., Pittsburgh, PA, 2nd edn., 1996.
- 23 R. D. JohnsonIII, Ed., in *NIST Standard Reference Database Number 101*, 2022.
- 24 M. K. Kesharwani, B. Brauer and J. M. L. L. Martin, *J. Phys. Chem. A*, 2015, **119**, 1701–1714.
- 25 J. P. Merrick, D. Moran and L. Radom, *J. Phys. Chem. A*, 2007, **111**, 11683–11700.
- 26 M. Bortoluzzi, I. Ciabatti, C. Cesari, C. Femoni, M. C. Iapalucci and S. Zacchini, *Eur. J. Inorg. Chem.*, 2017, **2017**, 3135–3143.
- 27 C. Joseph, S. Kuppaswamy, V. M. Lynch and M. J. Rose, *Inorg. Chem.*, 2018, **57**, 20–23.
- 28 E. H. Braye, L. F. Dahl, W. Hübel, D. L. Wampler, W. Hubel and D. L. Wampler, *J. Am. Chem. Soc.*, 1962, **84**, 4633–4639.
- 29 M. U. Delgado-Jaime, B. R. Dible, K. P. Chiang, W. W. Brennessel, U. Bergmann, P. L. Holland and S. DeBeer, *Inorg. Chem.*, 2011, **50**, 10709–10717.